CHALMERS
UNIVERSITY OF TECHNOLOGY

Usage of UWB Sensors for People Collision Avoidance at Construction Sites

Position Estimation of Construction Personnel Around an Excavator

Master's thesis in Master Programme Systems, Control and Mechatronics

MATTIAS GUDJONSSON
ANTON JOHANSSON

Department of Electrical Engineering
CHALMERS UNIVERSITY OF TECHNOLOGY
Gothenburg, Sweden 2018

Master's thesis EX081/2018

Usage of UWB Sensors for People Collision Avoidance at Construction Sites

Position Estimation of Construction Personnel Around an Excavator

MATTIAS GUDJONSSON
ANTON JOHANSSON

CHALMERS
UNIVERSITY OF TECHNOLOGY

Department of Electrical Engineering
Chalmers University of Technology
Gothenburg, Sweden 2018

Usage of UWB Sensors for People Collision Avoidance at Construction Sites
Position Estimation of Construction Personnel Around an Excavator
Mattias Gudjonsson
Anton Johansson

Supervisor: Per Björe Dahl, CPAC Systems
Examiner: Henk Wymeersch, Department of Electrical Engineering

Master's Thesis EX081/2018

Department of Electrical Engineering
Chalmers University of Technology
SE-412 96 Gothenburg
Telephone +46 31 772 1000

Cover: Picture of the excavator which the tests were performed on. Photo by Anton Johansson, 2018.

Typeset in LaTeX
Gothenburg, Sweden 2018

Usage of UWB Sensors for People Collision Avoidance at Construction Sites
Position Estimation of Construction Personnel Around an Excavator
MATTIAS GUDJONSSON
ANTON JOHANSSON
Department of Electrical Engineering
Chalmers University of Technology

Abstract

A problem with operating excavators and other heavy machinery on construction sites, are the many occurring blind spots. This is a safety issue, and because of the restricted field of view, accidents may occur. Today, there are solutions using cameras to cover blind spots, but these rely on the operator to look on screens. This Master's thesis intends to evaluate the use of ultra wideband (UWB) technology to cover these blind spots. The methods used for localization are, two way ranging (TWR) and time difference of arrival (TDOA). Two different types of filters, Extended Kalman filter (EKF) and Cubature Kalman filter (CKF), are used and evaluated to estimate a position. In addition to the filters, a non-linear programming solver is also used. To evaluate the system, tests and simulations have been conducted indoors and on a real excavator.

The results show that a TWR based system is more precise regarding accuracy and have a larger coverage around the machine. Although, a TDOA system shows good results in bearing, but the range tends to deviate. A TDOA system also scales better than a TWR system, with a larger amount of tags.

Keywords: ultra wideband, localization, position estimation, TOA, TDOA

Acknowledgements

We would like to express our gratitude to CPAC Systems AB for all the support during this thesis and a special thanks to our supervisor Per Björe Dahl at CPAC Systems AB. Further we would like to thank our examiner Henk Wymeersch and our advisor Alireza Sheikh at Chalmers University of Technology.

Mattias Gudjonsson and Anton Johansson, Gothenburg, June 2018

Contents

List of Figures

List of Tables

1
Introduction

In this chapter the background and the purpose of this Master's thesis are presented. The main objectives are defined, as well as the project scope and limitations. The thesis is done in collaboration with CPAC Systems AB and the work is performed in their facilities.

1.1 Background

At construction sites, heavy equipment are working in close proximity to construction site workers. One type of heavy equipment is excavators, in which the operator has a limited field of view. In extreme cases 270 degrees of the vision is blocked. Because of the limited field of view blind spots appear, which could lead to accidents, where the excavator might collide with workers [2]. Nowadays vision systems using cameras are used to get a bird's eye view to cover the blind spots. However, these vision systems are limited in range and relies on the operator to look on screens.

Instead of, or in addition to, using a vision system to cover the blind spots, a localization system based on UWB sensors can be used [3]. UWB sensors have a bandwidth of at least 25 % of the center frequency or an absolute bandwidth of at least 375 MHz [4]. The large bandwidth together with a low power level of the signals make UWB signals act as a background noise to other wireless communication systems [3]. The UWB sensors are also less power consuming compared to other wireless communication systems due to the lower power of the signal, as well as simpler architecture in the sensors [3].

There are different localization methods which can be used with UWB sensors. Using time, angle or signal strength, a position can be obtained [5]. Time based methods includes time of arrival (TOA) and TDOA. These methods utilize times to estimate a position. Angle of arrival (AOA) uses measured angles between reference nodes and a target node. The signal strength can be used to acquire a position by measuring the energy level of the signal at reference nodes. The energy levels are used to obtain distances. This is similar to TOA and TDOA methods, where times are used to obtain distances, which then are used to estimate the position. Reference nodes are hereby referred as anchors and target nodes as tags. The tags should be worn by the personnel or by the objects which shall be positioned, e.g., the tag could be mounted on the personnel's helmets.

UWB sensors are often used for indoor positioning [5]. In an indoor positioning system, the anchors are placed on walls, and therefore the tags will be inside an area defined by the anchors. In a positioning system used on an excavator, this is not the case. Due to this, it is unknown how the positioning methods work and therefore these methods will be evaluated in this thesis. A graphical representation of these two cases is seen in Fig. 1.1.

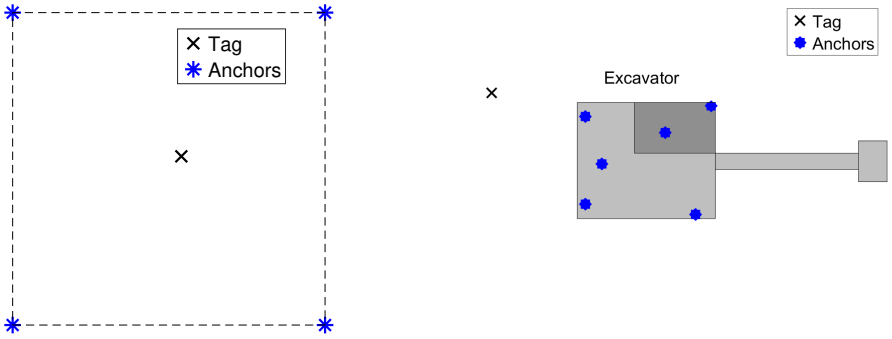

Figure 1.1: To the left, a standard case for indoor positioning with the tag inside the area defined by the anchors. To the right, the case studied in this thesis with the tag outside the area defined by the anchors.

1.2 Purpose

The purpose of this thesis is to study how a system of UWB sensors can be used in a construction site environment to localize workers in blind spots of an excavator. If workers can be detected in blind spots, the risk of collision can be decreased. This might improve the efficiency of the excavator, since the operator does not need to look at screens, in order to observe the surroundings.

1.3 Objective

The main objective in this Master's thesis is to investigate the possibility to position workers in the blind spots of an excavator with UWB sensors. Hence, a system must fulfill certain criteria. It must be accurate, have high enough update rate and cover all blind spots. To achieve this goal the objective is split into subobjectives, which is presented below:

- How does the UWB technology work when the tag is outside the area defined by the anchors?
- How accurate is a UWB positioning system?
- How many tags are possible to position simultaneously, in a UWB positioning system?
- What UWB sensors should be used?
- What are the characteristics of UWB sensors, i.e., how much noise is there, is there a bias?
- Which localization technique (time, angle or signal strength based) should be used?
- What localization algorithms exists and which should be used?
- What filters are needed to obtain a correct estimate of the position?
- How many anchors are needed and where should they be placed?

To fulfill above stated subobjectives, several system criteria is stated in Section 1.3.1. This includes, the limitations of the project, the requirements which the localization system has to fulfill, and how the performance of the system will be evaluated. A concept system is also developed, see Section 1.3.2, in order to evaluate the specified criteria.

1.3.1 System criteria

To investigate the feasibility of using UWB technology for people localization and collision avoidance on construction sites, tests are required. In order to evaluate the performance of the system, four main criteria will be investigated. They are, accuracy, range and coverage, update rate and scalability, and power consumption. A more in depth discussion of the different criteria and how to evaluate them follows in Section 1.3.1.1 to 1.3.1.4. Also, to cover the blind spots a position in 2D is adequate, but to accurately estimate the position relative to the machine, positioning in 3D is needed to take care of uneven terrain, i.e., heaps and holes, and people of different height.

1.3.1.1 Accuracy

One important property of a localization system is the accuracy of the position estimate. Therefore, the accuracy of UWB sensors have to be evaluated. This includes noise and bias of the sensors. Since UWB-technology is said to have an accuracy of ± 10 cm [6], a margin is added to be able to guarantee a certain accuracy. Hence, the system should be able to position a tag with an accuracy of ± 50 cm.

1.3.1.2 Range and Coverage

Another important property of an localization system are the range and coverage. Therefore, the effective range and resulting coverage of a localization system need to be evaluated, in order to know how far away it is possible to estimate a position.

The reach of a common high volume 20 ton excavator is between 9-16 m depending on configuration [7], and in order to have a large margin before a person enters the machine's reach, a working distance of 50 m is desired.

1.3.1.3 Update Rate and Scalability

Since a construction site might be crowded, a positioning system has to be able to position a large number of tags simultaneously. The ability to locate at least 10 people in close vicinity of the machine, should be enough to cover a normal situation. The possible update rate of the positions have to be determined. With an accuracy of ± 50 cm radius and an average walking speed of 2 m/s, an update rate of at least 2 Hz is needed in order for the next measurement to be within the accuracy radius of the previous measurement, and hence, always give a truthful position.

1.3.1.4 Power Consumption

The tags will be worn by construction site workers. Hence, they have to be powered by a mobile power source. In an industrialized product, this will most likely be done by a battery. Therefore, the wearable tag has to be powered by a battery for at least one working day. To minimize the size, weight and cost of the module, the UWB sensor have to consume as little energy as possible.

1.3.2 Concept system

A concept system will be developed in order to evaluate a positioning system in a real environment. As this will not be an industrialized system, no regards towards weatherproofing and manufacturability will be taken into account. In order to verify the system, the prototype will have to include the following features: hardware for the mobile tags and anchors, software to accompany the hardware, software to run the localization algorithms on a computational platform and a communication network to connect the hardware to the computational platform.

As the thesis is conducted within a limited time frame, commercial available UWB development kits will be used to shorten development time. This includes both hardware and software. This also introduce restrictions which are further explained in Chapter 6.

If a similar system would be implemented on a real construction site, faults may occur. The sensors might malfunction and positions of tags will therefore be lost. Those scenarios is dangerous if the operator of the excavator is not alerted. The thesis will discuss how these types of problems can be handled.

1.4 Ethical, Sustainability and Societal Aspects

All products that offer the user a safety system include ethical aspects. For example, in the context of autonomous cars, if the system fails for an unknown reason and an accident occurs, it is hard to determine whose fault it is. It could be the person driving the car, the manufacturer or the engineer who developed the function. The same scenario applies for this system. If the operator stops being alert while using the machine when an additional safety system is in use, and therefore manage to harm a coworker that the system does not recognize, it could be equally hard to determine who is to blame.

If a reliable detection system is implemented, the operator will not need to check around the excavator nor will the operator need to look on screens to ensure that the space around the excavator is free. Therefore, the excavator will not be idle for as long time as without such a system. A reliable detection system with UWB sensors should also reduce the risk of serious accidents on construction sites. A system with UWB sensors attached to an excavator could also be cheaper than a system with cameras, thus, more construction companies might install such a system on their equipment.

1.5 Thesis Structure

This section is intended to explain the thesis structure. Chapter 2 introduces UWB technology, as well as what hardware is used throughout this thesis. Chapter 3 covers the methods needed to obtain measurements from a radio frequency based localization system. Chapter 4 presents the theory needed to obtain a position from the measurements, obtained in Chapter 3. To obtain a smooth and precise position, filters are required. Necessary filter theory used in this thesis are presented in Chapter 5. In Chapter 6, the concept positioning system is introduced. This system combines the hardware presented in Chapter 2, the methods presented in Chapter 3, Chapter 4 and Chapter 5, into a complete positioning system. The concept system is used to evaluate if UWB is a viable solution for localization of construction personal. Chapter 7 presents the results of the system criteria using the system described in Chapter 6. Finally the results are discussed and suggested future work are presented in Chapter 8. The thesis is concluded in Chapter 9.

2
UWB-Sensors

In this chapter, basics of UWB technology is explained, and the UWB hardware used in this thesis is introduced.

2.1 UWB Technology

UWB is a wireless communication technology which is defined in different ways depending on the source. According to [8], the Federal Communications Commission defines UWB technology as any signal that occupies more than 500 MHz bandwidth in the 3.1 to 10.6 GHz band. Alternatively, [4] defines UWB as "any wireless transmission scheme that occupies a bandwidth of more than 25% of a center frequency, or more than 1.5 GHz". The conclusion is that UWB are signals which occupies a wide bandwidth, at least 375 MHz, and have a high center frequency. The spectra allocated for UWB transmissions varies depending on location. In USA, UWB transmission is allocated to the previously stated 3.1-10.6 GHz band, with a maximum mean power spectral density of 41.3 dBm/MHz [9]. Europe have a slightly different spectral band allocated to UWB transmissions. In Europe the main frequency slot used is 6-8.5 GHz, the maximum mean power spectral density is identical to the one used in USA [10]. The same maximum mean power spectral density is also allowed in other frequency regions, but in these regions other requirements on the amount of transmissions also apply [10]. UWB also transmit signals with a low power level, around 0.5 mW [11]. Despite the low power level, the data rate is high. The *Shannon-Hartley theorem* [11]

$$C = B \log_2 \left(1 + \frac{S}{N}\right) \tag{2.1}$$

shows the capacity of a channel, where C is the bits per second transmitted without errors, B is the bandwidth, S is the signal power and N is the power of a white uncorrelated Gaussian noise. From (2.1), one can infer that the capacity increases linearly with increasing bandwidth, whereas an exponential increase in signal power would be required for the same increase in capacity. Therefore, UWB technology is capable of transmitting large amounts of data using low power signals [11].

According to [11], the properties of UWB signals give the technology several advantages over traditional narrow-band wireless technologies. Among these a few stand out as they are directly beneficial to the purposes of this thesis. The low power level in the UWB signals also implies a low power consumption which results in a

long batterylife for wearable tags. The fine timings required by the high frequency high bandwidth signals of UWB gives it good multipath properties and therefore makes it ideal for local positioning systems [11]. Multipathing is when signals travel alternative routes, e.g., when a signal reflects on a wall before it is received.

Since the FCC release of the 3.1-10.6GHz band for unlicensed UWB communication, the use of UWB as a method for local positioning has increased [12]. Local positioning systems using other wireless technologies have been considered before, but with lower accuracy. Comparing several popular localization techniques, one can see that an UWB system outperforms the others [12].

2.1.1 IEEE802.1.14

IEEE802.1.14 or IEEE802.1.14-2011 is a standard for low-data-rate, low-power, and low-complexity, short-range radio frequency (RF) wireless communication, and is defined by the IEEE Standards Association [13]. This standard is often used in UWB applications. It includes multiple definitions of physical layers (PHY), which defines how the physical RF signals is composed, as well as a simple medium access control (MAC) layer, which defines how the transmitted data is formatted [13].

2.1.1.1 PHY

A frame, or a message, defined by IEEE802.1.14-2011 consists of four main parts, preamble, the start of frame delimiter (SFD), the PHY header (PHR) and the payload [1]. The first part of a frame is the preamble and it is followed by the SFD. These parts of the frame are used as an synchronization header. The synchronization header is followed by the PHR, which defines the length and data-rate of the following payload [1]. An graphical representation of an IEEE802.1.14-2011 frame is seen in Fig. 2.1.

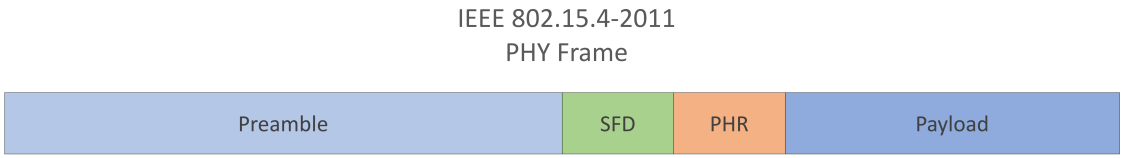

Figure 2.1: Layout of an IEEE802.15.4-2011 PHY frame.

The implementation of UWB defined in IEE802.15.4-20111 uses high speed RF pulses to transmit information. In order to send information, pulse modulation is needed. This particular implementation of UWB uses two different modulation techniques [1]. In the PHR and Payload section of the frame, the data is determined by a method called burst position modulation (BPM) which utilize binary phase shift keying [1]. During the synchronization header, the BPM is not used. Instead, a proprietary modulation technique is used [1]. The switch of modulation method is deterministic, this enables precise time stamps, which contributes to precise distance measurements [1].

2.1.1.2 MAC

The definition of the MAC layer is used to easily transmit and receive data in a structured manor. The MAC frame is sent in the payload portion of the PHY frame defined in Section 2.1.1.1. The structure of a MAC frame is shown in Fig. 2.2. A frame consists of several predetermined fields. First, a MAC header which, e.g., keeps track of the source and destination address of the transmitter and the receiver of the message [1]. After the header, the payload follows, which can contain any kind of data that the user want to transmit. The frame is then ended by the Frame Checking Sequence (FCS), which uses Cyclic Redundancy Check to determine if there was any error in the frame [1].

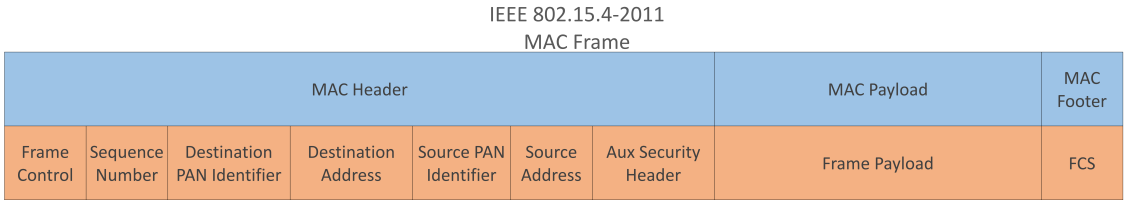

Figure 2.2: Layout of an IEEE802.15.4-2011 MAC frame

2.2 Test sensors

This section explains the hardware used throughout this thesis. This is done in two stages, first the hardware used for UWB transmissions and receptions is introduced. This is followed by the development kit used in the thesis which interfaces with the UWB sensor hardware.

2.2.1 UWB Sensor

The UWB sensor (DW1000) and its module (DWM1000), which are used in this thesis, are developed by the company Decawave.

2.2.1.1 Decawave DW1000

To be able to send and receive UWB messages, a UWB sensor is required. At the time of this thesis, a common sensor used in industry is the DW1000 developed by Decawave. The DW1000 is especially designed for use in local positioning systems and support localization methods as TWR and TDOA [6], see Section 3.1 and Section 3.2.

The DW1000 is a single chip UWB sensor which is low powered, low cost and compliant with IEEE802.15.4-2011 PHY and can be used with the IEEE802.15.4-2011 MAC layer. It can send data up to 6.8 Mbps and can achieve a distance accuracy of 10 cm [1]. The DW1000 is widely used and well documented, which makes it well suited for this thesis. This sensor provides several useful settings to adjust the properties of the transmitted messages. It is possible to adjust the transmission

speeds, center frequency, bandwidth, and preamble length in order to set up the sensor for maximum accuracy or maximum power efficiency [1]. The DW1000 can not operate on its own and needs a host microcontroller. To communicate between the sensor and the microcontroller, a Serial Peripheral Interface bus is used [6], and an application programming interface (API) is provided by Decawave.

2.2.1.2 Decawave DWM1000

The DW1000 comes in a small QFN-48 package without any of the required external components needed to operate properly [6]. Therefore it is hard to use the DW1000 directly. Hence, Decawave have developed the DWM1000 module which consists of a DW1000 sensor along with all the required external circuity and a built-in antenna [14]. This eliminates development time and is well suited for this thesis. The only drawback is that the DWM1000 module do not support external synchronization of the DW1000 [14], and thereby do not support wired clock synchronization which is needed for a wired TDOA implementation, see Section 3.2.

2.2.2 Development kit

To make it easier to interface with the DWM1000 module there exists several development kits from different manufacturers. The development kits provide a platform including the DWM1000 module, and a microcontroller to interface with the DWM1000. Occasionally extra sensors, such as an inertial measurement unit (IMU), are included. The development kit also includes the necessary firmware to instruct the DWM1000 to send and receive messages.

The development kit used in this thesis is available in two varieties. The first is an UWB tag which is mounted on a mini quadcopter. The other are nodes that can function as anchors or TWR tags [15]. Both varieties is built around the STM32F072 microcontroller.

Both versions of the development kit implements the localization methods, presented in Section 3.5. The nodes also have the ability to act as a "Sniffer", which listens and display the raw UWB data. The hardware and software is open source and is licensed under GNU Lesser General Public License v3.0 [15].

3
Localization Methods

In this chapter, different localization methods are described. First, different methods that are used to acquire times, time differences, angles or signal strength are explained. Later the methods which are used in this thesis to position tags are defined.

3.1 Time of Arrival

One method used to range wireless devices is TOA, sometimes called time of flight. With this method the time taken to send a message between a tag and an anchor is measured. This is done by comparing the time stamp when the tag sends a message, with the time stamp when the anchor receives the message. The distance can then be obtained by multiplying the time with the speed of light. The distance is a radius to a circle which the tag is positioned on, as shown in Fig. 3.1. Therefore a tag can be positioned by sending only one message to multiple anchors. The requirement for TOA to work is that the tag's and anchor's clocks are synchronized. Otherwise, the message which include the time stamp when the tag sent the message, cannot be compared with the time the anchor received the message. Therefore, the time it takes to send the message cannot be calculated. Also, if the synchronization would not be perfect, even a nanosecond affects the accuracy of the ranging since 1 ns is equal to a distance of approximately 30 cm (the speed of light multiplied by 1 ns gives approximately 30 cm).

A variant of TOA is TWR which is an asynchronous variant of TOA, i.e., the clocks of the tag and the anchor do not have to be synchronized. TWR measures the time it takes for a message to be sent back and forth to acquire a round trip time, therefore multiple numbers of messages must be sent before a tag can be positioned. There are different types of TWR [16], one is single sided TWR and another is double sided TWR [1].

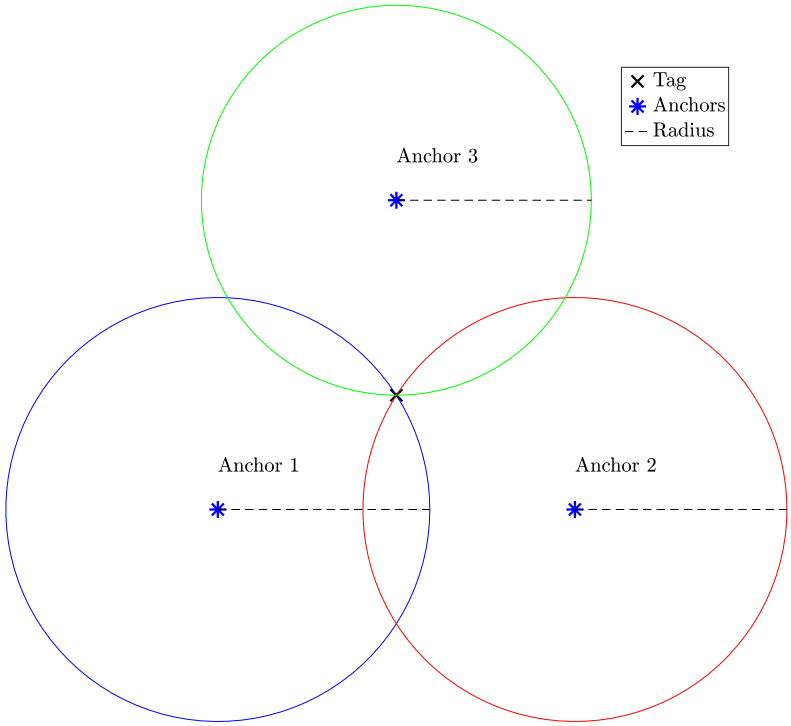

Figure 3.1: TOA. The radii are the distances from each anchor to the tag. Each circle is obtained by the radii and they represent the tag's possible positions. The true position of the tag is where all circles intersect.

3.1.1 Single Sided Two Way Ranging

The single sided TWR uses one round trip time to measure the time of arrival, i.e., the tag sends a message (called poll) to the anchor and the anchor answers (called answer), see Fig. 3.2. The time of flight, $\hat{T}$, is estimated by

$$\hat{T} = \frac{1}{2}\left(T_{round} - T_{reply}\right) \tag{3.1}$$

where T_{round} is the time it takes from that a poll is sent until an answer is received, and T_{reply} is the time between a poll is received and an answer is sent. According to [1], the single sided TWR is sensitive to clock errors. The error, e, is approximated as

$$e = \hat{T} - T \approx \frac{1}{2}(e_a - e_t)T_{reply} \tag{3.2}$$

where T is the time of flight, e_a and e_t are the offset error of the clocks nominal frequency in the anchor and the tag [1]. If T_{reply} is large and there is a too large clock error the estimated time of flight, $\hat{T}$, will become inaccurate, see Table 3.1.

T_{reply} \ Clock error	2 ppm	5 ppm	10 ppm	20 ppm	40 ppm
100 μ s	0.1 ns	0.25 ns	0.5 ns	1 ns	2 ns
200 μ s	0.2 ns	0.5 ns	1 ns	2 ns	4 ns
500 μ s	0.5 ns	1.25 ns	2.5 ns	5 ns	10 ns
1 ms	1 ns	2.5 ns	5 ns	10 ns	20 ns
2 ms	2 ns	5 ns	10 ns	20 ns	40 ns
5 ms	5 ns	12.5 ns	25 ns	50 ns	100 ns

Table 3.1: Typical clock induced errors in single sided TWR time of flight estimation [1].

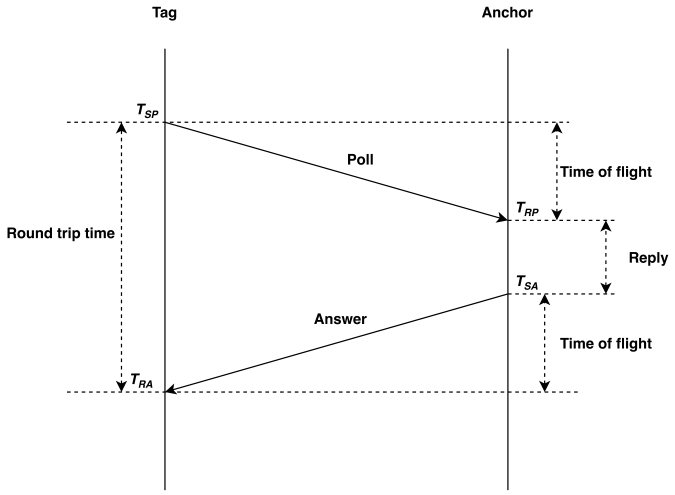

Figure 3.2: Schedule for single sided TWR.

3.1.2 Double Sided Two Way Ranging

The double sided TWR uses two round trip times. This is done by expanding the single sided TWR with an extra message called "Final", see Fig. 3.3. Since the communication scheme is different, compared to single sided TWR, double sided TWR estimate $\hat{T}$ as

$$\hat{T} = \frac{T_{round1}T_{round2} - T_{reply1}T_{reply2}}{T_{round1} + T_{round2} + T_{reply1} + T_{reply2}} \tag{3.3}$$

where T_{round1} and T_{round2} are the round trip times in Fig. 3.3, i.e., from T_{SP} to T_{RA} and T_{SA} to T_{RF}. The time it takes for a tag or an anchor to reply to a message after receiving one, is denoted by T_{reply1} and T_{reply2} in (3.3). With double sided TWR the clock induced error is smaller than single sided TWR. The error, e, can be approximated by

$$e = \hat{T}\left(1 - \frac{k_a + k_t}{2}\right) \tag{3.4}$$

where the clocks of the anchor and the tag runs at k_a and k_t times the desired clock frequency. The factors k_a and k_t are close to 1. According to [1], the worst case

specification is when the clock is 20 ppm apart, the factors, k_a and k_t, are then either 0.99998 or 1.00002.

In Fig. 3.3, the transmission schedule of double sided TWR is shown, where T_{SP} marks the time when the poll is sent, T_{RP} marks the time when the poll is received, T_{SA} marks the time when the answer is sent, T_{RA} marks the time when the answer is received, T_{SF} marks the time when the final is sent and T_{RF} marks the time when the final is received. The time of flight is the essential part to calculate the distance between an anchor and a tag. Double sided TWR can also include a message called "Report" which is sent after the final. "Report" is used if the measurement is to be processed by the tag instead of the anchor.

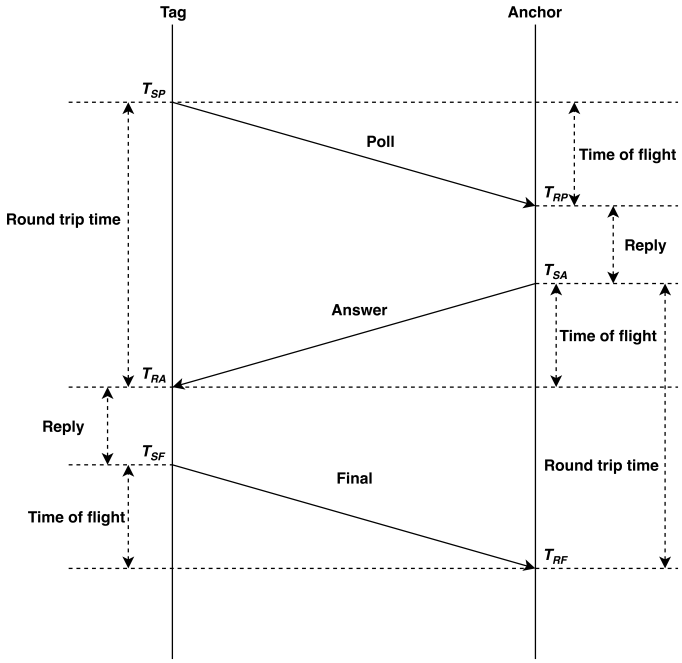

Figure 3.3: Schedule of double sided TWR.

3.2 Time Difference of Arrival

Another localization method is TDOA. TDOA uses time differences instead of time of flight, i.e., it compares the times when an anchor pair received a message from a tag. Hence, a tag can be positioned with only one message since the same message is received by all anchors, and can be compared by an arbitrary pair of anchors. TDOA is used in different types of positioning systems, e.g., to position air crafts [17]. Although, to be able to use TDOA the anchors require synchronized clocks. Otherwise, it is not possible to compare the different times with each other. The time differences results in hyperbolas, on where the tag's position is possible, see Fig. 3.4, in the same way as the circle created from the radius in the TOA method from Section 3.1.

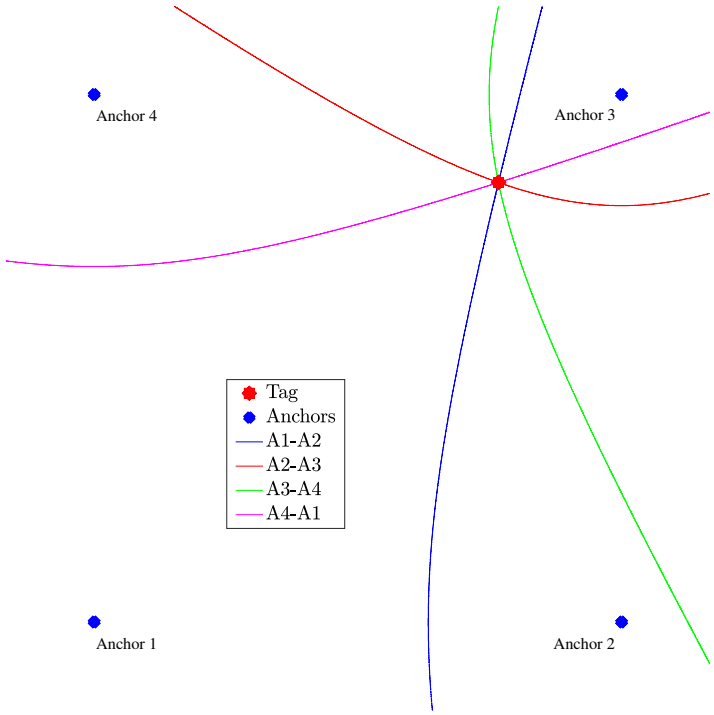

Figure 3.4: TDOA. The hyperbolas represent all possible positions of the tag for each anchor pair.

There is also an asynchronous method of TDOA which is called asynchronous time difference of arrival (ATDOA). This method does not require that the anchors are synchronized. With ATDOA, anchors send a poll, one at the time [18]. The poll are then received by a master anchor as well as a tag. The master anchor saves the time when it has received the message. The tag also receive the poll, and re-transmits the message to the master anchor. The master anchor will thereafter receive the

message from the tag, and has access to two times that is compared. ATDOA is illustrated in Fig. 3.5. From Fig. 3.5 the time difference is calculated by

$$T_{diff} = (T_{TB} + T_{AT}) - T_{AB} \tag{3.5}$$

when anchor B is the master anchor.

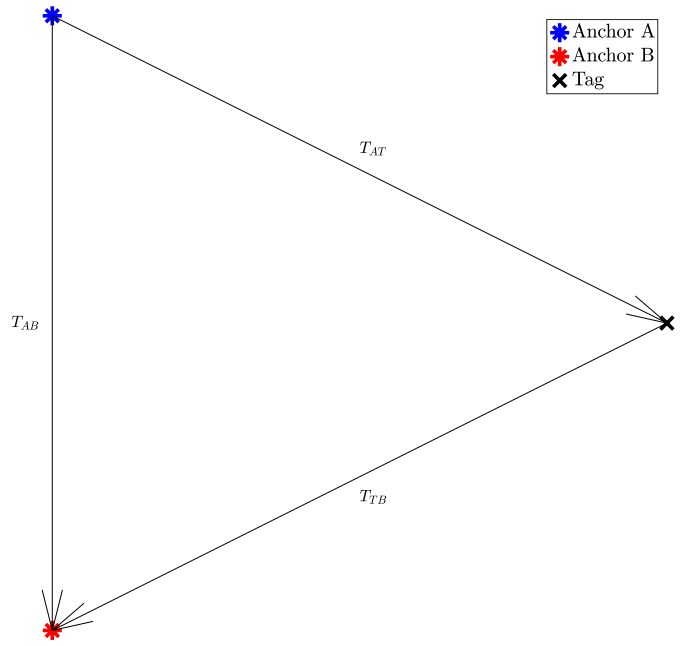

Figure 3.5: ATDOA. Anchor B is a master anchor.

3.3 Angle of Arrival

The AOA method uses angles to estimate a tag's position, see Fig. 3.6. To measure the angles from where the poll was sent, the anchors need to be equipped with antenna arrays [5].

3.4 Signal Strength

The distance between an anchor and a tag can be calculated by measuring the signal strength [5]. This method relies on a path-loss model and the channel characteristics have to be known. The same method is used to estimate a position with signal strength as with TOA.

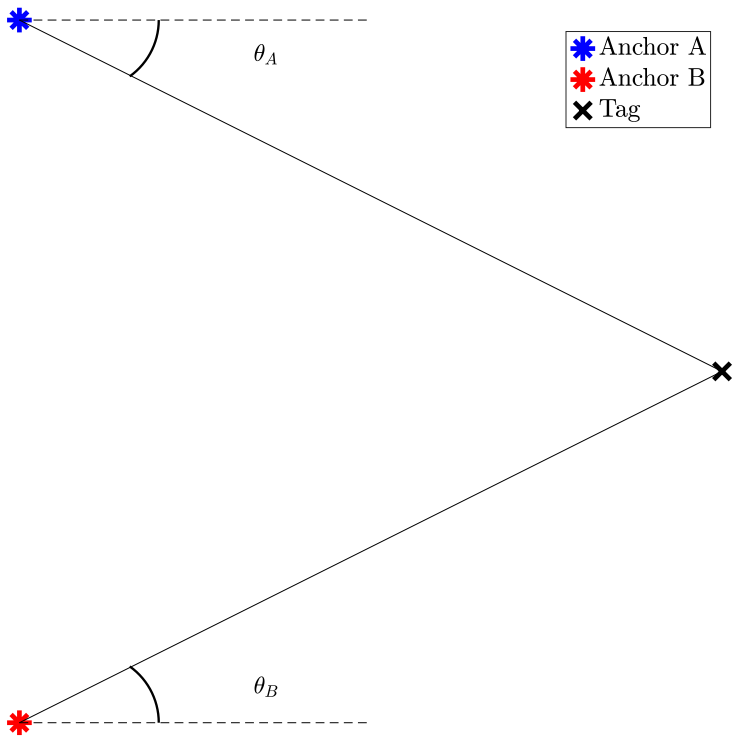

Figure 3.6: AOA. θ_A and θ_B are the angles of arrival.

3.5 Selected Methods

All of the different methods mentioned in this chapter are not implemented in this thesis. AOA is not further investigated because of the need for an antenna array, which is not equipped on the hardware used in this thesis. The method using signal strength to calculate distance is also ignored, since the channel depends on several unknown parameters [5].

The methods that are further studied are TOA and TDOA. In the TOA case, it is specifically the double sided TWR that is used due to its accuracy [1] and asynchronous property. TDOA with wireless synchronization is used, since the hardware limits the wired synchronization option, as mentioned in Section 2.2.

3.6 Scalability

As mentioned in Section 1.3.1, one important property of the system is that it needs to be scalable, i.e., the system must be able track at least the specified amount of tags at the specified update rate. There are different ways of implementing the different methods which affect the update rate. Double sided TWR gets a distance

from each anchor at the time, which leads to

$$N_{tot} = 3N_{anchor}N_{tag} \tag{3.6}$$

where N_{tot} is the total number of messages that are required to be sent until all tags have received distances to all anchors. The term N_{anchor} is the total number of anchors, and N_{tag} is the number of tags in the system. The number of anchors is multiplied by three, because of the number of messages (poll, answer and final) needed for the double sided TWR to obtain a distance. Although, [1] mentions an alternative implementation of the double sided TWR. With this implementation, the tag sends a poll to all anchors simultaneously. Then each anchor answer, one at the time. Lastly, the tag sends one final which is received by all the anchors. The formula for the total number of messages sent until the system has run one cycle is

$$N_{tot} = (N_{anchor} + 2)N_{tag} \tag{3.7}$$

due to the fact that each anchor sends a message for every tag and each tag sends two messages for every update cycle.

With TDOA the number of messages decrease. Only one message is needed to be sent for the system to obtain the time differences, which are used to acquire an estimated position of the tag. Therefore, the total number of messages sent per update cycle will be

$$N_{tot} = N_{tag} \tag{3.8}$$

i.e., it only depends on the number of tags. Although, this is with wired synchronization of the anchors' clocks. With a wireless implementation, which is done in this thesis, more messages are needed to synchronize the anchors' clocks.

3.7 Anchor Setup

A crucial property for an UWB system is the line of sight, i.e., there should not be anything in the way between the tags and anchors which try to communicate. Therefore, there must be enough anchors visible for the tags all the time for the system to work properly without measurement offsets, due to no line of sight. The geometry of the anchor setup can also create faulty estimations, e.g, if the anchors are all aligned there is an uncertainty for where the tag is [19].

For a system using TDOA there is also other aspects that need to be taken to account. According to [17], there are unfavorable zones outside the area defined by the anchors. In these unfavorable zones there may be multiple solutions for the multilateration algorithm, and the correct one might be hard to decide. Therefore, the TDOA system must be able to handle those kind of scenarios.

4

Positioning Algorithms

Depending on what is measured with the sensors, the positioning algorithm is different. For TOA methods, which provides times/distances, trilateration is used. For TDOA methods, which provides time/distance differences, multilateration is used. In this chapter the different algorithms for obtaining a position are described.

4.1 Trilateration

In 2D the distance between an anchor and a tag is calculated by

$$(x - x_i)^2 + (y - y_i)^2 = D_i^2 \tag{4.1}$$

where x and y are the positions of the tag and x_i and y_i denote the position of anchor i. Also, D_i is the measured distance between anchor i and the tag. In the 3D case, (4.1) is extended by a position on the Z-axis. The equation is then

$$(x - x_i)^2 + (y - y_i)^2 + (z - z_i)^2 = D_i^2 \tag{4.2}$$

where z is the tag's position on the Z-axis and z_i the anchor's position on the same axis.

To acquire the position of an object from distances obtained by the TOA methods, trilateration can be done [20]. Trilateration is to position an object with respect to measured distances. In 2D, two distances give two circles which intersect on two different points (if the tag is not exactly between the two anchors, then there is only one point). Therefore, three anchors are needed to obtain the position. Given as

$$\begin{aligned} (x - x_1)^2 + (y - y_1)^2 &= D_1^2 \\ (x - x_2)^2 + (y - y_2)^2 &= D_2^2 \\ (x - x_3)^2 + (y - y_3)^2 &= D_3^2 \end{aligned} , \tag{4.3}$$

where $i \in 1, 2, 3$, from (4.1).

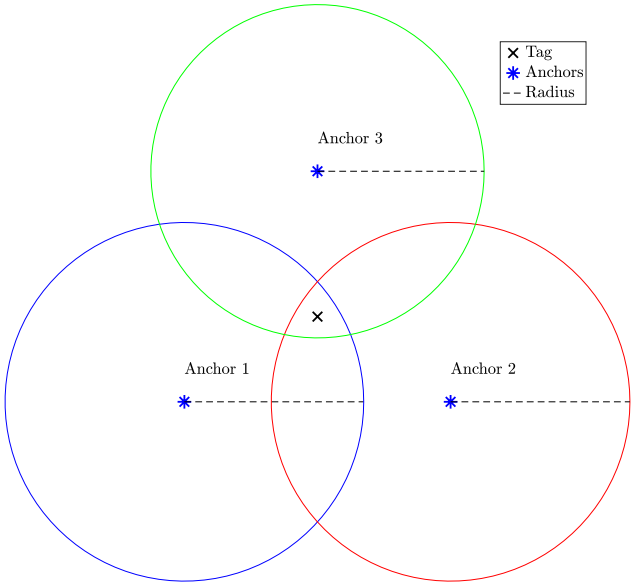

Figure 4.1: Localization problem when all circles do not intersect in one point.

Unfortunately, the sensors are not perfect and therefore not all distances correspond to exactly one point, as seen in Fig. 4.1. To obtain the correct position, i.e., the cross in Fig. 4.1, a linear least square (LLS) problem is solved. In order to solve (4.3) using linearization, one anchor is chosen as a reference anchor which the system is linearized around. In this case anchor $i = 1$ is the reference anchor. This results in the systems of equations, given as

$$\begin{aligned}(x_2 - x_1)x + (y_2 - y_1)y &= D_1^2 - D_2^2 + x_2^2 + y_2^2 - x_1^2 - y_1^2 \\ (x_3 - x_1)x + (y_3 - y_1)y &= D_1^2 - D_3^2 + x_3^2 + y_3^2 - x_1^2 - y_1^2\end{aligned}, \tag{4.4}$$

which in matrix form is

$$A\bar{x} = b \tag{4.5}$$

where

$$A = \begin{bmatrix} x_2 - x_1 & y_2 - y_1 \\ x_3 - x_1 & y_3 - y_1 \end{bmatrix}, \tag{4.6}$$

$$\bar{x} = \begin{bmatrix} x \\ y \end{bmatrix} \tag{4.7}$$

and

$$b = \begin{bmatrix} D_1^2 - D_2^2 + x_2^2 + y_2^2 - x_1^2 - y_1^2 \\ D_1^2 - D_3^2 + x_3^2 + y_3^2 - x_1^2 - y_1^2 \end{bmatrix}. \tag{4.8}$$

When the system is linearized the LLS problem is stated like

$$(A^T A)\bar{x} = A^T b\ . \tag{4.9}$$

The solution $\bar{x}$ is obtained by

$$\bar{x} = (A^T A)^{-1} A^T b \ . \tag{4.10}$$

The solution to the LLS problem is however not that accurate [21], although it can be used as an initial guess. To obtain an even better result, a non-linear programming solver is used. The cost function, J, is

$$J = \left(\sqrt{(\hat{x} - x_1)^2 + (\hat{y} - y_1)^2} - D_1\right)^2 + \left(\sqrt{(\hat{x} - x_2)^2 + (\hat{y} - y_2)^2} - D_2\right)^2 + \\ ... + \left(\sqrt{(\hat{x} - x_N)^2 + (\hat{y} - y_N)^2} - D_N\right)^2 \tag{4.11}$$

and is minimized with regards to $\hat{x}$ and $\hat{y}$ for N anchors. The cost function is designed to punish the difference between the measured distance D_i and the distance to the estimated position, $\sqrt{(\hat{x} - x_i)^2 + (\hat{y} - y_i)^2}$. The initial guess of $\hat{x}$ and $\hat{y}$ in the solver is the solution to the LLS problem, i.e.,

$$\begin{bmatrix} \hat{x} \\ \hat{y} \end{bmatrix} = \bar{x} \ . \tag{4.12}$$

With this iterative solver a more correct estimate of the position can be found.

The trilateration can also be viewed as a filtering problem, see Section 6.3.1.

4.2 Multilateration

There are different multilateration algorithms, some are mentioned in [17]. Even though most of the methods mentioned in [17] are applied on flying aircraft, there are some which are applied on aircraft on the ground. The scenario when an aircraft is on the ground can be compared with the scenario of this thesis. In [17], Fang's method is applied in the 2D case and Bancroft's method is applied in the 3D case to obtain a position. The book by Geyer, [17], also includes solutions by the use of LLS which is better to use when no exact solution can be derived, e.g., when there are noisy measurements.

In the 2D case the tag's position is (x, y). The anchors' positions are (x_i, y_i) for $i = 1, 2, 3$. Anchor 1 is chosen to be the common anchor and is in the origin. For simplicity $y_2 = 0$. Then

$$\begin{aligned} \Delta d_{12} &= \sqrt{(x)^2 + (y)^2} - \sqrt{(x - x_2)^2 + y^2} \\ \Delta d_{13} &= \sqrt{(x)^2 + (y)^2} - \sqrt{(x - x_3)^2 + (y - y_3)^2} \end{aligned} \tag{4.13}$$

where Δd represent the difference in distance between the different anchors. Each equation in (4.13) represent a hyperbola. The solution to this is the intersection of this hyperbolas. After re-arranging and squaring (4.13) becomes

$$x_2 - 2x_2 x - \Delta d_{12}^2 = -2\Delta d_{12}\sqrt{x^2 + y^2} \tag{4.14}$$

$$x_3^2 + y_3^2 - 2x_3x - 2y_3y - \Delta d_{13}^2 = -2\Delta d_{13}\sqrt{x^2 + y^2} \ . \tag{4.15}$$

Dividing (4.14) with (4.15) and re-arranging yields

$$y = Cx + D \tag{4.16}$$

where

$$C = \frac{\Delta d_{13}}{y_3}\frac{x_2}{\Delta d_{12}} - \frac{x_3}{y_3} \tag{4.17}$$

and

$$D = \frac{x_3^2 + y_3^2}{2y_3} - \frac{\Delta d_{13}^2}{2y_3} - \frac{\Delta d_{12}\Delta d_{13}}{2y_3}\left(\left(\frac{x_2}{\Delta d_{12}}\right)^2 - 1\right) \ . \tag{4.18}$$

Now the solution is described with a line, see (4.16). To obtain the location for x and y, an substitute for y in (4.14), is used. After squaring and re-arranging, the substitution yields

$$Ex^2 + Fx + G = 0 \tag{4.19}$$

where

$$E = 1 - \left(\frac{x_2}{\Delta d_{12}}\right)^2 + C^2 \ , \tag{4.20}$$

$$F = 2CD + x_2\left(\left(\frac{x_2}{\Delta d_{12}}\right)^2 - 1\right) \tag{4.21}$$

and

$$G = D^2 - \frac{\Delta d_{12}^2}{4}\left(\left(\frac{x_2}{\Delta d_{12}}\right)^2 - 1\right)^2 \ . \tag{4.22}$$

Now a position is obtainable by solving the quadratic equation which usually yields two candidates to the position on the x-axis. Then substitute those values into (4.16) to find the corresponding value for y. To determine which one is correct, the candidates are substituted into (4.13).

Although, this algebraic solution is hard to implement and is not feasible for all possible values for x and y. Rather, an iterative solver is used to obtain an estimated position, much like the trilateration case.

For the multilateration problem, the same non-linear programming solver is used as for the trilateration problem. However, the cost function is modified due to the differences to obtain measurements. The cost function is now

$$\begin{aligned} J = &\left(\left(\sqrt{(\hat{x} - x_2)^2 + (\hat{y} - y_2)^2} - \sqrt{(\hat{x} - x_1)^2 + (\hat{y} - y_1)^2}\right) - \Delta D_1\right)^2 \\ &+ \left(\left(\sqrt{(\hat{x} - x_3)^2 + (\hat{y} - y_3)^2} - \sqrt{(\hat{x} - x_2)^2 + (\hat{y} - y_2)^2}\right) - \Delta D_2\right)^2 \\ ... &+ \left(\left(\sqrt{(\hat{x} - x_N)^2 + (\hat{y} - y_N)^2} - \sqrt{(\hat{x} - x_{N-1})^2 + (\hat{y} - y_{N-1})^2}\right) - \Delta D_N\right)^2 \end{aligned} \tag{4.23}$$

where ΔD is the measured distance difference and N is the number of distance differences.

The multilateration can also be viewed as a filtering problem, see Section 6.3.2.

5
Filter design

In this chapter basics of Bayesian filtering is explained along with the description of the Kalman filter (KF), the EKF and the CKF.

5.1 Bayesian filtering

Bayesian filtering uses Bayesian statistics [22], in order to estimate a state vector x_k given sensor measurements $y_{1:k} = \{y_0, y_1, ..., y_k\}$ from one or several sensors. This is done by recursively computing the posterior distribution

$$p(x_k|y_{1:k}) \tag{5.1}$$

at time k.

From (5.1) one can see that the distribution is a conditional probability. Therefore it is possible to apply Bays rule, which, in a generic form, results in

$$P(A|B) = \frac{P(B|A)P(A)}{P(B)} \ . \tag{5.2}$$

Another assumption that can be made is the Markov property. In this context the state at time k, x_k, only is conditionally dependent on the state at the previous time step, x_{k-1}. The same property applies for the measurements. This result in

$$p(x_k|x_{k-1}, ..., x_0) = p(x_k|x_{k-1}) \tag{5.3}$$

$$p(_k|x_k, ..., x_0) = p(y_k|x_k) \ . \tag{5.4}$$

When applying these two assumptions together the resulting posterior density can be written as

$$p(x_k|y_{1:k}) = p(x_k|y_k, y_{1:k-1}) = \frac{p(y_k|x_k, y_{1:k-1})p(x_k|y_{1:k-1})}{p(y_k|y_{1:k-1})} = \frac{p(y_k|x_k)p(x_k|y_{1:k-1})}{p(y_k|y_{1:k-1})} \ . \tag{5.5}$$

The result from (5.5) can also be viewed as

$$\text{Posterior} = \frac{\text{Likelihood} \cdot \text{Prior}}{\text{Normalization factor}} \tag{5.6}$$

which is

$$\text{Posterior} \propto \text{Likelihood} \cdot \text{Prior} \ . \tag{5.7}$$

The Bayesian filtering process is divided into different steps to finally estimate the posterior density. The first step is the prediction step which computes the prior by the Chapman-Kolomogorov equation

$$p(x_k|y_{1:k-1}) = \int p(x_k|x_{k-1})p(x_{k-1}|y_{1:k-1})\, dx_{k-1} \ . \tag{5.8}$$

The second step is the update step, which given the measurement y_k, the posterior distribution can be calculated by

$$p(x_k|y_{1:k}) = \frac{1}{Z_k} p(y_k|x_k)p(x_k|y_{1:k-1}) \tag{5.9}$$

where Z_k is the normalization factor from (5.6), and therefore, $p(x_k|y_{1:k})$ can be written as

$$p(x_k|y_{1:k}) \propto p(y_k|x_k)p(x_k|y_{1:k-1}) \ . \tag{5.10}$$

5.2 Kalman filter

One well known filter that utilizes Bayesian filtering is the KF [22]. The KF is applied to models which are linear Gaussian,

$$x_k = A_{k-1}x_{k-1} + q_{k-1} \tag{5.11}$$
$$y_k = H_k x_k + r_k \tag{5.12}$$

where $q_{k-1} \sim \mathcal{N}(0, Q_{k-1})$ is the process noise, $r_k \sim \mathcal{N}(0, R_k,\ A_{k-1})$ is the transition matrix of the motion/process model and H_k is the measurement model matrix.

The KF consists of two steps, the prediction step and the update step. The predicted states, $\hat{x}_{k|k-1}$, and covariance matrix, $P_{k|k-1}$, are calculated by the prediction step as

$$\hat{x}_{k|k-1} = A_{k-1}\hat{x}_{k-1|k-1} \tag{5.13}$$
$$P_{k|k-1} = A_{k-1}P_{k-1|k-1}A_{k-1}^T + Q_{k-1} \ . \tag{5.14}$$

The estimated states, $\hat{x}_{k|k}$, and the estimated covariance matrix, $P_{k|k}$, are calculated by the update step as

$$\hat{x}_{k|k} = x_{k|k-1} + K_k v_k \tag{5.15}$$
$$P_{k|k} = P_{k|k-1} - K_k S_k K_k^T \tag{5.16}$$

where

$$S_k = H_k P_{k|k-1} H_k^T + R_k \tag{5.17}$$
$$v_k = y_k - H_k \hat{x}_{k|k-1} \tag{5.18}$$
$$K_k = P_{k|k-1} H_k^T S_k^{-1} \ . \tag{5.19}$$

The result from the KF is a Gaussian density with the mean $\hat{x}_{k|k}$ and the covariance $P_{k|k}$ at the time k.

Although, the linear KF cannot be used in this thesis, since it cannot handle non-linear models. Therefore, other versions of the KF needs to be reviewed.

5.3 Extended Kalman Filter

Often the process and measurements models are non-linear. In these cases the regular KF is not appropriate. Instead an EKF can be used [22]. The EKF is an extension to the KF for non-linear filtering problems. The EKF uses Taylor series approximations to linearize the non-linearities. The EKF model can be written as

$$\boldsymbol{x_k} = f_{k-1}(x_{k-1}) + q_{k-1} \tag{5.20}$$
$$y_k = h_k(x_k) + r_k \tag{5.21}$$

where x is the state vector, y is the measurements, $f(\cdot)$ is the process dynamics, $h(\cdot)$ is the measurement model, q is the process noise, and r is the measurement noise.

The prediction step for the EKF is

$$\hat{x}_{k|k-1} = f_{k-1}(\hat{x}_{k-1|k-1}) \tag{5.22}$$
$$P_{k|k-1} = F_{k-1}(\hat{x}_{k-1|k-1})P_{k-1|k-1}F_{k-1}^T(\hat{x}_{k-1|k-1}) + Q_{k-1} \tag{5.23}$$

where $F(\cdot)$ is the Jacobian to the process model $f(\cdot)$.

The update step for the EKF is

$$\hat{x}_{k|k} = \hat{x}_{k|k-1} + K_k v_k \tag{5.24}$$
$$P_{k|k} = P_{k|k-1} - K_k S_k K_k^T \tag{5.25}$$
$$v_k = y_k - h(\hat{x}_{k|k-1}) \tag{5.26}$$
$$S_k = H_k(\hat{x}_{k|k-1})P_{k|k-1}H_k^T(\hat{x}_{k|k-1}) + R_k \tag{5.27}$$
$$K_k = P_{k|k-1}H_k^T(\hat{x}_{k|k-1})S_k^{-1} \tag{5.28}$$

where $H(\cdot)$ is the Jacobian to the measurement model $h(\cdot)$.

The benefit with the EKF over other non-linear filters is that it is relatively simple compared to its performance. It is relatively easy to implement as long as the process and measurement model are differentiable. Although, the noise must be Gaussian for the EKF to work properly and it has problems with too extensive non-linearities.

5.4 Cubature Kalman Filter

There are other filters then the EKF that handles non-linearities even better. One of them is the CKF [22]. Basically, it uses sigma points to approximate Gaussian

integrals of the form

$$\int f(x)\mathcal{N}(x;\hat{x},P)\,dx \approx \sum_{i=1}^{N} W^{(i)} f(\mathcal{X}^{(i)}) \tag{5.29}$$

where W are weights and $\mathcal{X}$ are the sigma points.

The first step of the CKF's prediction step, is to form a set containing of $2n$ sigma points, where n is the number of states in the state vector. Then the sigma points are formed like

$$\mathcal{X}_{k-1}^{(i)} = \hat{x}_{k-1|k-1} + \sqrt{n}\left(P_{k-1|k-1}^{\frac{1}{2}}\right)_i, \quad i = 1, ..., n \tag{5.30}$$

$$\mathcal{X}_{k-1}^{(i+1)} = \hat{x}_{k-1|k-1} - \sqrt{n}\left(P_{k-1|k-1}^{\frac{1}{2}}\right)_i, \quad i = 1, ..., n \tag{5.31}$$

where $P_i^{\frac{1}{2}}$ is the i:th column of $P^{\frac{1}{2}}$. The weights are set by

$$W^{(i)} = \frac{1}{2n}, \quad i = 1, ..., 2n\ . \tag{5.32}$$

Then the predicted states and the covaraince matrix are estimated by

$$\hat{x}_{k|k-1} \approx \sum_{i=1}^{2n} f(\mathcal{X}_{k-1}^{(i)}) W_i \tag{5.33}$$

$$P_{k|k-1} \approx Q_{k-1} + \sum_{i=1}^{2n} \left(f(\mathcal{X}_{k-1}^{(i)}) - \hat{x}_{k|k-1}\right)\left(f(\mathcal{X}_{k-1}^{(i)}) - \hat{x}_{k|k-1}\right)^T W_i\ . \tag{5.34}$$

In the update step, a new set of $2n$ sigma points are created and formed as

$$\mathcal{X}_{k-1}^{(i)} = \hat{x}_{k|k-1} + \sqrt{n}\left(P_{k|k-1}^{\frac{1}{2}}\right)_i, \quad i = 1, ..., n \tag{5.35}$$

$$\mathcal{X}_{k-1}^{(i)} = \hat{x}_{k|k-1} - \sqrt{n}\left(P_{k|k-1}^{\frac{1}{2}}\right)_i, \quad i = 1, ..., n \tag{5.36}$$

with the weights

$$W^{(i)} = \frac{1}{2n}, \quad i = 1, ..., 2n\ . \tag{5.37}$$

The estimated states and the covariance matrix are finally obtained by

$$\hat{x}_{k|k} = \hat{x}_{k|k-1} + P_{xy} S_k^{-1}(y_k - \hat{y}_{k|k-1}) \tag{5.38}$$

$$P_{k|k} = P_{k|k-1} - P_{xy} S_k^{-1} P_{xy}^T \tag{5.39}$$

where

$$\hat{y}_{k|k-1} \approx \sum_{i=1}^{2n} h(\mathcal{X}_k^{(i)}) W_i \tag{5.40}$$

$$P_{xy} \approx \sum_{i=1}^{2n} \left(\mathcal{X}_k^{(i)} - \hat{x}_{k|k-1}\right)\left(h(\mathcal{X}_k^{(i)}) - \hat{y}_{k|k-1}\right)^T W_i \tag{5.41}$$

$$S_k \approx R_k + \sum_{i=1}^{2n} \left(h(\mathcal{X}_k^{(i)}) - \hat{y}_{k|k-1}\right)\left(h(\mathcal{X}_k^{(i)}) - \hat{y}_{k|k-1}\right)^T W_i\ . \tag{5.42}$$

6
Concept System

To investigate the feasibility of using UWB for positioning personnel around heavy machinery, a concept/test system is needed. A concept system requires both hardware and software. The utilized hardware is introduced in Section 2.2.2. The methods used in this concept system are introduced in Chapter 3, 4 and 5. In this chapter, the implemented concept system is introduced and described.

6.1 Overview

This concept system is split into two different platforms, both including hardware and software. They are a UWB platform and a computer platform. The UWB platform uses up to 7 sensors. Depending on what localization method used, the constellation of the number of anchors and tags can be different. The anchor setup is further explained in Section 6.5 and Section 6.6. Although, the system only includes one tag, multiple tags can easily be added, which also have been done as a proof of concept. The different platforms each have their own distinct purposes. The UWB platform is responsible for acquiring distance or distance difference data, by utilizing the localization methods described in Chapter 3. The computer platform is responsible for estimating a position from the raw measurements, given by the sensors, using the methods explained in Chapter 4 and Chapter 5. To connect these two platforms, a communication channel is needed. In this concept system, all measurements are available in the wearable tag, and therefore, the tag is connected to the computer platform via a secondary RF link, or USB.

To combine the two platforms into a functioning positioning system, special software are developed. There are three different parts of software needed. On the UWB platform, the microcontroller needs special firmware in order to obtain TWR or TDOA measurements. How this firmware is developed is presented in detail in Section 6.4. On the computer platform, the algorithms described in Chapter 4 and the filters in Chapter 5, are implemented. How this is done is described in Section 6.3. Apart from these algorithms, there is a need for a system to manage incoming UWB data and execute the algorithms. This software is called the positioning framework and is further described in Section 6.2.

A graphical overview of how the system is interconnected is shown in Fig. 6.1. The rest of this section intend to give a short description of the system work flow. Firstly, note that the concept system can operate in two different modes, TWR or TDOA,

which are specified on both platforms. In the TWR mode, the system supports up to 3 tags and 4-6 anchors. In the TDOA mode, the system supports 1 tag and up to 6 anchors. The following description is using TWR mode, TDOA behaves similarly, but using time differences and different algorithms.

To be able to locate a tag, the tags starts sending the TWR messages to each anchor in the system. After each TWR cycle a distance is calculated by the UWB platform. Then, the obtained distances are transferred to a computer through USB or the RF link. On the computer platform, the positioning framework reads the incoming data and forwards it to the positioning algorithms which estimate a position.

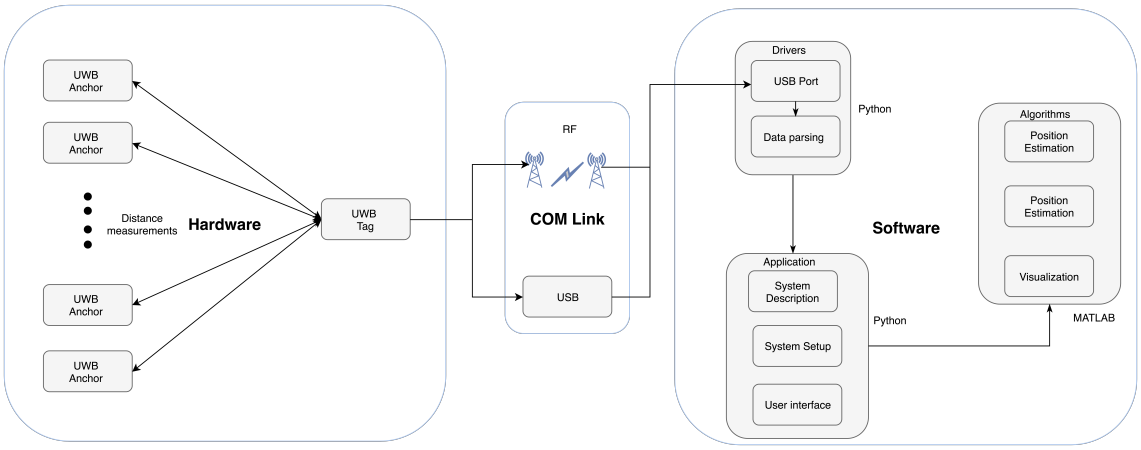

Figure 6.1: Overview of the system architecture.

6.2 Positioning Framework

A part of the concept system is the positioning framework, which is software designed and developed to run on a computer or an embedded platform. As previously stated, its purpose is to connect the UWB hardware to a computer, and execute the position estimation calculations, see Section 6.3, using the methods described in Chapter 3 and Chapter 4. The framework is developed in Python and runs in a command line environment. The framework is built in two layers, in order to make it dynamic and easy to add support for new hardware. A more in depth description of the two layers follows in Section 6.2.1 and Section 6.2.2.

6.2.1 Application Layer

The application layer's purpose is to provide the user with an interface to interact with the system. There is three main features of the application layer, and they are as follows. Firstly, displaying raw sensor data to the user and collecting the data, to make it available for offline analyses and testing. Secondly, executing the positioning algorithms, to obtain a real time position estimation, and displaying this position relative to the anchors. Lastly, the application layer has a set of settings in a configuration file, making it possible to change important settings. These settings

are: anchor position, number of active tags and anchors, plot settings for the real time positioning and which method to connect to the hardware.

6.2.2 Driver Layer

The drivers interact closely with the UWB platform, and are responsible for data collection. This is the part of the system that connects the hardware through USB, or RF, and parsing it to a predetermined format, to make it useful for later processing. Since the UWB platform can interface with a computer in two different ways, there are two different drivers available in the framework. There is also a driver for computer generated measurements for quick prototyping and testing of the framework itself.

6.3 Algorithms Used for Position Estimation

The concept system uses different algorithms for the position estimation. These algorithms are presented in this section. The algorithms are implemented as MATLAB functions which are called by the position framework, through a MATLAB Python API. Some of the algorithms are specific for each of the two modes, TWR and TDOA, while others are used in both modes. The specific ones are the trilateration implementation for TWR, and the multilateration for TDOA. For each mode, position estimates are obtained by a non-linear programming solver as well as with two different filters, see Section 6.3.1 and Section 6.3.2. For every filter there are also two different process models, a constant velocity model and a random walk model. The former uses the states $x = \begin{bmatrix} X & Y & Z & v_x & v_y & v_z \end{bmatrix}^T$, where X is the position on the x-axis, Y is the position on the y-axis, Z the position on the z-axis, v_x the velocity in x, v_y the velocity in y and v_z the velocity in z. The latter uses the states $x = \begin{bmatrix} X & Y & Z \end{bmatrix}^T$. The algorithms that are used for both modes are described in Section 6.3.3 and Section 6.3.4.

6.3.1 Implementation of Trilateration

One of the trilateration methods implemented in this thesis is a non-linear programming solver. It is used to get a representation of the position without filtering. It consists of a cost function which is the same as (4.11) where N is the number of anchors and measurements. The non-linear programming solver used is MATLAB's *fminsearch*. The initial guess to the solver is obtained by the solution of the LLS problem, see (4.10). Also, in the thesis two different filters are used, an EKF and an CKF, for each localization system, and each filter is evaluated with two different process models, a random walk and a constant velocity model.

The filters are an alternative way of implementing trilateration, which include prediction models. If the prediction model is good enough, the filters should not deviate too much even if the measurements would not be satisfying. Also, the filter approach

is an easy way of implementing a system with a varying number of sensors and measurements. For every sensor used in an update cycle, the update step of the filter is recalled with the related measurement.

The first versions of the EKF and CKF used with the TWR mode, use a constant velocity model in the prediction step. The process model for the predicted states is

$$f = \begin{bmatrix} X + t_0 v_x & Y + t_0 v_y & Z + t_0 v_z & v_x & v_y & v_z \end{bmatrix}^T . \tag{6.1}$$

The EKF needs a Jacobian for the process model, which is

$$F = \begin{bmatrix} 1 & 0 & 0 & t_0 & 0 & 0 \\ 0 & 1 & 0 & 0 & t_0 & 0 \\ 0 & 0 & 1 & 0 & 0 & t_0 \\ 0 & 0 & 0 & 1 & 0 & 0 \\ 0 & 0 & 0 & 0 & 1 & 0 \\ 0 & 0 & 0 & 0 & 0 & 1 \end{bmatrix} . \tag{6.2}$$

The second version of the filters use a random walk model instead of a constant velocity model. The process model for the prediction step is

$$f = \begin{bmatrix} X + \Delta_x \\ Y + \Delta_y \\ Z + \Delta_z \end{bmatrix} \tag{6.3}$$

where $\Delta_{x,y,z}$ are random values which represent motion in a direction.
The Jacobian for the EKF is formed as

$$F = \begin{bmatrix} 1 & 0 & 0 \\ 0 & 1 & 0 \\ 0 & 0 & 1 \end{bmatrix} . \tag{6.4}$$

In the update step, the distance measurements from the UWB sensors are compared with the predicted measurement from the measurement model. The measurement model is the same for the different versions of filters since the different process models only affect the prediction step. The measurement model for the distance is

$$h = \sqrt{(X - x_i)^2 + (Y - y_i)^2 + (Z - z_i)^2} \tag{6.5}$$

where (X, Y, Z) are the predicted position of the tag and (x_i, y_i, z_i) are the position of the anchor i. The EKF also needs a Jacobian for the measurement model and it is

$$H = \begin{bmatrix} \frac{X - x_i}{\sqrt{(X-x_i)^2+(Y-y_i)^2+(Z-z_i)^2}} \\ \frac{Y - y_i}{\sqrt{(X-x_i)^2+(Y-y_i)^2+(Z-z_i)^2}} \\ \frac{Z - z_i}{\sqrt{(X-x_i)^2+(Y-y_i)^2+(Z-z_i)^2}} \\ 0 \\ 0 \\ 0 \end{bmatrix}^T . \tag{6.6}$$

The tuning of the filters' Q and R matrices is done by trial and error.

6.3.2 Implementation of Multilateration

Much like the trilateration case, an estimate is obtained by non-linear programming solver. The cost function for the multilateration case is on the same form as (4.23). The solver used is MATLAB's *fminsearch*. As in the trilateration case, position estimations are also obtained by the use of filters. The filter implementation of the multilateration is done by the use of an EKF and a CKF. It is done in the same way as the trilateration described in Section 6.3.1 with some slight differences which is described in this section.

The prediction steps for the different EKFs and CKFs in the TDOA mode are the same as their counterparts in the TWR mode. The process model for the filters with a constant velocity model is (6.1), and the EKF has the Jacobian (6.2). The process model for the filters with a random walk model is (6.3), and the EKF has the Jacobian (6.4).

The measurement model however, differs from the model in Section 6.3.1. Due to that the measurements are distance differences instead of distances, the model needs to be different. The measurement model becomes

$$h = \sqrt{(X - x_{i+1})^2 + (Y - y_{i+1})^2 + (Z - z_{i+1})^2} - \sqrt{(X - x_i)^2 + (Y - y_i)^2 + (Z - z_i)^2}\,. \tag{6.7}$$

For the EKF the Jacobian becomes

$$H = \begin{bmatrix} \frac{X-x_{i+1}}{\sqrt{(X-x_{i+1})^2+(Y-y_{i+1})^2+(Z-z_{i+1})^2}} - \frac{X-x_i}{\sqrt{(X-x_i)^2+(Y-y_i)^2+(Z-z_i)^2}} \\ \frac{Y-y_{i+1}}{\sqrt{(X-x_{i+1})^2+(Y-y_{i+1})^2+(Z-z_{i+1})^2}} - \frac{Y-y_i}{\sqrt{(X-x_i)^2+(Y-y_i)^2+(Z-z_i)^2}} \\ \frac{Z-z_{i+1}}{\sqrt{(X-x_{i+1})^2+(Y-y_{i+1})^2+(Z-z_{i+1})^2}} - \frac{Z-z_i}{\sqrt{(X-x_i)^2+(Y-y_i)^2+(Z-z_i)^2}} \\ 0 \\ 0 \\ 0 \end{bmatrix}^T . \tag{6.8}$$

The tuning of the filters' Q and R matrices is done by trial and error.

6.3.3 Anchor Selector

Since the suggested anchor setup on the excavator, see Section 6.6, does not allow the tag to have line of sight to every anchor all the time. Hence, the anchors which do not have line of sight should be excluded from the calculations. Therefore, a selector needs to be implemented to the system. This selector is heuristic by dividing the area around the excavator into different zones. For TWR, when the tag's predicted position is in a specific zone, 4 decided anchors are chosen with their respective measurements. For TDOA, there are instead 4 decided anchor pairs which are chosen. In Fig. 6.2 it is seen how the zones are assigned.

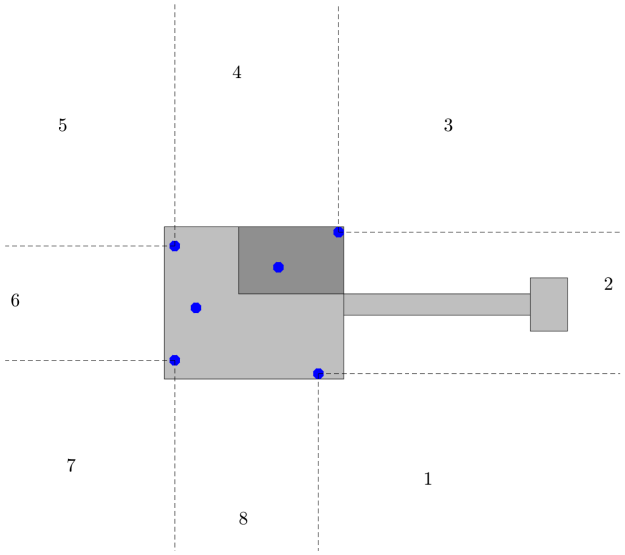

Figure 6.2: Illustration of how the zones from the anchor selector are assigned. Every number marks a different zone.

6.3.4 Outlier Rejector

To avoid outliers that may appear, e.g., if there is no line of sight, an outlier rejector is implemented. For the TWR system the distance between the current state and the anchor is compared with the measurement. If the comparison is greater than a threshold the measurement is rejected and the update step is not performed for the specific measurement. The outlier rejector for the TDOA system works similarly as the one for TWR but the comparison is with distance differences instead.

6.4 Firmware

To implement different localization methods, tweak the sensors performance and implement scheduling algorithms, the firmware in the UWB platform is modified. The main differences are changed settings for the DW1000. The settings are: communication speed of 6800 kbps, the use of channel 5, preamble length of 2048, preamble code 9 and the maximum transmission power. The transmission power is set to maximum to provide the best possible measurements at the maximum distance. Due to the absence of a spectrometer that measures frequencies over 6 GHz, it is unknown if the transmissions is within regulations.

The UWB platform includes open source implementations of TWR and TDOA. To save development time, the implementation of localization methods is based on these open source implementations. Due to this, the more compact double-sided TWR is not implemented, nor ATDOA.

6.4.1 Implementation of Two Way Ranging

The TWR implementation is done as explained in Section 3.1.2, but with one extra report message. It also includes a scheduling protocol.

When only one tag is present in the system, there is no need to consider how and when the messages are transmitted, as there is no other devices to interfere. When there are two or more tags, multiple tags might try to transmit at once. Since all devices uses the same channel, air, the messages have a large chance to interfere with each other. Therefore, to build a positioning system that can support multiple tags, a scheduling scheme is required.

When using the TWR mode, one tag has to send multiple messages to each anchor separately. When analyzing the test system, one can measure the time required to send a message and the time required for a full TWR cycle of one anchor. With the stated DW1000 settings, one complete cycle uses approximately 3 ms. During the machine test, there are six anchors in the system. The suggested scheduling scheme is seen in Fig. 6.3 and Fig. 6.4.

Fig. 6.3 visualizes the timings of a complete TWR sequence of 6 anchors using one tag. The time is divided into 6 slots, one for each anchor, which is 5 ms long. Each slot starts with a poll to one anchor. Then, there is time for the polled anchor to respond, if it receives the poll. If the anchor responds, the time between the slots is used to send and receive the messages required for TWR. If there is no response form the anchor, nothing is sent until the poll for the next anchor. With this setup, the total time for a position estimation update, using 6 anchors and one tag, is 30 ms.

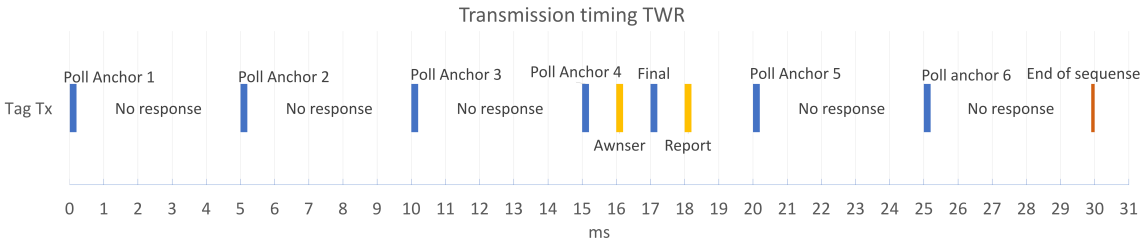

Figure 6.3: Illustration of how the TWR message scheme is designed.

With the TWR transmission scheme suggested in Fig. 6.3, a corresponding schedule is purposed in Fig. 6.4. A method using 3 tags to obtain an update rate of 10 Hz is derived. As each round of TWR cycles for one tag uses 30 ms, it is possible for 3 tags to obtain distances to all anchors within a window of 100 ms. However, this is different from the objective stated in Section 1.3.1, since the development kit only

includes 7 sensors and the concept system requires at least 4 anchors. Therefore, 10 Hz is used to maximize the update rate for the available tags.

Therefore, the tags need to be synchronized to not overlap each other. In the thesis the following method for synchronization is used. The tag with the lowest ID, in this case tag 1, acts as a master, and executes its TWR cycles in a period of 100 ms. Tag 2 do not have a periodic scheduling. Instead, it listens to the master's transmissions and when the master poll the last anchor, tag 2 starts its TWR cycle. After it is done it switches back to listen to the master. Tag 3 acts similar to tag 2, but instead of listening to tag 1, it listens to tag 2.

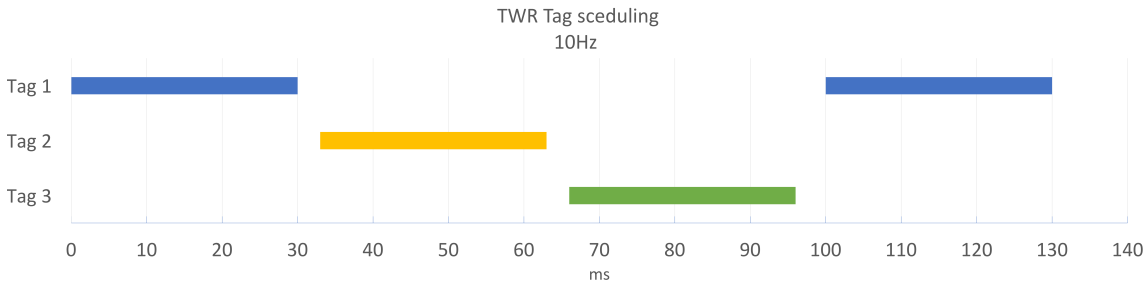

Figure 6.4: Illustration of the TWR message scheme. It shows how the scheme is designed to avoid interference.

6.4.2 Implementation of Time Difference of Arrival

The implementation to obtain TDOA measurements is different from what is described in Section 3.2. Due to the fact that the DWM1000 does not allow an external clock to synchronize the clocks of the DW1000. This implementation synchronize the anchor clocks wirelessly. Synchronization messages is sent and therefore use some of the available transmission time. The time is divided into 6 slots, one for every anchor and every time slot is 2 ms. In these time slots, the anchors sends their synchronization messages. In slot 1, anchor A_1 sends its message, in slot 2, anchor A_2 sends its message and so on. Also in this implementation, the tags do not need to send a message for localization. Instead the tags listens to the synchronization messages for localization. Because of this, there is a possibility of using another type of communication for reporting the time-difference measurements, in order to free up channel usage.

The synchronization algorithm used infers limitations. The distance differences can only be obtained between two anchors in consecutive order. Thus, the first measurement is obtained from the difference between anchor A_i and A_{i+1}, the second measurement is acquired from anchors A_{i+1} and A_{i+2} and so on where $i = 1, ..., 6$ in the system. The sixth measurement is the difference between anchors A_6 and A_1.

6.5 Anchor Setup for Indoor Testing

The indoor testing is conducted in a small sports hall, which is an open area without any visible obstacles. Due to the restricted area there are two different anchor setups to utilize as much of the hall as possible, for different tests. The first setup is presented in Table 6.1 and the second setup is presented in Table 6.2. The first setup has its origin in the rear left corner of the sports hall, to acquire as long distances as possible. In the first setup the anchors are faced forward in the hall's direction. The second setup is placed in the middle of the hall to allow testing around the setup. In the second setup the anchors are faced outwards to simulate that they are mounted on an excavator.

	x	y
A_1	-1500	1500
A_2	1500	-1500
A_3	1500	1500
A_4	-1500	1500

Table 6.1: The anchors' positions for the first anchor setup. The origin is located in the rear left corner of the sports hall.

	x	y
A_1	3400	6350
A_2	8400	6350
A_3	8400	10350
A_4	3400	10350

Table 6.2: The anchors' positions for the second anchor setup. The origin is located in the center of the sports hall.

6.6 Anchor Setup on Excavator

The anchor setup on the excavator is, as mentioned in Section 3.7, an important part of the system. The objective is to have line of sight to at least 4 anchors everywhere around the excavator. A restriction for the test system in this thesis is that there are only 6 available anchors, which may interfere with the line of sight objective. Both the TWR and TDOA system use the same anchor setup in the tests on the excavator. The positions of the anchors are presented in Table 6.3. The origin is in a point below anchor 6, A_6, which is in front right corner of the machine, 1400 mm above the ground.

	x	y	z	Description
A_1	-750	2000	2180	On top of the cabin
A_2	380	2660	1700	Front left
A_3	-2700	2400	1400	Rear left
A_4	-2700	250	1400	Rear right
A_5	-2300	1240	1640	Rear center
A_6	0	0	1070	Front right

Table 6.3: The anchors' positions on the excavator. The unit is mm. $z = 0$ is 1400 mm over the ground.

7

Test Results

In this chapter, the test results of the concept system from Chapter 6, are presented. These tests are conducted indoors and outdoors, for the TWR and TDOA modes. Computer simulations are also included in this chapter.

7.1 Sensor Characterization

To get an initial understanding for how the measurements from the UWB-sensors behave, static indoor-testing is performed using TWR to obtain distances and TDOA to obtain distance differences. A graphical representation of the testing setup can be seen in Fig. 7.1, the first anchor setup is used, Table 6.1. The results of the tests can be seen in Appendix A, for TWR, and Appendix B, for TDOA. In Appendix A the measurements have a deviation of approximately ±150 mm and a bias of approximately −300 mm. The bias is most likely due to sensor delays which are not correctly compensated for in the firmware. Although, the bias can easily be compensated for by adding the offset to the measurement in the positioning framework. The distance differences have a deviation of approximately ±150 mm, see Appendix B. There are some bias but it does not appear to be consistent. Instead, it appears to depend on the anchor pair and the position of the tag.

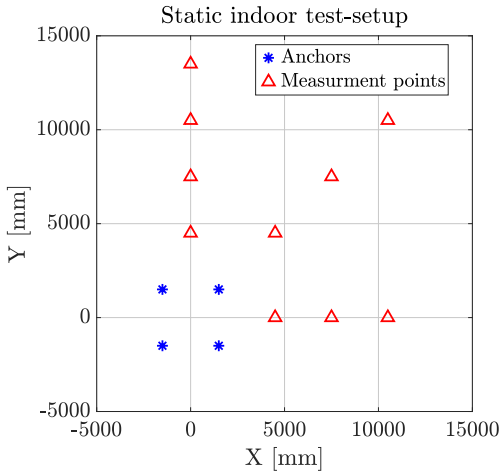

Figure 7.1: Illustration of the anchor setup with the position of measurement points.

7.2 Accuracy for Two Way Ranging

To determine the accuracy of the concept system, using TWR mode, several tests are conducted and the results evaluated. The accuracy of the system is affected by two main sources. The accuracy of the sensors and external disturbances are the main contributing factors to the overall accuracy. There also exists a secondary factor, which is the trilateration technique used to estimate the position. To evaluate all factors the following tests are conducted. Computer simulations of static test cases, static test with real hardware and lastly dynamic test with real hardware.

7.2.1 Simulations

To analyze how trilateration algorithms and anchor placement affect the accuracy of a TWR system, simulation is used in order to study the affect of the algorithms in an ideal environment. The simulation is done by using the same positioning algorithms as in the concept system, with the exception of simulated distance data and anchor positions. Therefore, the output will be the same as the real system if provided with white noise distance data.

The case tested in these simulations are stationary measurements. To do this, an evenly spaced grid of measurement points are generated. At each point the true distance to each anchor is calculated, and white noise is added. Afterwards, a position estimation of the noisy distances is calculated. This process is then repeated 200 times at each point. This produce a group of measurements which spread out in the XY-plane and approximate a probability density function of a position estimation at the specific point.

As described in Section 6.3.1, for trilaterating a position using TWR measurements, two different approaches are evaluated. Although, simulations are performed using only the non-linear programming solver.

The simulations are presented in two different types of plots. To get an overview how the position error propagates over a large area at a high resolution, a three dimensional surface plot is used. To study what shape the position estimates form, a scatter plot is used. Three different scenarios are simulated using the non-linear solver. The first scenario is a square anchor placement, like the anchor setup in Table 6.1, and the result of this is shown in a scatter plot, Fig. 7.2, and surface plot, Fig. 7.3. The second scenario have a slightly asymmetrical anchor placement, but still resembles a square. The result of this case is shown in Fig. 7.4. In the last scenario, the anchors are aligned in the Y-axis. The result of this case is shown in Fig. 7.5.

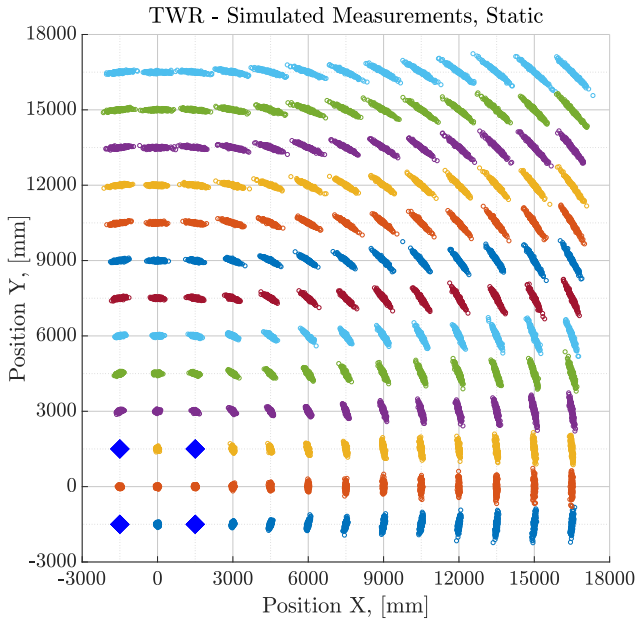

Figure 7.2: Simulation of position estimation using a non-linear programming solver with anchors placed in a square formation.

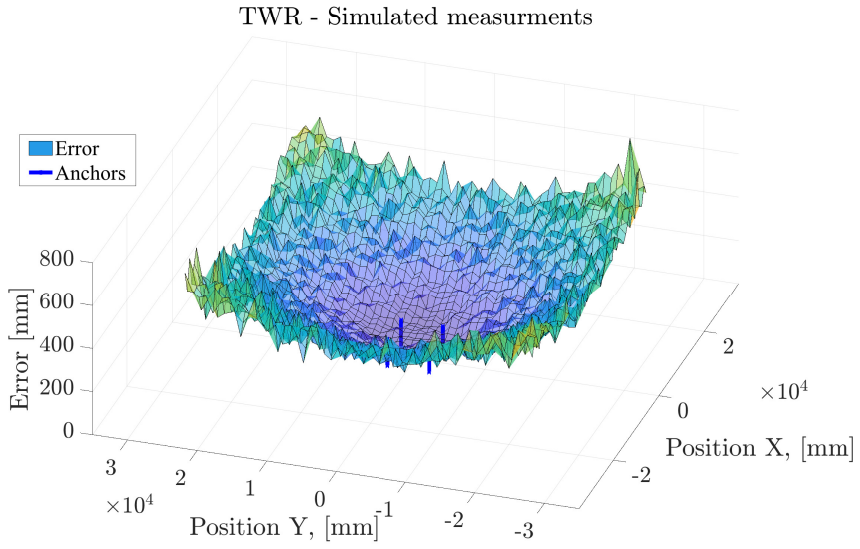

Figure 7.3: Simulation of position estimation using non-linear programming solver with anchors placed in a square formation. Measurements position in X- and Y-axis, mean square of the standard deviation in Z-axis.

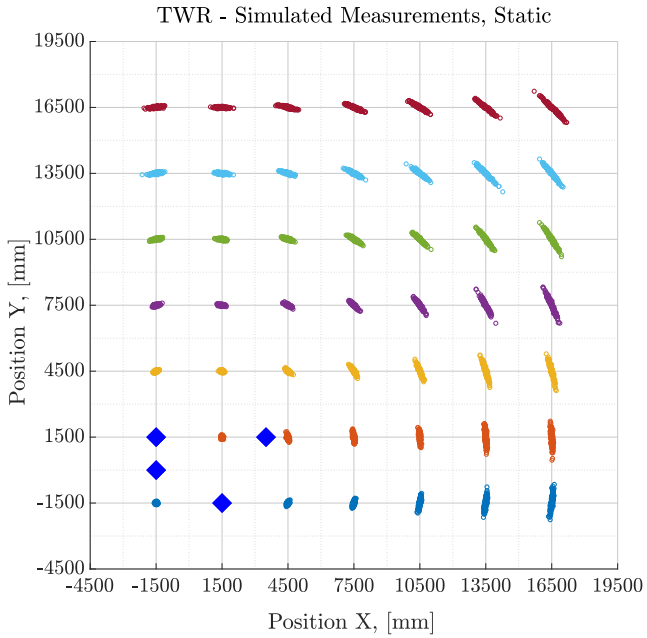

Figure 7.4: Simulation of position estimation using a non-linear programming solver, with anchors placed in a slightly asymmetrical square formation.

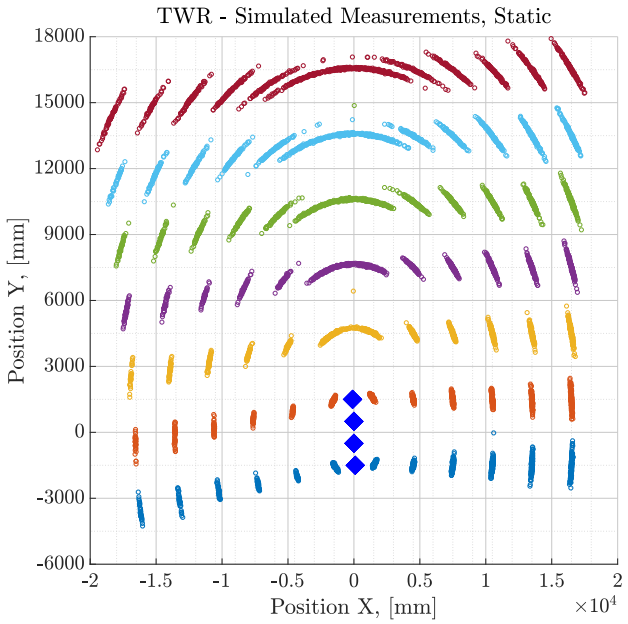

Figure 7.5: Simulation of position estimation using a non-linear programming solver, with anchors aligned.

As seen in Fig. 7.2, the approximated probability density of the position grows as the distance from the anchors center increases. This is due to the fact that, with a larger distance from the center, the relative distance between the anchors

decreases, and eventually appears to originate from the same point. Because of this, the circles produced around the anchors when trilaterating, coincide in a larger region. Due to this, a small variation in distance may contribute to a large shift in position. A graphical representation of this behaviour can be viewed in Appendix C. This phenomena exhibits a predictable behaviour and when comparing Fig. 7.2, which have a symmetrical anchor placement, with Fig. 7.4, one can see that anchor placement dose not affect the precision greatly. This is true as long as the anchors are not aligned with one and another. In that case the accuracy decrease significantly in and around the same line as the anchors are placed. This is shown in Fig. 7.5, where the anchors have been placed almost aligned. In Fig. 7.5, the propagation is increased, and some measurements from the same point are divided on both sides of the anchor line.

7.2.2 Indoor Tests

The indoor testing is done to obtain understandings of how the concept system works, as well as collecting data for comparison and tuning. The indoor testing utilize two different anchor setups which are described in Section 6.5.

7.2.2.1 Static

The computer simulations give a good insight in how the position error propagates in the XY-plane, but this only shows the behaviour in ideal conditions. Therefore, to acquire a greater understanding of how the sensors behave in a real world situation, the same test cases shown in Fig. 7.2 and 7.3, are replicated using the concept system. During the static tests, the first anchor setup, Table 6.1, is used and all distance measurements are used to estimate the position.

A difficulty when performing real world test is to accurately measure and place the correct test points. As this test intends to show the noise at different positions around the anchors, the absolute positions are not as important as when measuring an actual distance between two points. Therefore the measurements do not align to the intended points perfectly. The result of these tests is shown in Fig. 7.6 using the non-linear programming solver.

As suggested by the simulation results in Section 7.2.1, the position error should be distributed evenly around the anchor center at a given distance. In these tests, Fig. 7.6, it is seen that for the trilateration algorithm the position estimations are subjected to very large disturbance at certain points. At other points, at the same distance from the anchor centers, the position estimations appear to follow the disturbance characteristics given by the simulation. To ensure that this disturbances were not due to human errors, several extra measurements on the same test points where performed with the same results. This concludes that this is due to interference created by the environment and/or multipathing, and that the real world measurements resembles the simulation.

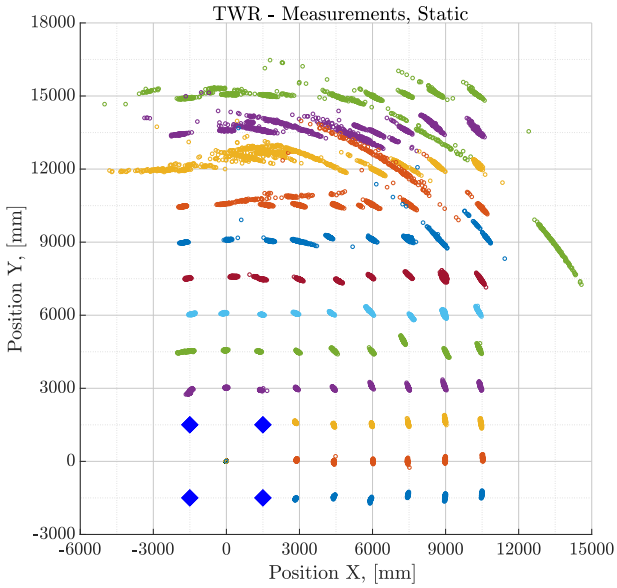

Figure 7.6: Measurements of position estimation using the non-linear solver with anchors placed in a square formation.

7.2.2.2 Dynamic

The real world application of this system is to track people. Hence, dynamic test are necessary, and therefore conducted indoors. To make the most use of the available area three different test cases are designed and evaluated. The dynamic tests are performed with either the first anchor setup, Table 6.1, or the second setup, Table 6.2. During the test all of the distance measurements to all of the four anchors where used to estimate a position.

Case one uses the first anchor setup, Table 6.1. The case starts at anchor A_4 and ends at anchor A_2. This path utilizes all available space, and therefore the tag is adjacent to the wall, which might have introduced disturbances. The tag moves along this rectangular path at as close to constant velocity as possible. The result of this test is seen Fig. 7.7.

Fig. 7.7 displays the result of test case one. It is seen that there is a large amount of interference in the upper right corner of the path. If this point is correlated with the stationary test, Fig. 7.6, it is apparent that this disturbance is present in both tests. This further strengthen the hypotheses that there is an environmental inflicted disturbance source. Further, by only using the position estimation from a non-linear programming solver provides a very good position estimation when there is no disturbance present. But, when there is disturbance, the position becomes rough and jerky. Using an EKF or a CKF drastically smoothed out the position estimates, and also provide good position estimates in a no disturbance situation. When disturbance is present, the position estimate using an EKF or a CKF, is not affected as much as only using an iterative method.

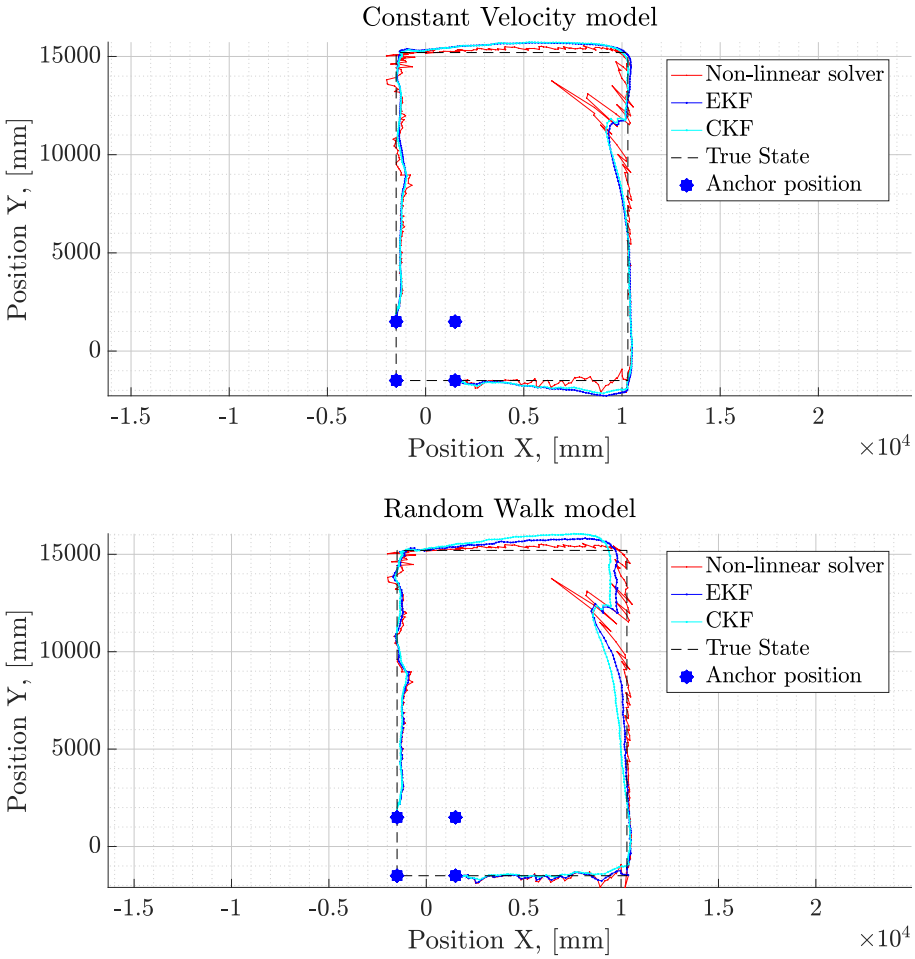

Figure 7.7: Plot of dynamic test case one, position estimation using EKF, CKF and non-linear solver. The filters are using a constant velocity model and a random walk model.

Case two uses the second anchor setup, Table 6.2, which accommodates a complete pass around the anchor setup. Once again the path is walked in close to constant velocity and distance measurements are collected. The result is seen in Fig. 7.8.

In Fig. 7.8 the results of test case two are displayed. It is seen that there is no large amount of disturbance, and therefore all of the positioning methods produce a good position estimate. As with test case one, the EKF and CKF produce a smother trajectory. At a distance of 12 m the position estimate is accurate to roughly 20 cm. Overall, the the random walk model is the highest performer, using of both filters.

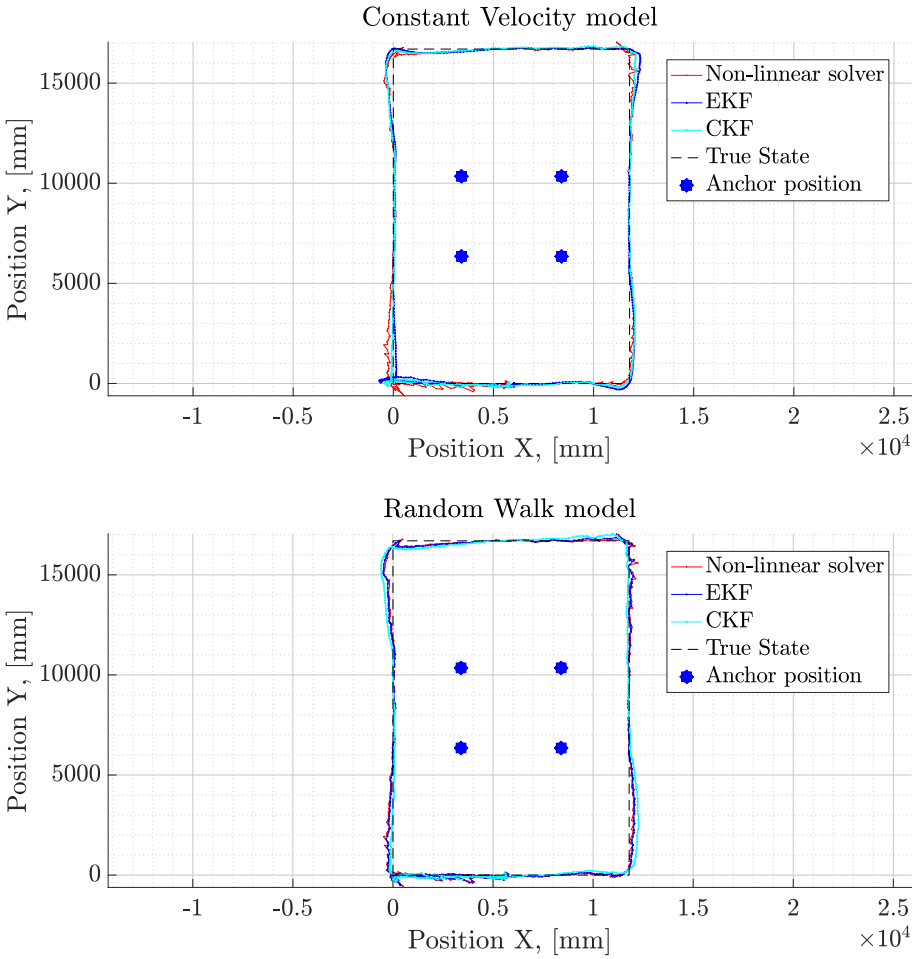

Figure 7.8: Plot of dynamic test case two, position estimation using EKF, CKF and non-linear solver. The filters are using a constant velocity model and a random walk model.

The third test uses the first anchor setup, Table 6.1. In this test case, the tag moves in a pattern which is similar to an "8", with straight edges. This pattern is used to study the behaviour of the system during several sudden directions changes. Once again the tag where moved at constant velocity. The result is seen in Fig. 7.9.

In Fig. 7.9, the result of test case three is shown. As with test case one, there are large disturbances present in some part of the path. If this regions are cross checked with the stationary test, it is seen that the disturbances exists in both tests, see Fig. 7.6, except from the region around $(4000, 7000)$. Here the non-linear programming solver approach suffer significantly from the disturbance, but during low noise conditions outperforms the CKF and EKF regarding accuracy. The filters suffers from a slight drift, from the true state, which is unfavorable. This is a trade off for having a straighter trajectory and more resistance to noise. Overall, the UWB system is capable to capture the more complex movement pattern. As in test case two, the CKF with random walk model is the highest performing filter.

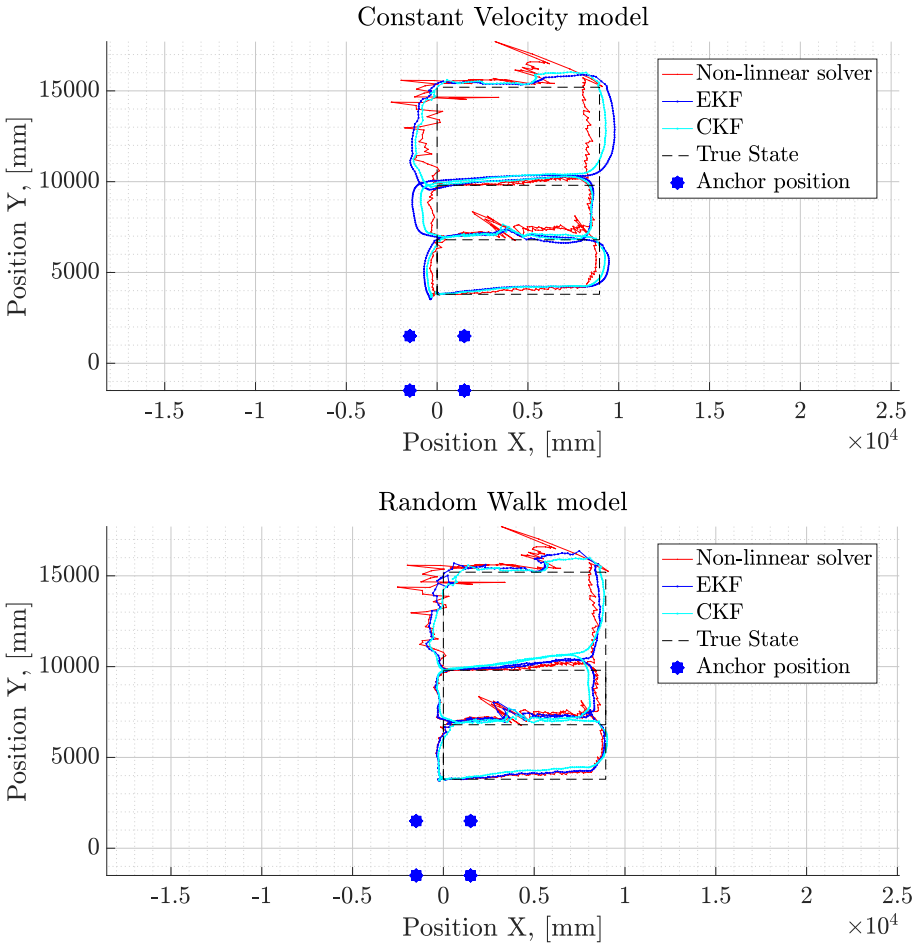

Figure 7.9: Plot of dynamic test case three, position estimation using EKF, CKF and non-linear solver. The filters are using a constant velocity model and random walk model.

7.2.3 Machine Tests

In order to evaluate the concept system in a real setting, extensive outdoor testing is performed. This is done using a real excavator. The anchors are mounted on the machine as described in Section 6.6. Using this setup, dynamic and static tests are performed. The machine is placed at a remote location with good visibility around the machine, except for vegetation. The outcome of these tests are presented in this section. During all test scenarios, the outlier rejector and the anchor selector are in use.

7.2.3.1 Static

A series of static test cases is conducted with the system, mounted on a real machine. Due to the geometry of the machine and the terrain of the test site, not as many static test points where evaluated as in the inside test. Instead of using an evenly distributed grid of points, nine well selected test points is used. The points selected are three points on each side of the machine, excluding the front, and at

three distances, 3 m, 5 m and 11 m away. These points where selected in order to get an overview of how the position error behaves on critical points around the machine. These points can be viewed in Fig. 7.10.

As seen in Fig. 7.10, the result resembles the indoor test well, and there is no apparent region that produces more or less disturbances. Although, the positions where the measurements are done do not seem to align in all cases. This is presumably due to the human factor. The filters perform almost as well as the non-linear solver in terms of accuracy, but create a different shape. This is probably due to the process model that restricts movement. As in previous test, the random walk CKF is the highest performer.

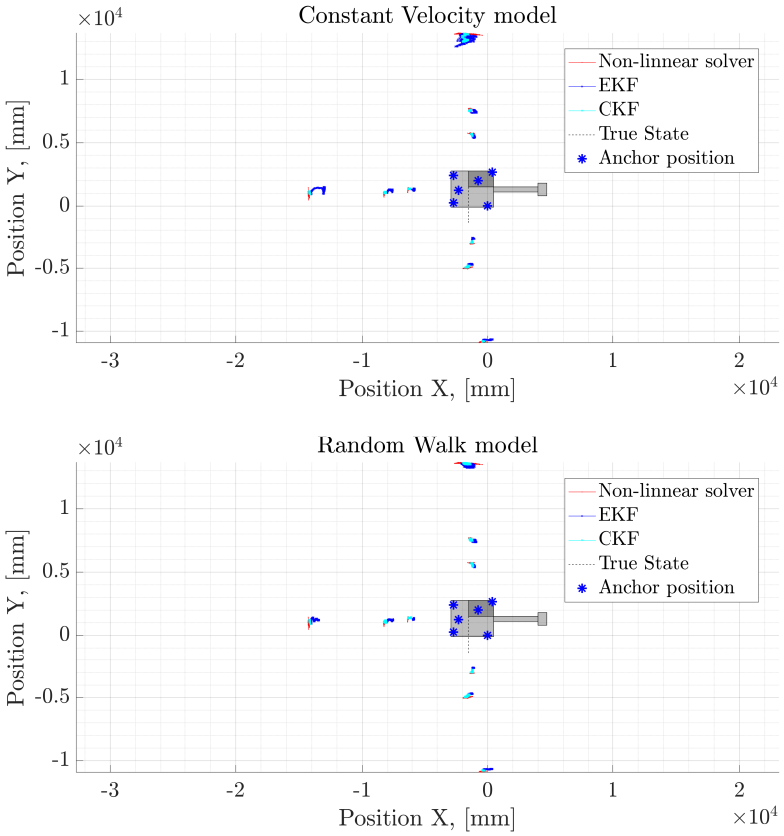

Figure 7.10: Plot of the static tests on a real machine, position estimation using EKF, CKF and non-linear solver. The filters are using a constant velocity model and random walk model.

7.2.3.2 Dynamic

To simulate the real application as close as possible, dynamic tests, using the system mounted on a machine, have been conducted. Nine different dynamic test cases have been evaluated in order to properly evaluate the system accuracy performance in an realistic environment. Six of the test cases are similar to the static cases, where the tag is moved in a circular pattern with its center in the mid right side, the mid back and the front left side (position of anchor A_2), with the radius of 5 m and 11 m. The results are displayed in Fig. 7.11-7.13.

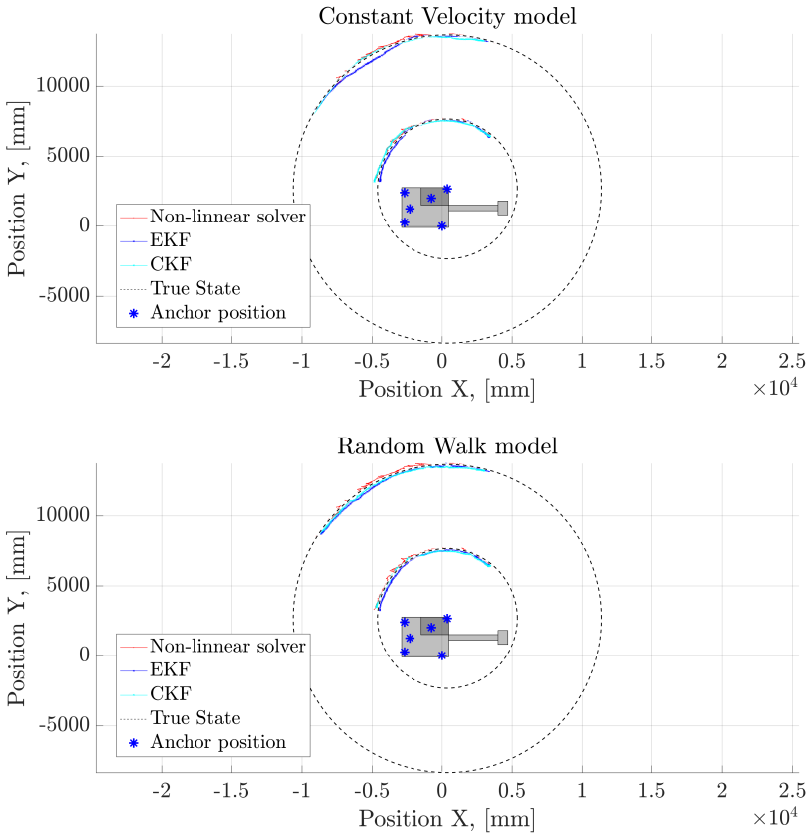

Figure 7.11: Plot of dynamic tests on a real machine, tag moving in circular trajectory at 5 and 11 m away from the machine, on its left side. Position estimation using EKF, CKF and non-linear solver. The filters are using a constant velocity model and a random walk model.

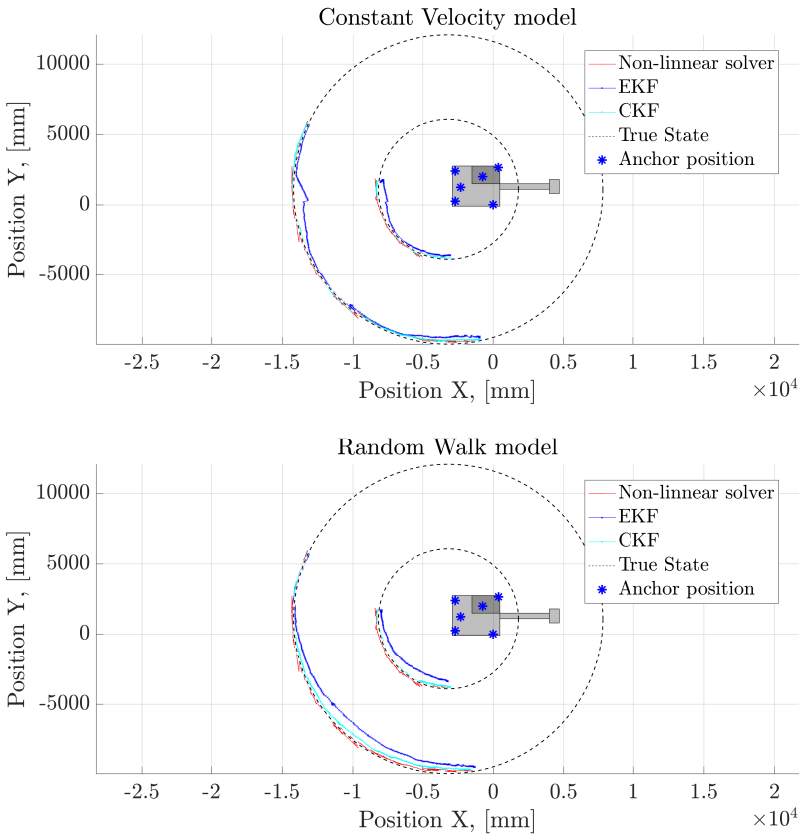

Figure 7.12: Plot of dynamic tests on a real machine, tag moving in circular trajectory at 5 and 11 m away from the machine, behind it. Position estimation using EKF, CKF and non-linear solver. The filters are using a constant velocity model and a random walk model.

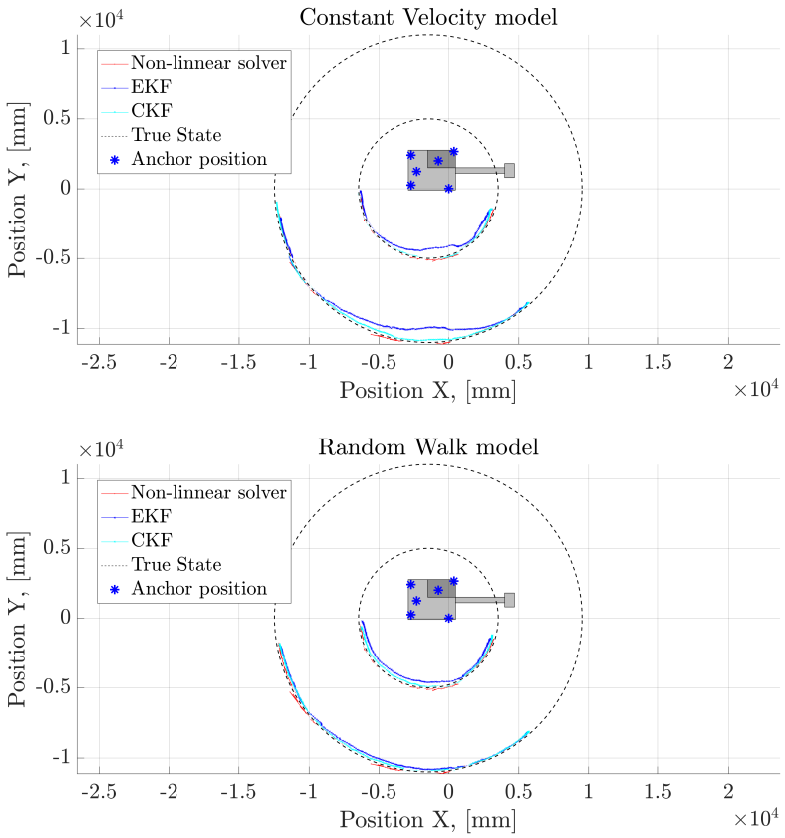

Figure 7.13: Plot of dynamic tests on a real machine, tag moving in circular trajectory at 5 and 11 m away from the machine, on its right side. Position estimation using EKF, CKF and non-linear solver. The filters are using a constant velocity model and a random walk model.

As seen in Fig. 7.11-7.13, the non-linear solver as well as the filters follows the true state closely. The filter produces a smother trajectory. Overall the filter provides a desirable result, but the EKF provides a few false position changes, which is not present in the CKF. Regarding the process model, both produce a similar result.

Apart from this six initial tests, three more extensive tests are preformed. The seventh test is a large path around the machine. This test is designed to be able to evaluate if the system is able to track a person moving around the machine at a fairly large distance. This test case can be seen in Fig. 7.14. The eighth test is performed by moving the tag in a long straight line past the machine. This is in order to evaluate how the concept system performs when people are walking by, and also to evaluate how long effective range the TWR mode has. The result is seen in Fig. 7.15. In the ninth scenario the tag is stationary but the excavator is rotating back and forth, with short stops in between. This is done in order to evaluate how the system behaves when the machine is moving. The result is seen in Fig. 7.16.

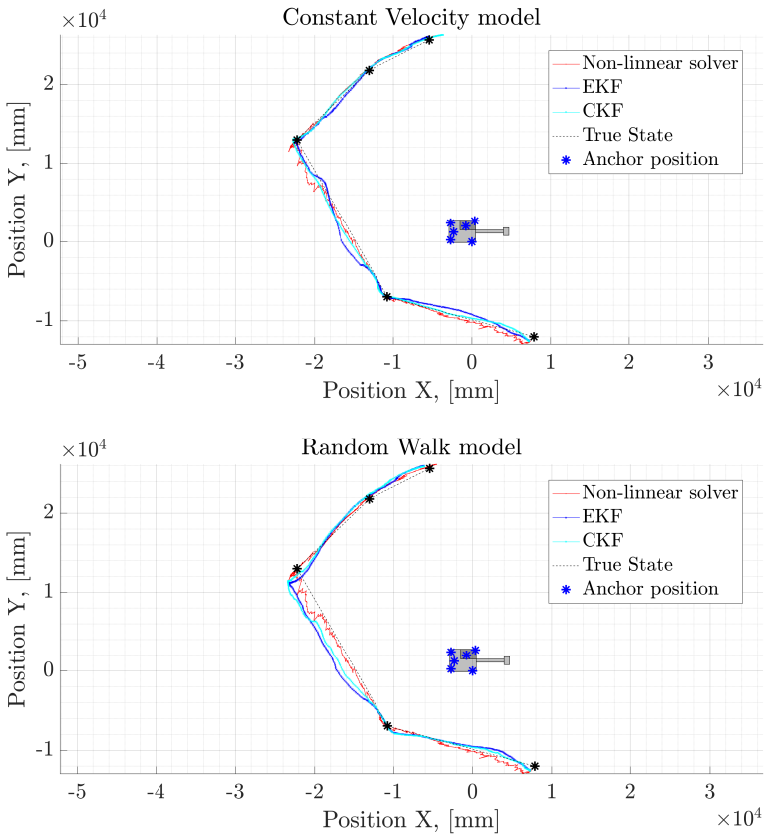

Figure 7.14: Plot of dynamic tests on a real machine. The tag is moving from the bottom of the plot and upwards. Position estimation using EKF, CKF and non-linear solver. The filters are using a constant velocity model and a random walk model.

The results seen in Fig. 7.14 differs depending on the process model, as well as which filter type is used. The CKF is the best filter, but the different models are better or worse on different parts of the path.

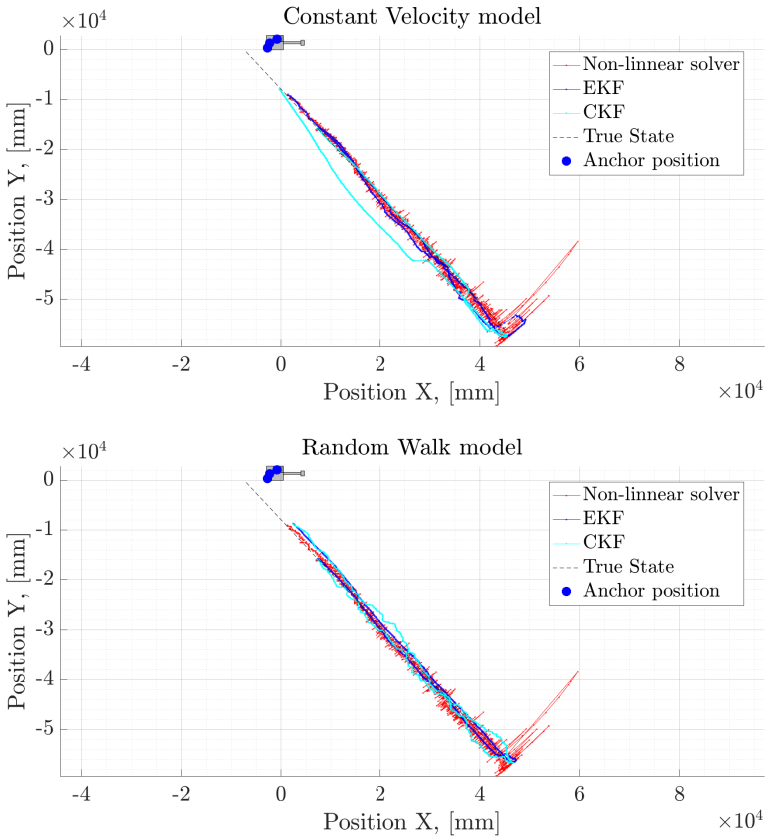

Figure 7.15: Plot of dynamic tests on a real machine. The tag is moving far away from the machine to test the range. Position estimation using EKF, CKF and non-linear solver. The filters are using a constant velocity model and a random walk mode.

As seen in Fig. 7.15, the system is able to track a moving person over a large distance. All methods of positioning works adequately, but the filters produce a smoother trajectory. The measurements start to deviate in a circular pattern as the distance increase, as predicted in the simulations, Fig 7.2. In this test the EKF is the highest performer, the random walk and constant velocity model perform equally except for the turn at the end of the path. The CKF with constant velocity is the worst performer.

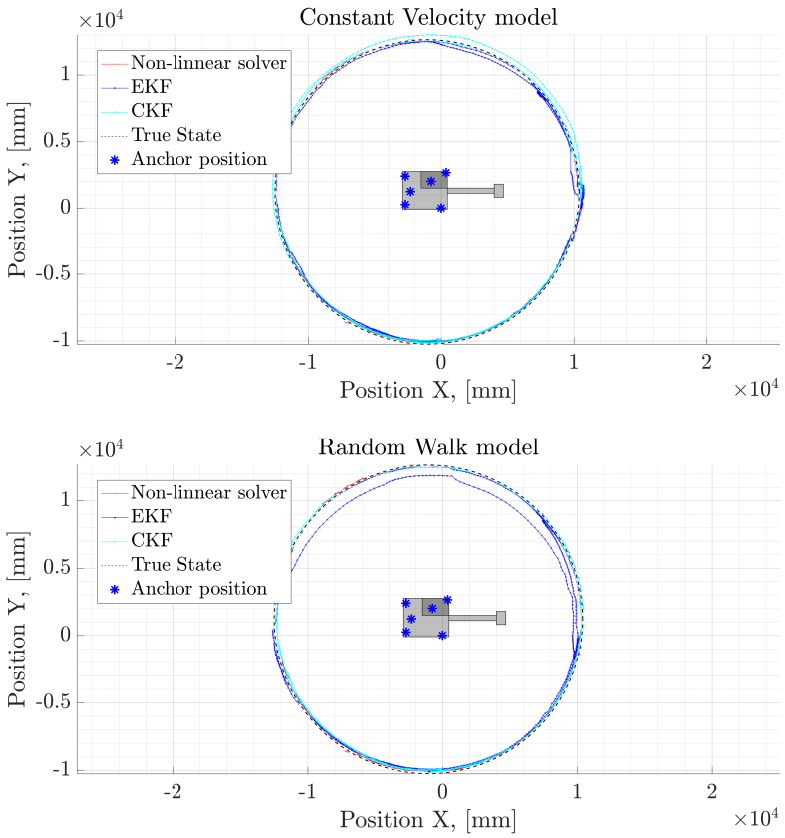

Figure 7.16: Plot of dynamic tests on a real machine. The tag is stationary while the machine is rotating. Position estimation using EKF, CKF and non-linear solver. The filters are using a constant velocity model and a random walk model.

From Fig. 7.16 it is seen that the measurements create an even circle, since it can be compared with the tag moving around the machine. The filters is able to capture the movement well, with some minor difficulties when the machine is changing direction, especially with the constant velocity model. The EKF using random walk gives a few wrong position estimations, while the CKF using random walk captures the movement perfectly.

7.3 Accuracy for Time Difference of Arrival

The approach of testing and evaluating is the same for TDOA as it is for TWR, see Section 7.2. As discussed in Section 7.2, there exist several sources of inaccuracies for the estimations. This section presents the results of computer simulations, indoor testing and outdoor testing. There are differences from the TWR testing. For a TDOA system the approach of using an iterative non-linear solver does not yield a fair result. As seen in Appendix C, a small deviation of the distance differences, results in large deviation in position, when minimizing the cost function (4.23). This error is many magnitudes larger that the filters, and therefore this method will not be presented further in this section.

7.3.1 Simulations

For TWR, the inaccuracy is easily understandable and distributes in circles around the anchor setup's center. In a TDOA system, hyperbolas is created and their expansion in the XY-plan is harder to visualize. Hence, computer simulation is not only good for acquiring a rough estimate of how the error behaves. It is also an important tool for selecting a proper anchor placement. The simulations for the TDOA system are performed in the same manor as the TWR cases described in Section 7.2.1. Fig. 7.17-7.21 show the error for different anchor placements.

As it is harder to visualize how the error will propagate in a TDOA system, the first simulation in Fig. 7.17 is of an triangle anchor setup. This is done to verify the unfavorable zones mentioned in Section 3.7, which appears depending on the geometry of the anchor setup.

To be able to compare the accuracy of a TDOA system against a TWR system the same test cases are simulated using a TDOA system, Fig. 7.21. To accompany this test case further, tests on a larger distances are conducted and are shown in Fig. 7.19-7.20.

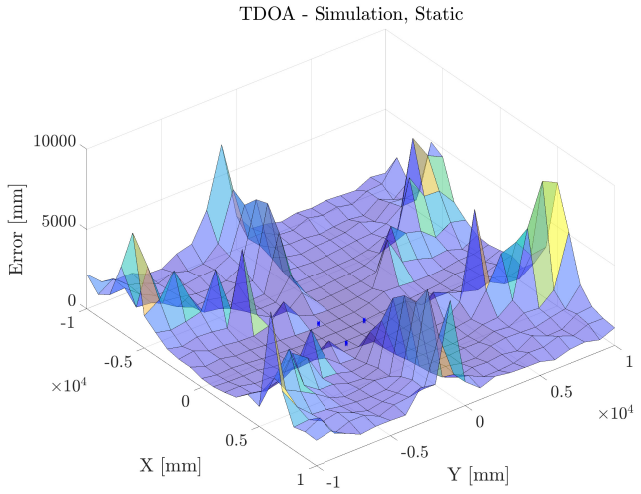

Figure 7.17: Simulation of position estimation using EKF with anchors placed as a triangle. Measurements position in X-axis and Y-axis, mean square of the standard deviation in Z-axis.

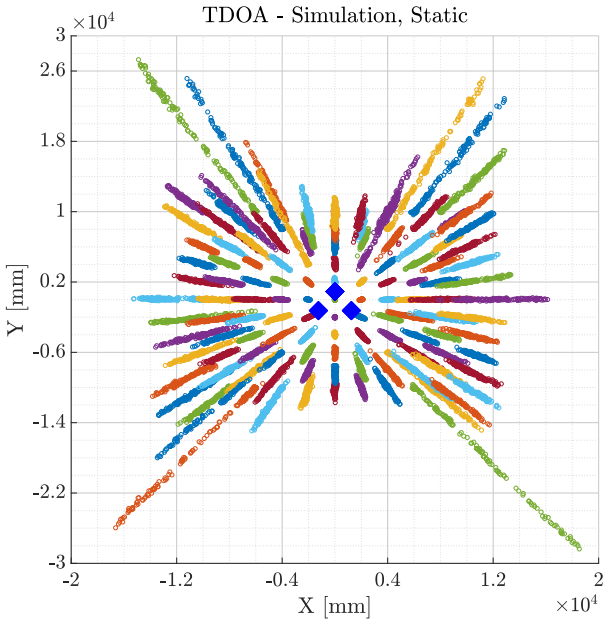

Figure 7.18: Scatter plot of a simulation using TDOA with an EKF. The anchors are placed as a triangle. The points are position estimates. Points with the same color, close to each other originate from the same true state.

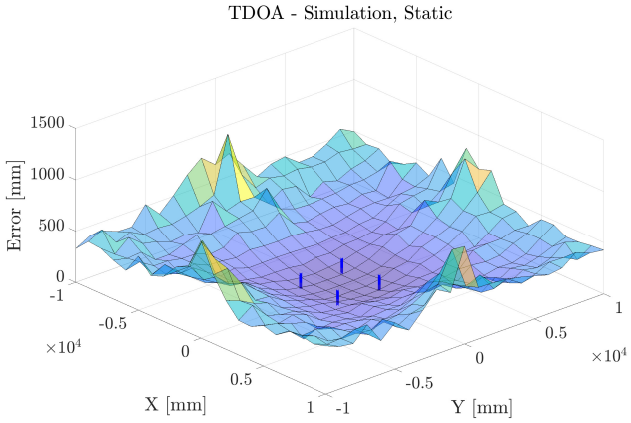

Figure 7.19: Simulation of position estimation using EKF with anchors placed as a cube. Measurements position in X-axis and Y-axis, mean square of the standard deviation in Z-axis.

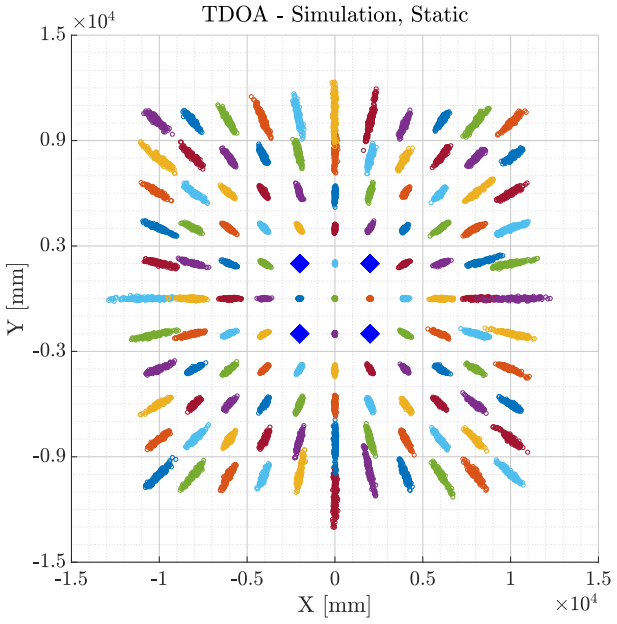

Figure 7.20: Scatter plot of a simulation using TDOA with an EKF. The anchors are placed as a cube. The points are position estimates. Points with the same color, close to each other originate from the same true state.

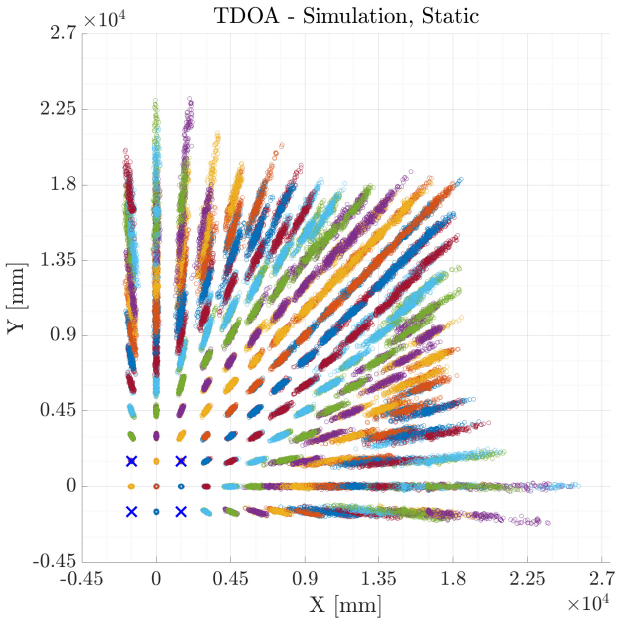

Figure 7.21: Scatter plot of a simulation using TDOA with an EKF. The anchors are placed as a cube. The points are position estimates. Points with the same color, close to each other originate from the same true state. This simulation represents the setup used for the indoor testing.

As seen in Fig.7.17-7.21, the error of a TDOA based system does not propagate in a circular pattern around the anchor centers. Instead they form asymptotes, which coincide to a imaginary line drawn from the anchor centers to the true position. This phenomena is due to the hyperbolas coinciding in long lines. The area of coinciding hyperbolas are larger and also appear at a closer distance than the circles coinciding in a TWR system, Fig. 7.2. This behaviour can further be seen in Appendix C. Due to this behaviour the accuracy of a TDOA based system will deteriorate faster and at a shorter range than a TWR based system.

In Fig. 7.17 and Fig. 7.18, it is seen that estimations on the extended baselines of the triangle, that the anchor setup defines, are more dispersed than the rest of the points. On these lines the hyperbolas, created from the baseline anchor pair, create a long line of possible positions. Therefore, a large area where it is equally probable that the tag is located is created. Hence, even with an ideal noise free environment, it is hard to accurately position the tag. If noise is added, the position estimates deviates more in this area, and make it impossible to estimate the tag's position.

In Fig. 7.19 and Fig. 7.20, it is seen when two anchor pairs provide the same distance differences, the ones mirrored around the X- and Y-axis, generates worse results. This behaviour is due to the hyperbolas coinciding. Therefore, small disturbances result in greater diversities than around the rest of the anchor setup.

Fig. 7.21 shows the same scenario as the indoor testing. The same behaviour as in

Fig. 7.20, is present in Fig. 7.21 as well.

7.3.2 Indoor Tests

The indoor testing for the TDOA system is conducted in the same way as the TWR testing, Section 7.2.2. There are two different anchor setups, see Table 6.1 and Table 6.2.

7.3.2.1 Static

The results of the static tests, using the EKF are seen in Fig. 7.22.

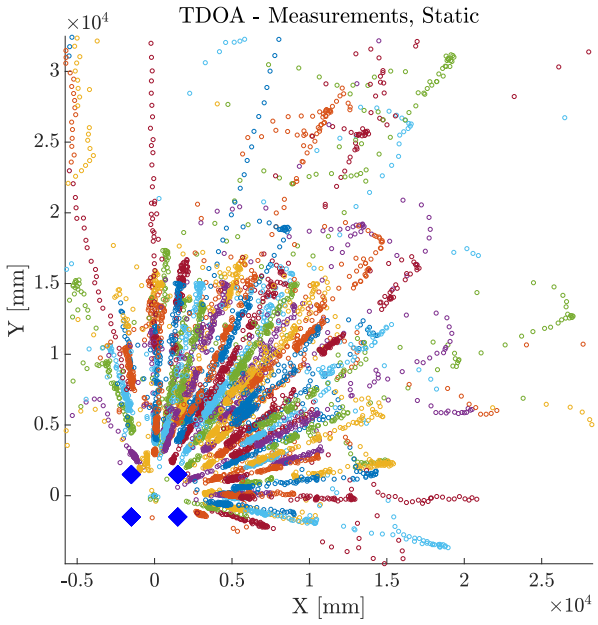

Figure 7.22: Position estimates for the static indoor testing. The estimations are obtained by the use of the EKF. Points close to each other with the same color share the same true state. Remark that this plot is zoomed in, there are estimates that are further away.

In Fig. 7.22 it is seen that the real behaviour of the static tests are similar to the simulations. Although, the results are worse. The estimated positions are scattered over a significantly larger area then in the simulations. This is due to more noise. For distances larger than 5 m, the deviations of the estimations are too large to accurately determine the position.

7.3.2.2 Dynamic

The dynamic indoor test cases are the same as the dynamic indoor testing for the TWR system, see Section 7.2.2.2, except the third case is not performed. The results are seen in Fig. 7.23 and Fig. 7.24.

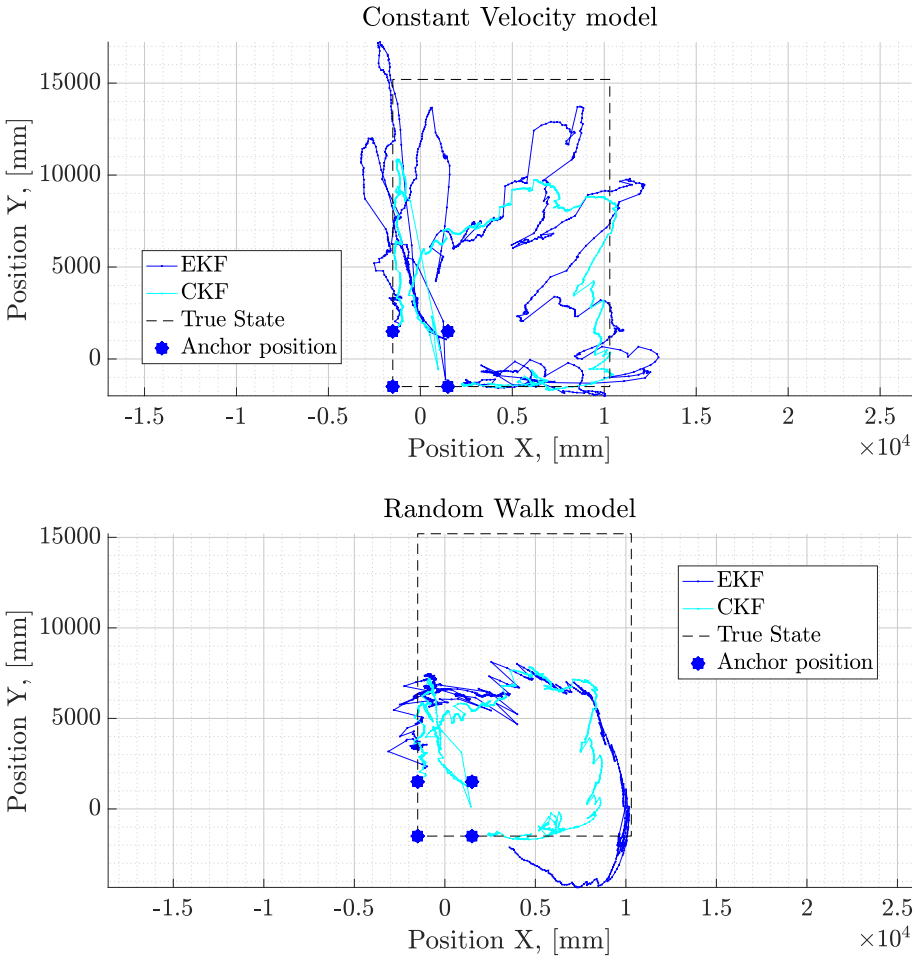

Figure 7.23: Plot of dynamic tests, tag moving along trajectory one. Position estimation using EKF and CKF. The filters are using a constant velocity model and a random walk model.

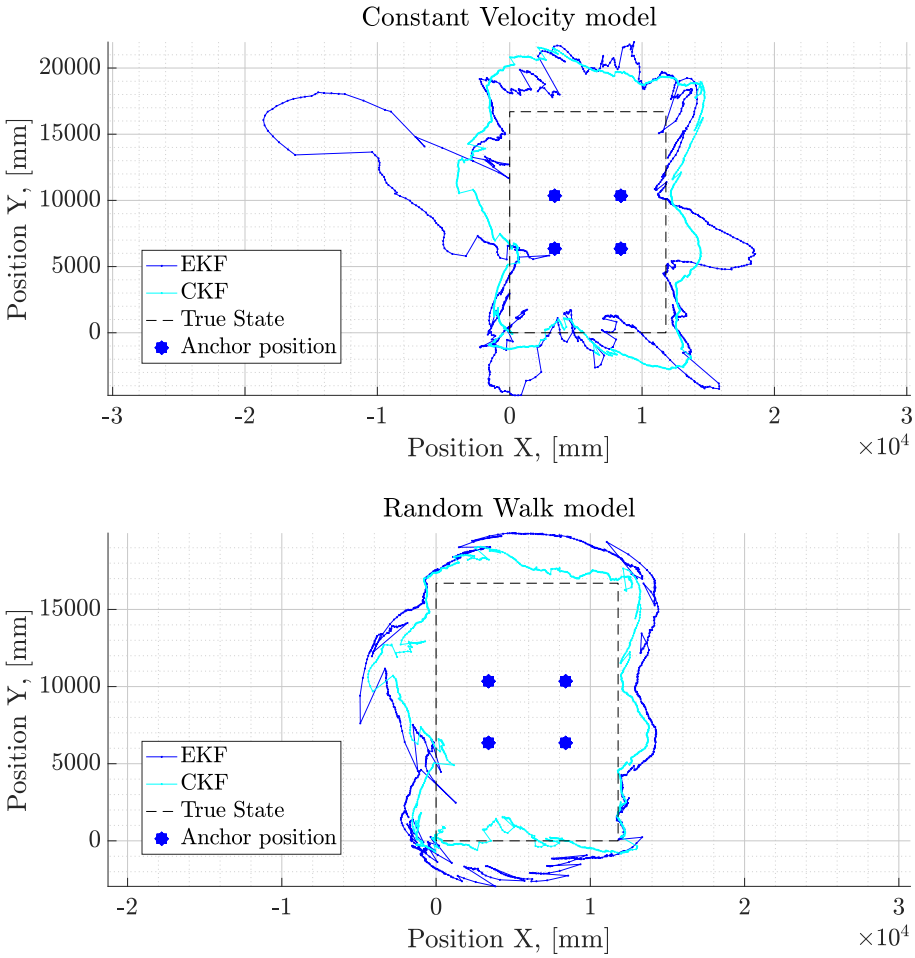

Figure 7.24: Plot of dynamic tests, tag moving along trajectory two. Position estimation using EKF and CKF. The filters are using a constant velocity model and a random walk model.

In Fig. 7.23 the result of case one is displayed. The filters are able to track the position, but only to a distance of roughly 5-6 m. After this point, the measurements become too noisy, as mentioned in Section 7.3.2.1. Therefore, the TDOA system is not capable of tracking a person in this case.

In Fig. 7.24, the result of test case two can be seen. As this test is conducted closer to the anchors, both filters are able to estimate the position adequately, and therefore, TDOA is a viable solution for localization at this distance. Although, the EKF with constant velocity model drifts away for some parts. The CKF does not have the same behaviour for either of the process models, and follows the true state satisfactorily.

7.3.3 Machine Tests

The machine tests are conducted in the same way for the TDOA system as for the TWR system, see Section 7.2.3. The anchor setup is also the same, see Table 6.3.

7.3.3.1 Static

The results of the static tests are seen in Fig. 7.25.

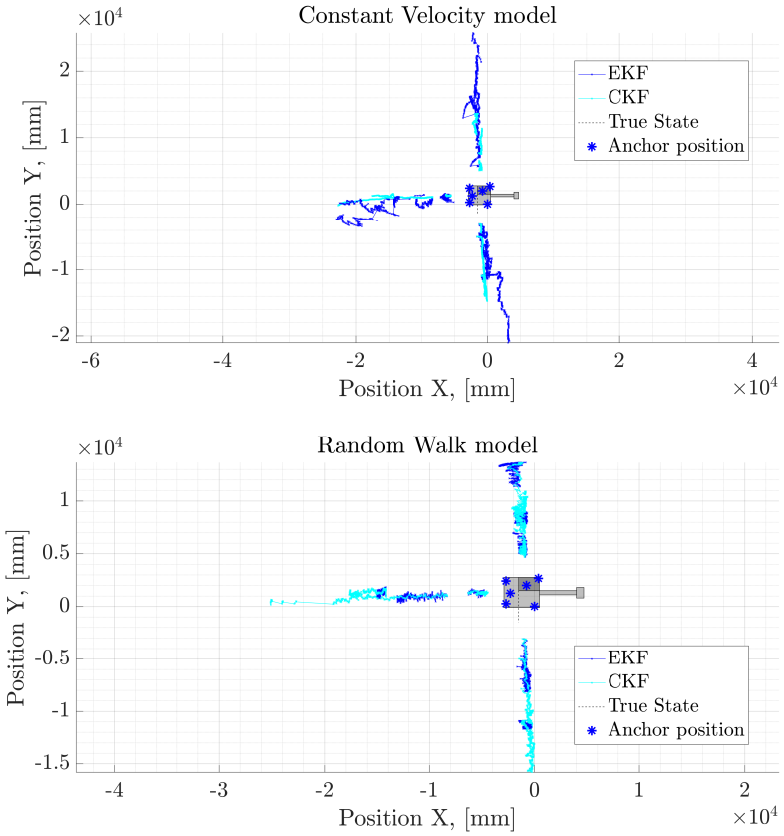

Figure 7.25: Plot of static tests on a real machine. Position estimation using EKF and CKF. The filters are using a constant velocity model and a random walk model.

In Fig. 7.25, it is seen that the direction of the estimations are correct, but the there are diversities in the range. The behaviour is similar to the behavior for the simulations and the indoor tests.

7.3.3.2 Dynamic

The dynamic tests for the TDOA system are done in the same way as for the TWR system, except the case when the excavator is rotating. The results for the cases when the tag moves in circular paths are seen in Fig. 7.26, the case when the tag is moving in a path around the excavator is seen in Fig. 7.27, and the case when the tag is moving away from the excavator is seen in Fig. 7.28. The rest of the test results are seen in Appendix D.

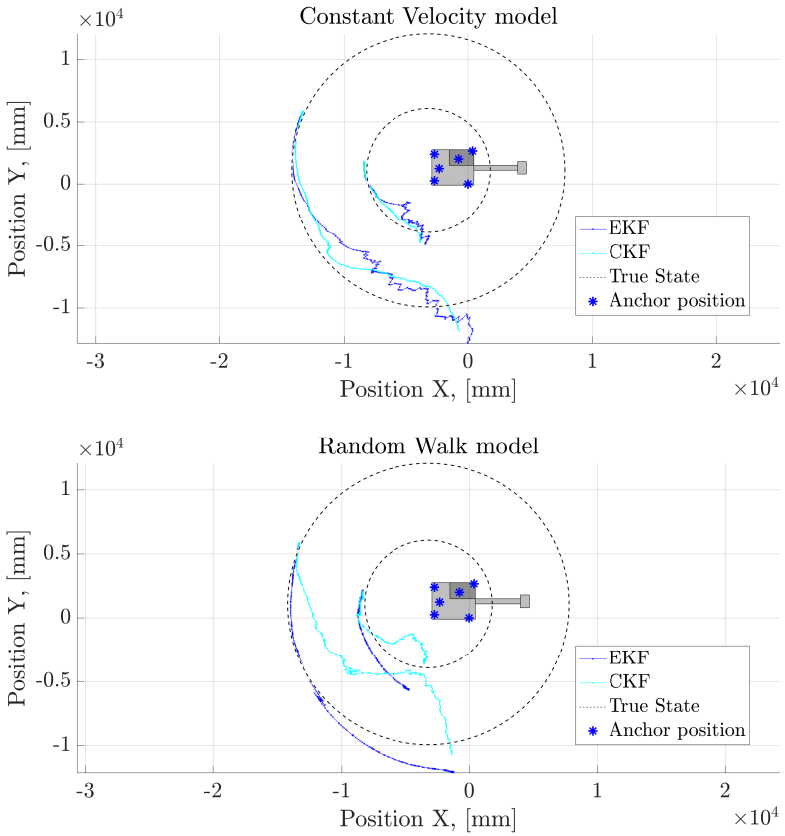

Figure 7.26: Plot of dynamic tests on a real machine. The tag is moving in circular trajectory at 5 m and 11 m away from machine, behind it. Position estimation using EKF and CKF. The filters are using a constant velocity model and a random walk model.

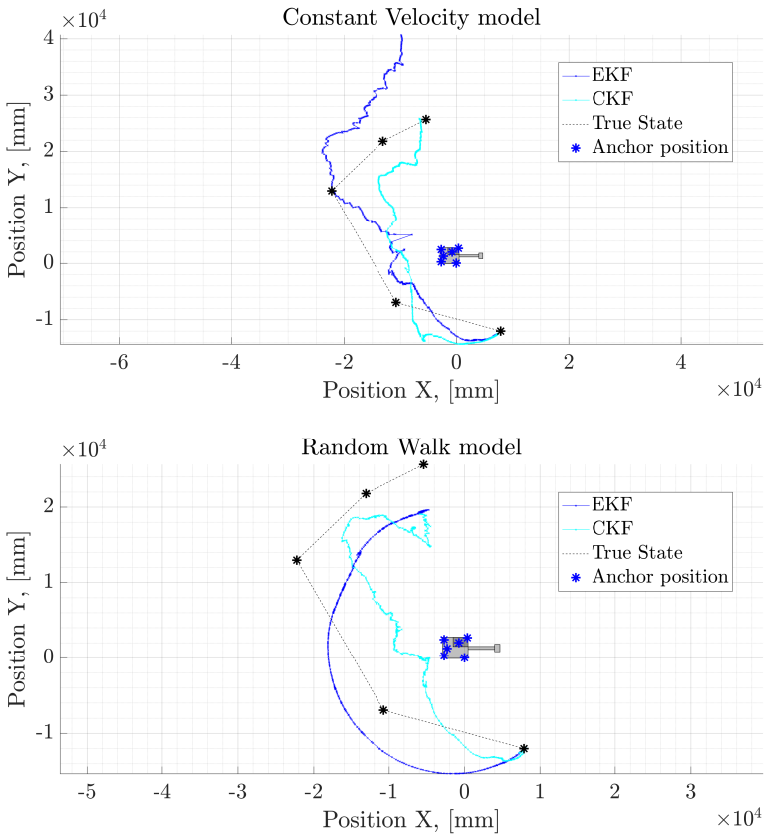

Figure 7.27: Plot of dynamic tests on a real machine. The tag is moving along a trajectory which starts in the bottom of the plot. Position estimation using EKF and CKF. The filters are using a constant velocity model and a random walk model.

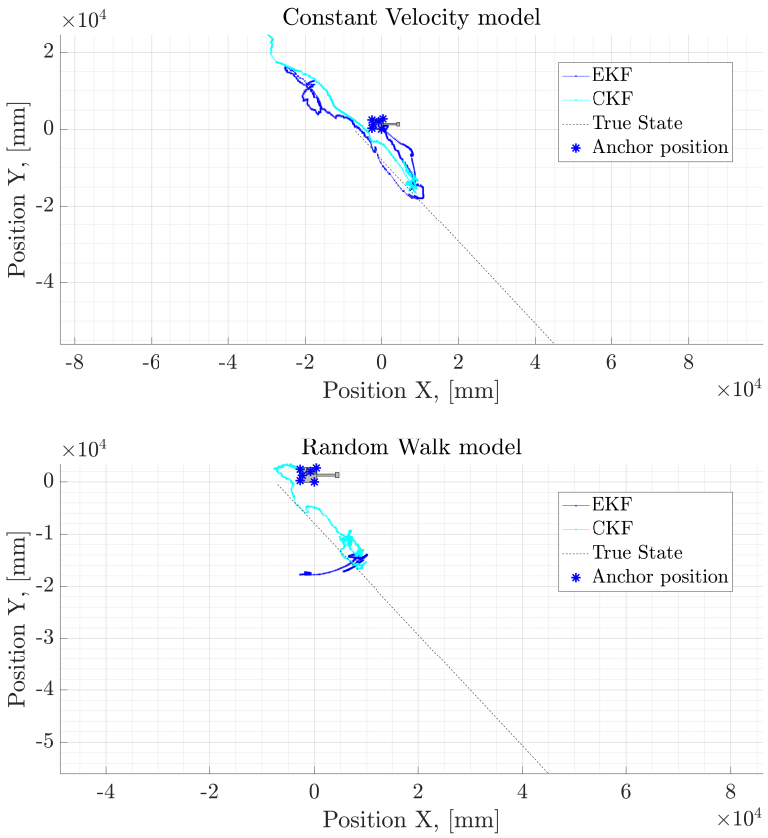

Figure 7.28: Plot of dynamic tests on a real machine. The tag is moving along a trajectory to test the range for TDOA. Position estimation using EKF and CKF. The filters are using a constant velocity model and a random walk model.

The same behaviour is seen in Fig. 7.26 as in Section 7.3.3.1. The filters are good at estimating a direction, but they are not as good in estimating a distance to the machine. In the case shown in Fig. 7.27, the filters are able to track the position to some extent. As in test case one, the direction estimation is correct but the filters do not manage to estimate the correct distance. As this affect both filters and both models there is no apparent top performer. The results displayed in Fig. 7.28 follows the same behaviour as previously presented test cases.

7.4 Filter Computational Time

The filters and the iterative solver used to obtain a position differs in computational requirement. To evaluate how computationally heavy each algorithm is, the execution time of each technique is measured. The result of these measurements are presented in Table 7.1.

	Non-linear solver	**EKF RW**	**EKF CV**	**CKF RW**	**CKF CV**
TWR	9.8	1.2	1	13.3	16.1
TDOA	17.5	2.8	1.4	14	9.8

Table 7.1: Table of average normalized execution times for CKF, EKF and the non-linear solver. The time for TWR using EKF with the constant velocity model is the reference time.

As seen in 7.1, the EKF filter is the least computational heavy algorithm. The non-linear solver and CKF approach is considerably slower.

7.5 System Range

During the dynamic machine test shown in Fig. 7.15, the maximum working range of the concept system is tested. This is done to evaluate if UWB technology is capable to locate workers at long enough distance. The test reveals, Fig. 7.29, that the TWR system can communicate over a distance of 70 m. The test could unfortunately not measure the maximum distance, as the available testing space is too small. Some anchors lost connection to the tag at a closer range, these are the anchors mounted on the opposite side of the machine. Hence, they experienced severe no line of sight conditions. These anchors still provided distance measurements up to a distance of roughly 32 m away from the machine. Also, there is a line of sight anchor that lost connection at 35 m. Although, it reconnected again at the return trip at 65 m. As this behaviour did not occur on the other line of sight anchors, this might be due to hardware issues. Based on this, the system using TWR has a guarantied range of a circle with a radius of 35 m, but in most cases a working distance of 70 m.

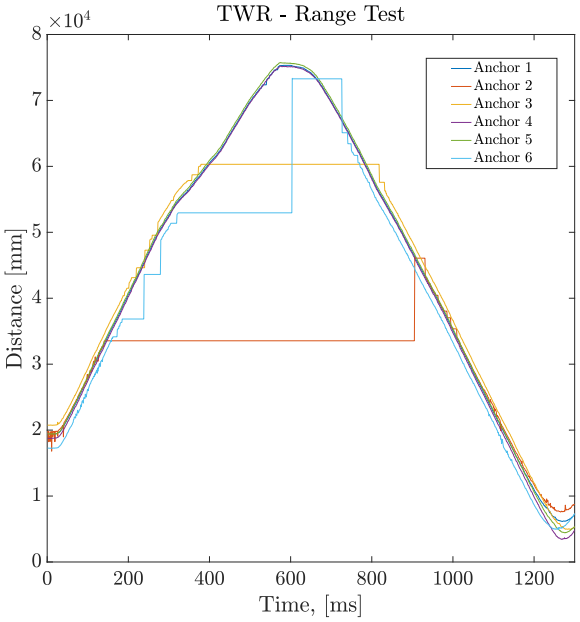

Figure 7.29: Plot of the distances to the different anchors during the range test.

In earlier tests (see Section 7.3), it is seen that the TDOA system becomes unreliable at distances greater than 5 m. However, measurements were obtained at the same distance as TWR.

7.6 Scalability with Two Way Ranging

The double sided TWR can have up to 27 tags in a system with an update rate of 2 Hz, while using 6 anchors, see (3.6). Although, the implemented double sided TWR yields a system with a capacity of 15 tags with an update rate of 2 Hz, due to the extra report message and the margins to avoid message collisions.

7.7 Scalability with Time Difference of Arrival

Using the implementation of TDOA described in Section 6.4, synchronization messages are sent every 2 ms. Therefore, half of the available time is used by the synchronization, which leaves 500 ms for the tags to report their position. This implies a maximum of 250 tags at 2Hz, without regards to extra time for a scheduling algorithm.

7.8 Power consumption

To ensure that the system is able to function throughout the day, the power consumption are measured for the different proposed systems. In table 7.2, the power consumption for a TWR and a TDOA based system is compared.

Power consumption	No UWB	TWR	TDOA
Min Power (mW)	372	913	978
Max Power (mW)	383	1091	1132
Avg Power (mW)	378	1002	1055
Percentage (%)		100	105.3

Table 7.2: Table of measured power consumption using both TWR and TDOA protocol.

In 7.2 it is seen that the power consumption of TWR and TDOA are similar, but the TDOA system is slightly more power consuming. This might be due to the wireless synchronization needed by the TDOA protocol. Because of this, the tag receives a synchronization message at 500 Hz, which is more often than what a TWR system encounters. As the development kit includes several status LEDs, which blinks, the measurements are affected. The large deviation in the measured values in 7.2, is due to this blinking LEDs. This is because in this test the current is measured in a single time instance, and in some instances all LEDs are off, corresponding to a low value, and in other all are on, corresponding to a high value. Since the LEDs draws power, and the order in which they blink depends on if TWR or TDOA is used, there is a possibility that the increase in power using TDOA is due to the LEDs rather than the localization method.

8

Discussion and Future Work

In this chapter the different localization methods, position estimation techniques, scalabiltity and overall system behaviour is discussed and evaluated.

8.1 Test Results

In this section, the test results are discussed. First, the TWR system, and secondly the TDOA system.

8.1.1 Results for the Two Way Ranging Method

As the results from Chapter 7 show, using UWB sensors and a TWR localization method, performs overall satisfactory. The accuracy of the system is greater than what is stated as necessary for this application, see Section 1.3.1. It also has a longer range than desired. Although, the settings for the DWM1000 sensor are set for maximum transmission power, which may not be allowed depending on which country it operates in. Unfortunately, the transmission power has not been measured, since no measurement unit has been acquired.

When comparing the accuracy performance of the system, one can see that the different algorithms behaves quite differently. It is seen that the non-linear solver, using a low pass filter, would perform well in terms of accuracy, in low disturbance situations. Since, the method generates an estimate close to the true position in those cases. A drawback of this approach is the time complexity. Due to this, as well as the inability to cope with large disturbances, the non-linear solver approach might not be optimal in an industrialized system with a large number of tags, as this would require a fairly powerful CPU to compute the positions at a satisfactory update rate.

A better method is to use one of the implemented filters. The CKF filter yields the best performance of the filters. Although, a CKF has a higher computational complexity compared to an EKF, due to all the sums it needs to calculate, see Section 5.4. It is hard to estimate if the computational complexity would make it sub-optimal for a industrialized system, but it would be the filter of choice if the hardware allows it. Regarding the most suitable process model one can see in Section 7.2 that both the random walk model and the constant velocity have their pros and cons. The constant velocity model yields a better result when the tag is moving in a straight line, but have difficulties taking care of sudden changes in direction

and during large disturbances. The random walk, on the other hand, provides good results in most of the cases, but are not as good when moving in straight lines. Therefore, a random walk model is the model of choice in most cases. It is reasonable that the constant velocity model works best when moving in straight lines, since it is made to predict the next state in the same direction. The random walk model, however, predict a state in a random direction.

As mentioned in Chapter 3, TWR suffers from a slow update rate and therefore has a limited scalability, for the implemented TWR method. As presented in Section 7.6, there is a limit of 15 tags at 2 Hz. This might be increased by a more efficient scheduling algorithm, e.g., the implementation generating (3.7), which is mentioned in Section 3.6. Changes to the DWM1000 settings could also increase the update rate, by changing the message length etc. To obtain a reasonable amount of tags in the system, the update rate could be lowered, as 30 tags would be able to fit if the update rate is 1 Hz. Further improvements to the communication scheme could improve the scalability without changing the communication speed. An example of this is to not update with all anchors during one update cycle. Due to no line of sight conditions, a better implementation of the tags could be to only update with the necessary anchors in order to save air utilization. The update rate could also be changed dynamically depending on the amount of tags in the system. When only one tag is present in the system, it can be allowed to communicate uninterrupted in order to obtain a high update rate. When more tags join the system, the update rate can be decreased. A further improvement of this technique would be to dynamical change the update rate depending on the distance from the machine. As tags at a distance of more than 20 m are irrelevant to track at high speed, as they do not endanger the machine. The tag could instead be allowed to communicate at 1 Hz, but when the tag is at a distance of 5 m, it might benefit from a update rate of 20 Hz.

8.1.2 Results for the Time Difference of Arrival Method

The main advantage of using the TDOA method is the minimal number of messages needed to obtain a position. Therefore it is ideal for a system that are required to track a large number of tags at high speeds. Also, if a wired clock synchronization is used, TDOA might be more power efficient as the tag does not need to receive as many messages.

Unfortunately the advantages end there. Firstly, the need for synchronized clocks require a complex synchronization algorithm, if this is to be done wirelessly. Otherwise, a custom hardware design is necessary, if a wired method is to be used. This synchronization might increase the measurement noise due to synchronization inaccuracy. This is most sensitive in the wireless case.

The main disadvantage is the trait of multilateration. When multilaterating outside the area defined by the anchors, the hyperbolas coincide which leads to highly inaccurate position estimations, but an accurate bearing estimation. Because of this, a

TDOA method, by itself, is not a favorable choice for this application.

From the results, see Section 7.3, one see that the TDOA can provide an acceptable position estimation, in some cases. Although, if the distance to the anchors surpasses 5 m, the estimations are unusable. In these results the filter is tuned to trust heavily on the process model. Here the initial state is set to the true state. Therefore, the filter is able to track the movement decently. If the initial state to the filter is far away from the true state, the filter is not able to track the movement. Therefore TDOA is not a robust system and heavily dependent on a good initial guess of the states.

8.1.3 Concept Evaluation

Based on the results in Chapter 7, and the previous discussion, localization of construction workers on construction sites is possible using UWB technology. To obtain a good range of the position estimations as well as the desired accuracy, the localization system has to use the TWR method. With this said, the concept system evaluated in this thesis is not a fully functional system, and further tests and improvements have to be made in order to get a working positioning system.

As seen in Chapter 7, the random walk model is superior in certain cases and the constant velocity model in others. Hence, there is no obvious model that would yield perfect results in all situations. To solve this, an approach using a dynamic process model could be applied. In this way, the system could switch between the different models depending on behaviour and environment, e.g., when the outlier rejector detect a noisy environment the process model could switch to a constant velocity model with heading, and during long turns to a random walk model.

Generally for the evaluated systems, there are spots around the machine that suffers from no line of sight conditions, for one or several anchors. Therefore, the accuracy at different positions around the machine is better or worse. Although, a six anchor setup using TWR works satisfactory, but more anchors would yield a more consistent coverage around the machine. For a TDOA system this would be even more beneficial as it requires line of sight to two anchors to obtain one measurement.

As previously mentioned the tags would be battery powered in a industrialized system. When analyzing the power consumption presented in 7.8, the average power consumption of the TWR system is around 1 W. Therefore, if the tag is powered by a Li-ion battery with a nominal voltage of 3.7 V, it would draw 270 mA. A common 18650 Li-ion battery cell have a capacity of 2500-3000 mAh. Therefore this system could be powered for 10 hours without any modifications, which is longer than a ordinary working day. Further with bespoke hardware the LEDs could be removed and thereby the power consumption be lowered and the battery life extended.

Since the concept system is meant to be used for safety issues, it is necessary to have redundancy. To make the system redundant, two separate UWB systems could be

used, which runs on different channels to not interfere one another. When not both systems are functioning, a warning could alert the machine operator. With the use of multiple systems other opportunities emerge, which is further discussed in Section 8.2.11.

8.2 Improvements and Future Work

In this section, different improvements which could be included to the system are discussed as well as other future work.

8.2.1 Sensor Integration

The use of external sensors might aid the position estimation, e.g., an IMU could be included with the tag, by the use of sensor fusion. The use of data from the IMU could help to decide a heading, with magnetometer and/or gyro, and also tell when the tag is moving, with data from the accelerometer.

8.2.2 Robust Wireless Clock Synchronization

The implementation of wireless clock synchronization used in this thesis is based on an open source implementation, see Chapter 6. Decawawe, the manufacturer of the UWB sensors, have their own implementation of wireless synchronization. Wirelesses synchronization is hard to accomplish when the desired clock difference is in the nanosecond range. As this thesis uses a free implementation of the synchronization it is probable that the commercial version developed by the manufacturer offers a more exact synchronization and thereby a higher accuracy, as well as the possibility to obtain time difference from a dynamically selected pair of anchors. In this way the TDOA system might both become more accurate as well as able to handle no line of sight condition in a more dynamic and efficient manner.

8.2.3 Wired Clock Synchronization of Anchors

An even more robust clock synchronization could be achieved by investigating the possibility of using a wired clock synchronization of the anchors. As any wireless synchronization are susceptible to disturbances when synchronizing, a completely wired solution would greatly improve the accuracy performance. As previously discussed, see Section 2.2.1, the DW1000 IC support an external clock signal in order to achieve synchronized clocks. As the DWM1000 module do not support this, a new hardware platform would be needed.

8.2.4 Synchronous Time of Arrival

As seen in the results, Chapter 7, the TWR protocol outperforms TDOA in terms of accuracy. This is mainly due to how trilateration differs from multilateration. TDOA on the other hand, outperforms TWR in the terms of scalability, as it is a synchronous system, and does not need to send multiple messages to obtain a

measurement. A possible solution to get the best from both methods would be to develop a synchronization scheme to synchronize the tags to the anchors' clocks. This would be a synchronous TOA technique which would exhibit the positive accuracy effects on TWR and the scalability performance of TDOA. Since, the TOA method produces circles rather than hyperbolas and the synchronized clock would eliminate the need for two way communication, reducing the three needed messages of the double sided TWR implementation to only one per anchor.

8.2.5 Bespoke Hardware

An untouched subject in this thesis is how the hardware design around the DWM1000 module affects the performance. In this thesis one hardware design has been used, although a different platform were used in early tests. This tests have showed a slight difference in the system behaviour. However, the reason for this is unknown. It could be due to different software implementation or it might be due to the different hardware design. A more bespoke hardware design would also remove any unnecessary power consuming components and reduce size in order for the system to be developed in to a industrialized product.

8.2.6 Radio Frequency Design

The DWM1000 module includes a complete RF design, and therefore the RF designs relation to performance have not been evaluated. A larger or more omnidirectional antenna might yield better results, and might not contribute to performance degradation when the anchors are turned away form the tag, which would increase performance.

8.2.7 Bespoke Software

To be able to evaluate the use of UWB technology for positioning around an excavator, available hardware and software have been used in order to shorten development time. This is great for a proof of concept system, but for a industrialized system, a bespoke embedded software in the anchors and tags are required. In the test system, there are unnecessary functions that requires processing power and the system is hard to adapt to fully suit the new application, e.g., it is hard to dynamically switch settings for the DW1000 module. If this would be possible, a more dynamic localization system could be developed, where the signal strength and transmission speed could change with the distance between the tag and anchors, and with the number of active tags in the system. It could also make it possible to switch between TWR and TDOA dynamically depending on location. It could e.g. be desirable to increase scalability when personnel are close enough to the machine, by using TDOA.

8.2.8 Collaborative Position Estimation

As the system is implemented, there are predetermined anchors and tags in the system, and they only acts as anchors and tags respectively. An alternative and

maybe higher performing method, is to dynamically use the tags as both anchors and tags. As the UWB standard allows for information to be transmitted, as well as distance measurements, a network of tags could collaborate. There are two main advantages of this. The first and main one, is that if the tags broadcast their own position to all other tags, a tag outside the reach of the main anchors could use the position of the closer tags as anchors instead. This would result in a larger range of the system. The second advantage is the event if a tag have a connection to an anchor on the machine, it might be in a no line of sight condition and therefore it would give a wrong measurement. Instead other tags in the vicinity could be used as anchors to get a better position estimation. Essentially, this approach would yield a drastically higher anchor density.

8.2.9 Multipathing

A source of disturbance that probably is present in the results, but not studied and evaluated, is the affect of multipathing. To get a well functioning and robust system, the effects of multipathing need to be studied in order for the software and algorithms to handle this situations accordingly.

8.2.10 Multiple Machines

On large construction sites there might be multiple machines present. That scenario would lead to problems for the system as it is implemented in this thesis. Since the TWR mode is scheduled to send messages to all anchors, multiple machines leads to a long update time for each tag. Also, since the TDOA is implemented by wireless synchronization, the different setups of the machines might interfere each other while trying to synchronize.

Although, there are possible fixes to these problems. If TWR is used, a system which consists of subsystems for every machine could be implemented. Then each tag could connect to the closest subsystem, dynamically, i.e., the tags are able to change subsystem continuously. For this to work, every subsystem would need to run on an own frequency to not interfere each other. The wireless TDOA could work in a similar way, with subsystems running on their own frequencies to not interfere one another.

Another solution could be to use TDOA with wired clock synchronization of the anchors. With such a system implemented, multiple machines would not be a major problem, since the anchors are passive and only listens to the tags. Therefore, the tags only need to follow a scheduling protocol and then broadcast their signal to all anchors with one message. Each machine would then be able to obtain a position estimate of each tag. Such a system could be improved if the different machines are connected to each other and could share information. Then measurements from multiple machines could be used to obtain a position estimate.

8.2.11 Hybrid TWR/TDOA System

An interesting way of implementing a localization system would be to merge the TWR and TDOA methods. This could increase scalability without the sacrifice of accuracy. A hybrid system consisting of updates of both TWR and TDOA measurements could work since the TDOA gives estimates with a good bearing and the TWR gives a good distance. Therefore several TDOA measurements could be used, which have good scalability properties, and just one TWR measurement, which has good accuracy properties. If the implementation is done by the use of a KF, the filter could be designed to weigh the TDOA and TWR measurements differently. Therefore, one can design the filter to let the TWR update to have a greater effect than the TDOA updates, even though there are more updates with TDOA measurements than updates with TWR measurements.

If the system is to be redundant, and two subsystems are used simultaneously, a hybrid system could easily be implemented. One subsystem could use TDOA, at a high update rate, and the other could use TWR, with a low update rate. This would create two completely isolated systems, which could either operate independently or together. It would also simplify the redundancy, as if one of the systems would stop functioning the operator could be alerted, as further discussed in Section 8.1.3.

9
Conclusion

The conclusion of this thesis is that a system consisting of UWB sensors could be able to cover the blind spots of an excavator, by estimating the positions of workers. Although, TWR has to be used since it is the only method that is accurate enough outside the area defined by the anchors. With TWR the accuracy goal, ±50 cm, is fulfilled within a distance of 25 m from the excavator. TWR also fulfills the scalability goals as it is able to position 15 tags at 2 Hz.

In this thesis the DW1000 UWB sensor has been used. The characteristics of the sensor equipped on a microcontroller are, for the TWR mode, a deviation of approximately ±150 mm and a bias of approximately -300 mm. For the TDOA mode there is a deviation of approximately ±150 mm. There is also some bias but it is not consistent and therefore hard to verify.

There exists multiple localization methods for positioning with UWB sensors, but in this thesis TWR and TDOA have been used. For each localization method there are multiple algorithms which can be used to estimate a position. In this thesis the trilateration and multilateration problem have been solved by non-linear KFs and by non-linear programming, with satisfying results.

In this thesis 6 anchors have been used during the machine tests. As this tests have fulfilled the accuracy requirement, no more anchors are needed, but with further testing and improved anchor placement less anchors might yield similar results.

The system could be improved if the parts discussed in Chapter 8 are further investigated and implemented.

Bibliography

[1] *DW1000 USER MANUAL*, Decawave Ltd.

[2] J. W. Hinze and J. Teizer, "Visibility-related fatalities related to construction equipment," *Safety science*, vol. 49, no. 5, pp. 709–718, 2011.

[3] R. S. Kshetrimayum, "An introduction to UWB communication systems," *IEEE Potentials*, vol. 28, no. 2, pp. 9–13, March 2009.

[4] J. Foerster, E. Green, S. Somayazulu, and D. Leeper, "Ultra-wideband technology for short-or medium-range wireless communications," in *Intel technology journal*. Citeseer, 2001.

[5] S. Gezici, Z. Tian, G. B. Giannakis, H. Kobayashi, A. F. Molisch, H. V. Poor, and Z. Sahinoglu, "Localization via ultra-wideband radios: a look at positioning aspects for future sensor networks," *IEEE signal processing magazine*, vol. 22, no. 4, pp. 70–84, 2005.

[6] *DW1000 Datasheet*, Decawave Ltd.

[7] *EC200 Brochure*, Volvo CE. [Online]. Available: https://www.volvoce.com/europe/en/products/excavators/crawler/ec220e/

[8] G. R. Aiello and G. D. Rogerson, "Ultra-wideband wireless systems," *IEEE microwave magazine*, vol. 4, no. 2, pp. 36–47, 2003.

[9] "FCC UWB rules." [Online]. Available: https://transition.fcc.gov/Bureaus/Engineering_Technology/Orders/2002/fcc02048.pdf

[10] Eir-lex.europa.eu, "EUR-Lex - 32014D0702," 2014. [Online]. Available: http://eur-lex.europa.eu/eli/dec_impl/2014/702/oj#document1

[11] R. S. Kshetrimayum, "An introduction to uwb communication systems," *IEEE Potentials*, vol. 28, no. 2, pp. 9–13, 2009.

[12] M. R. Mahfouz, A. E. Fathy, M. J. Kuhn, and Y. Wang, "Recent trends and advances in UWB positioning," in *2009 IEEE MTT-S International Microwave Workshop on Wireless Sensing, Local Positioning, and RFID*, Sept 2009, pp. 1–4.

[13] "IEEE standard for low-rate wireless networks," *IEEE Std 802.15.4-2015 (Revision of IEEE Std 802.15.4-2011)*, pp. 1–709, April 2016.

[14] *DWM1000 Datasheet*, Decawave Ltd.

[15] "Loco, bitcraze uwb localization system." [Online]. Available: https://www.bitcraze.io/loco-pos-system//

[16] M. Kwak and J. Chong, "A new double two-way ranging algorithm for ranging system," in *Network Infrastructure and Digital Content, 2010 2nd IEEE International Conference on*. IEEE, 2010, pp. 470–473.

[17] M. Geyer and John A. Volpe National Transportation Systems Center (US), *Aircraft navigation and surveillance analysis for a spherical earth*. Volpe National Transportation Systems Center, 2014.

[18] S. He, X. Dong, and W.-S. Lu, "Localization algorithms for asynchronous time difference of arrival positioning systems," *EURASIP Journal on Wireless Communications and Networking*, vol. 2017, no. 1, p. 64, 2017.

[19] L. Huang, F. Wang, C. Ma, and W. Duan, "The analysis of anchor placement for self-localization algorithm in wireless sensor networks," in *China Conference on Wireless Sensor Networks*. Springer, 2012, pp. 117–126.

[20] Y. Zhou, "An efficient least-squares trilateration algorithm for mobile robot localization," in *Intelligent Robots and Systems, 2009. IROS 2009. IEEE/RSJ International Conference on*. IEEE, 2009, pp. 3474–3479.

[21] F. Izquierdo, M. Ciurana, F. Barceló, J. Paradells, and E. Zola, "Performance evaluation of a TOA-based trilateration method to locate terminals in WLAN," in *Wireless Pervasive Computing, 2006 1st International Symposium on*. IEEE, 2006, pp. 1–6.

[22] S. Särkkä, *Bayesian Filtering and Smoothing*, ser. Institute of Mathematical Statistics Textbooks. Cambridge University Press, 2013.

A

Appendix A

Plots of the distance measurements for the sensor characterization. The measurement points are presented in Fig. 7.1.

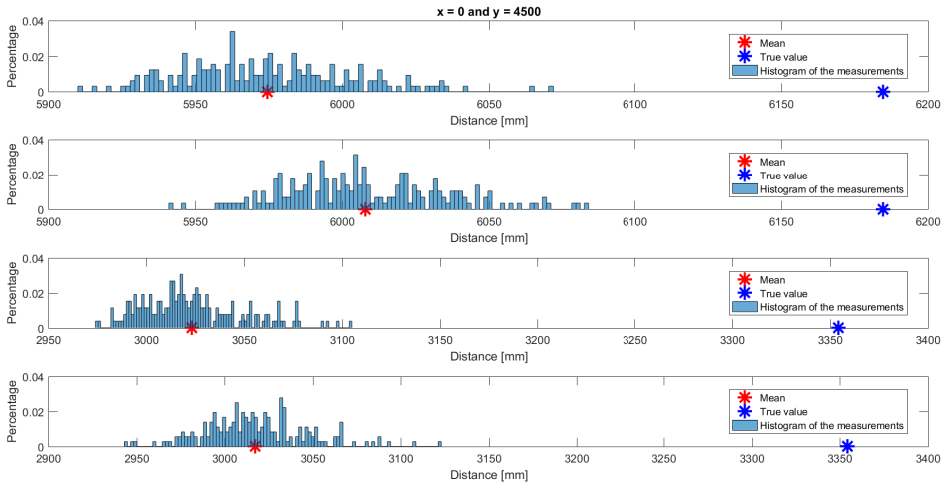

Figure A.1: Plot which shows the distribution, mean value and true value for the distance measurements in the point $(0, 4500)$ with TWR.

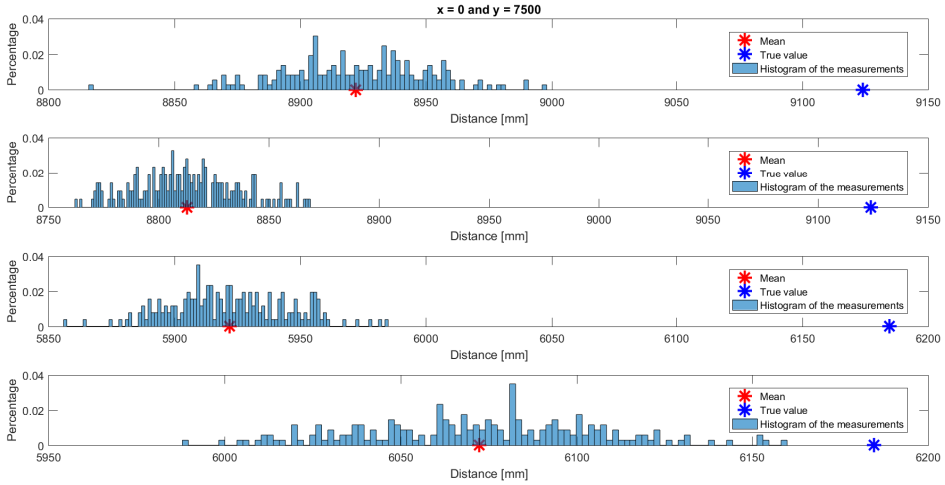

Figure A.2: Plot which shows the distribution, mean value and true value for the distance measurements in the point $(0, 7500)$ with TWR.

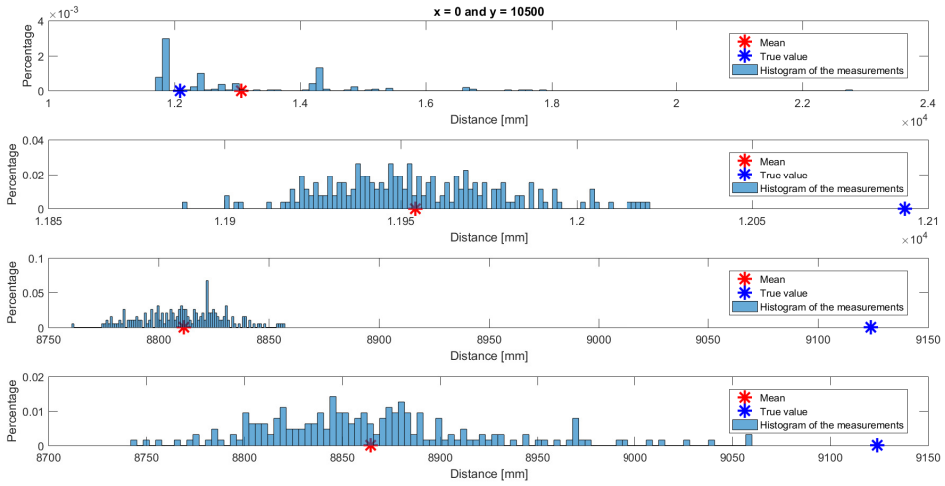

Figure A.3: Plot which shows the distribution, mean value and true value for the distance measurements in the point $(0, 10500)$ with TWR.

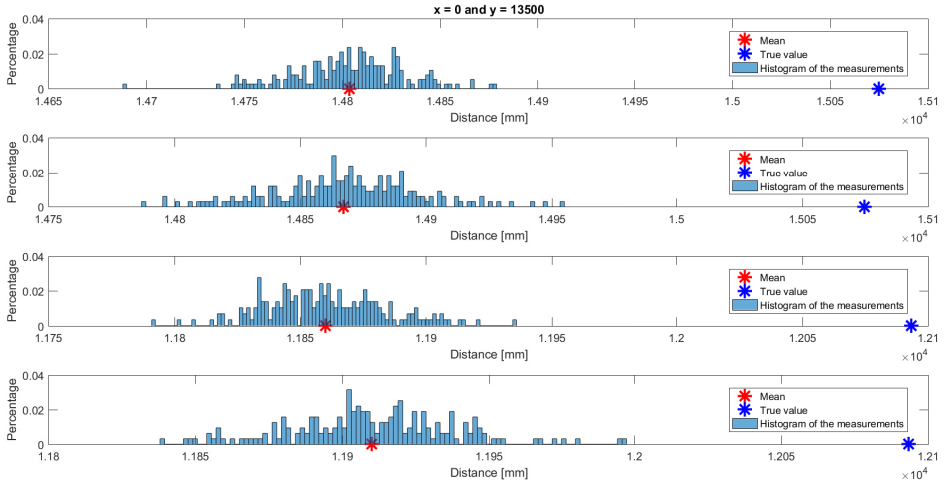

Figure A.4: Plot which shows the distribution, mean value and true value for the distance measurements in the point $(0, 13500)$ with TWR.

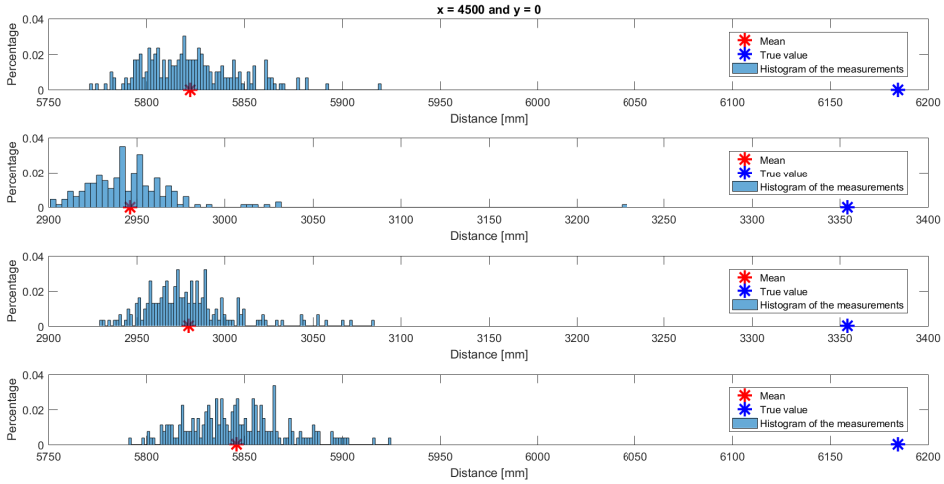

Figure A.5: Plot which shows the distribution, mean value and true value for the distance measurements in the point $(4500, 0)$ with TWR.

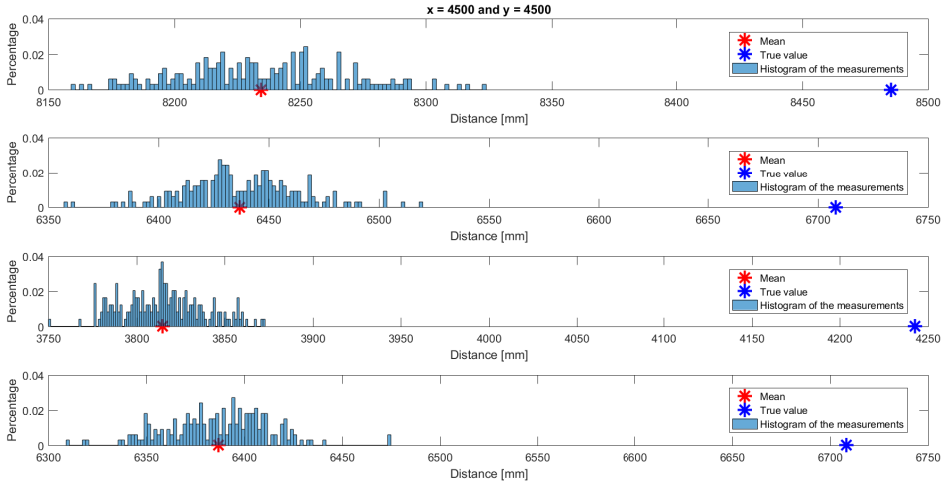

Figure A.6: Plot which shows the distribution, mean value and true value for the distance measurements in the point $(4500, 4500)$ with TWR.

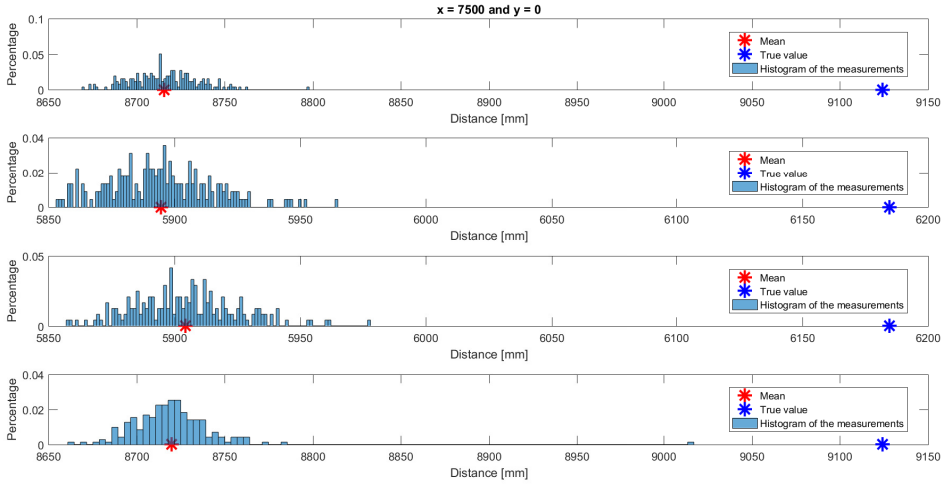

Figure A.7: Plot which shows the distribution, mean value and true value for the distance measurements in the point $(7500, 0)$ with TWR.

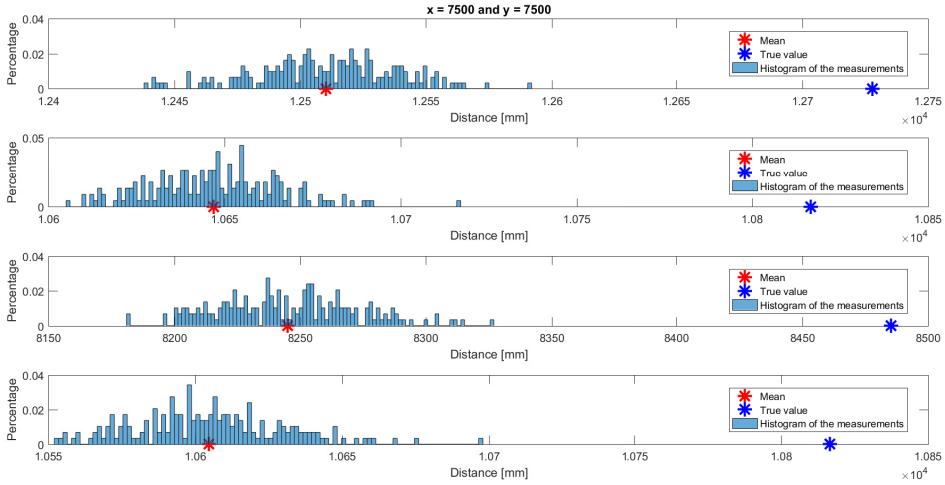

Figure A.8: Plot which shows the distribution, mean value and true value for the distance measurements in the point $(7500, 7500)$ with TWR.

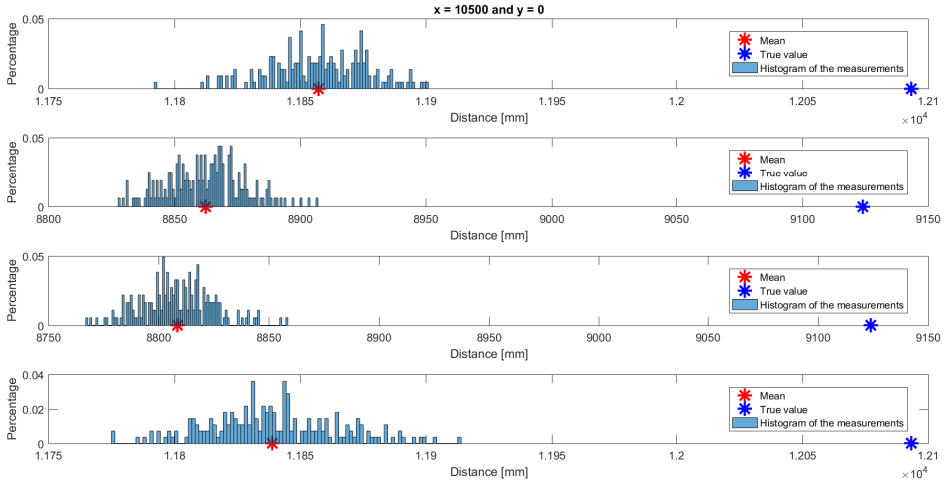

Figure A.9: Plot which shows the distribution, mean value and true value for the distance measurements in the point $(10500, 0)$ with TWR.

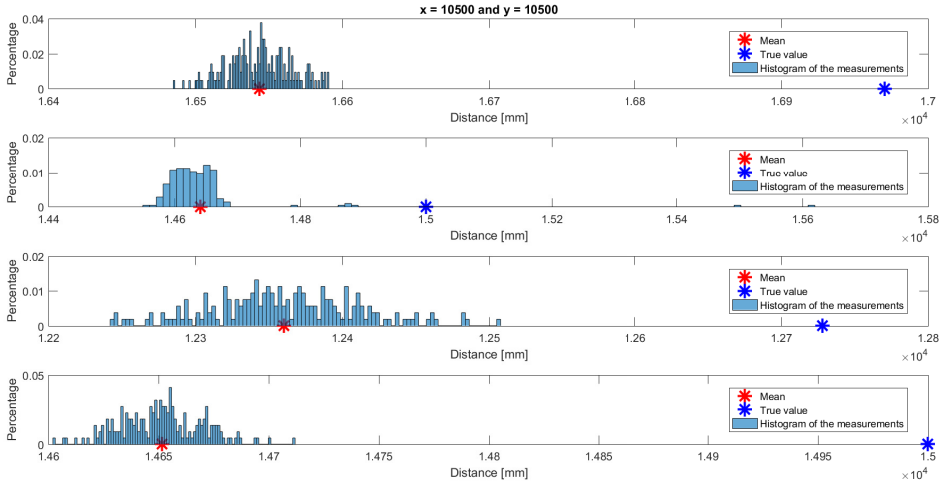

Figure A.10: Plot which shows the distribution, mean value and true value for the distance measurements in the point $(10500, 10500)$ with TWR.

B

Appendix B

Plots of the distance difference measurements for the sensor characterization. The measurement points are presented in Fig. 7.1.

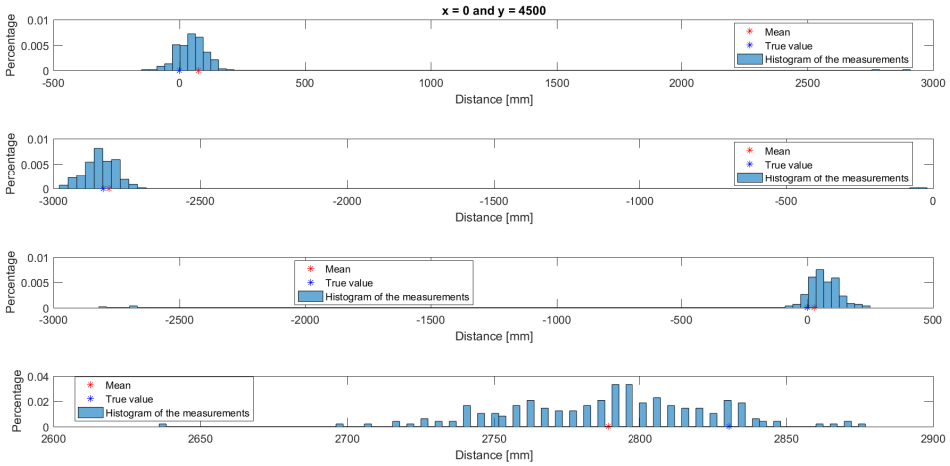

Figure B.1: Plot which shows the distribution, mean value and true value for the distance difference measurements in the point $(0, 4500)$ with TDOA.

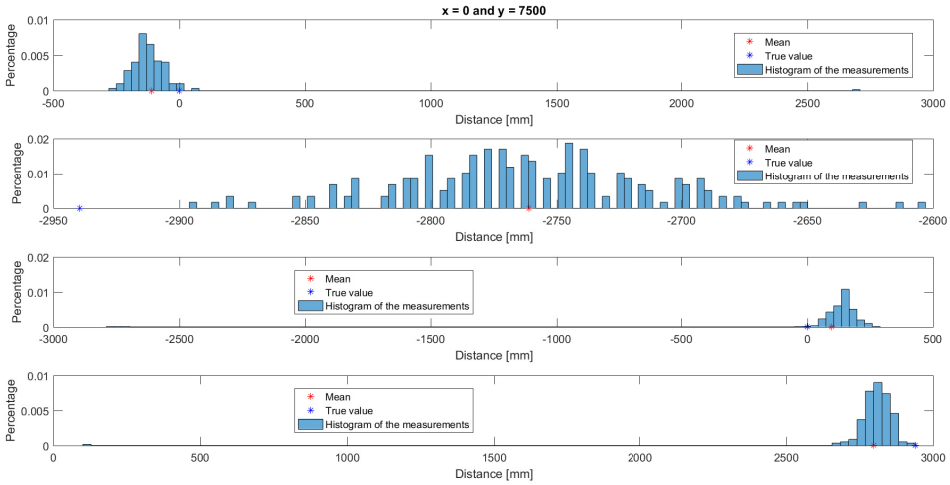

Figure B.2: Plot which shows the distribution, mean value and true value for the distance difference measurements in the point $(0, 7500)$ with TDOA.

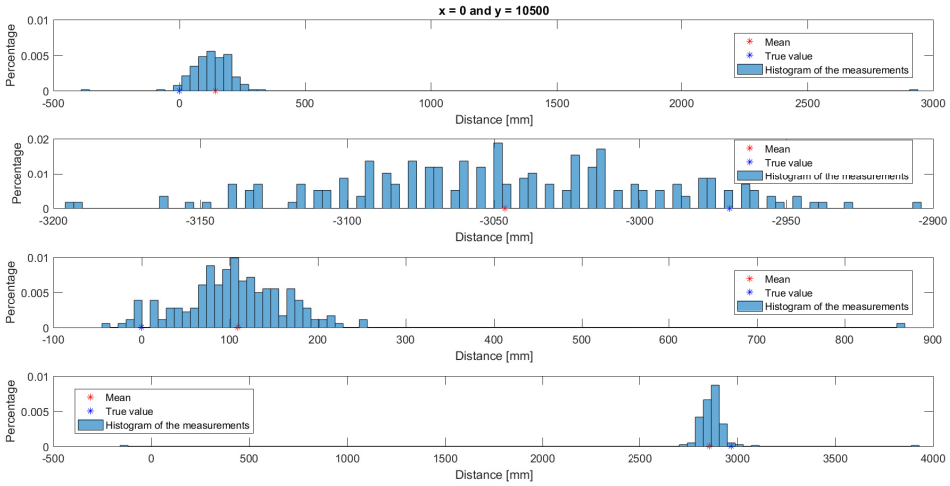

Figure B.3: Plot which shows the distribution, mean value and true value for the distance difference measurements in the point $(0, 10500)$ with TDOA.

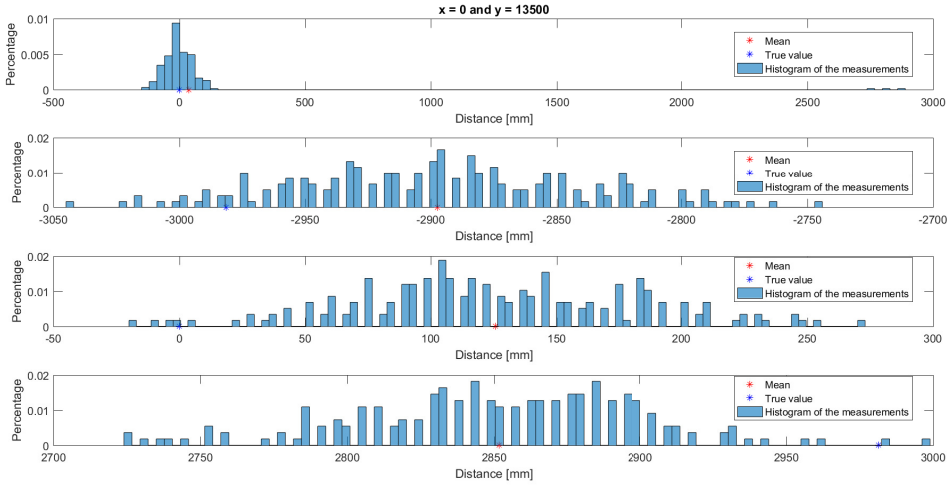

Figure B.4: Plot which shows the distribution, mean value and true value for the distance difference measurements in the point $(0, 13500)$ with TDOA.

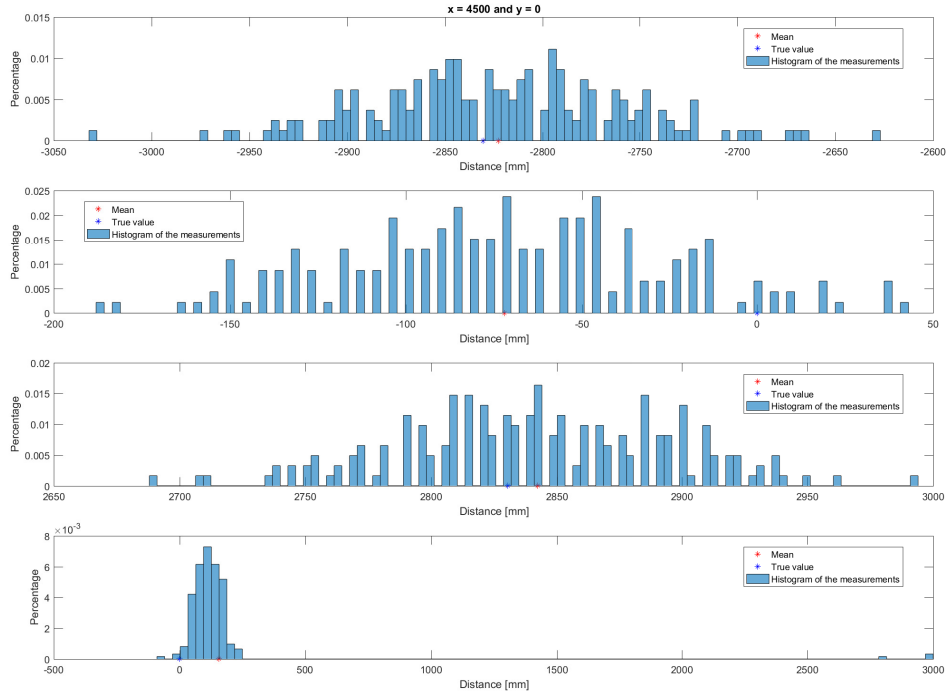

Figure B.5: Plot which shows the distribution, mean value and true value for the distance difference measurements in the point $(4500, 0)$ with TDOA.

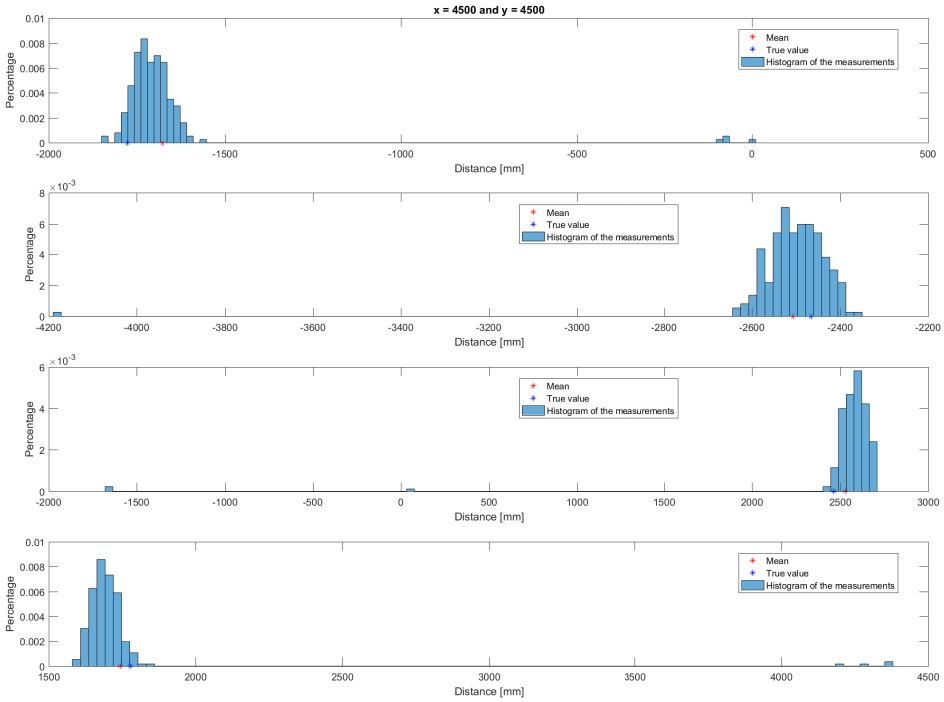

Figure B.6: Plot which shows the distribution, mean value and true value for the distance difference measurements in the point $(4500, 4500)$ with TDOA.

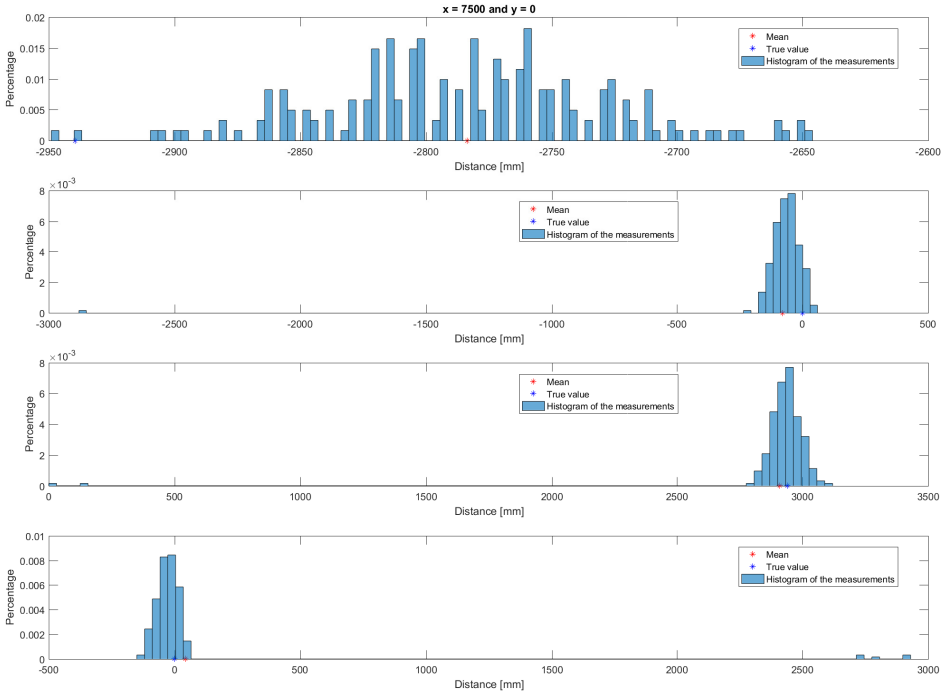

Figure B.7: Plot which shows the distribution, mean value and true value for the distance difference measurements in the point $(7500, 0)$ with TDOA.

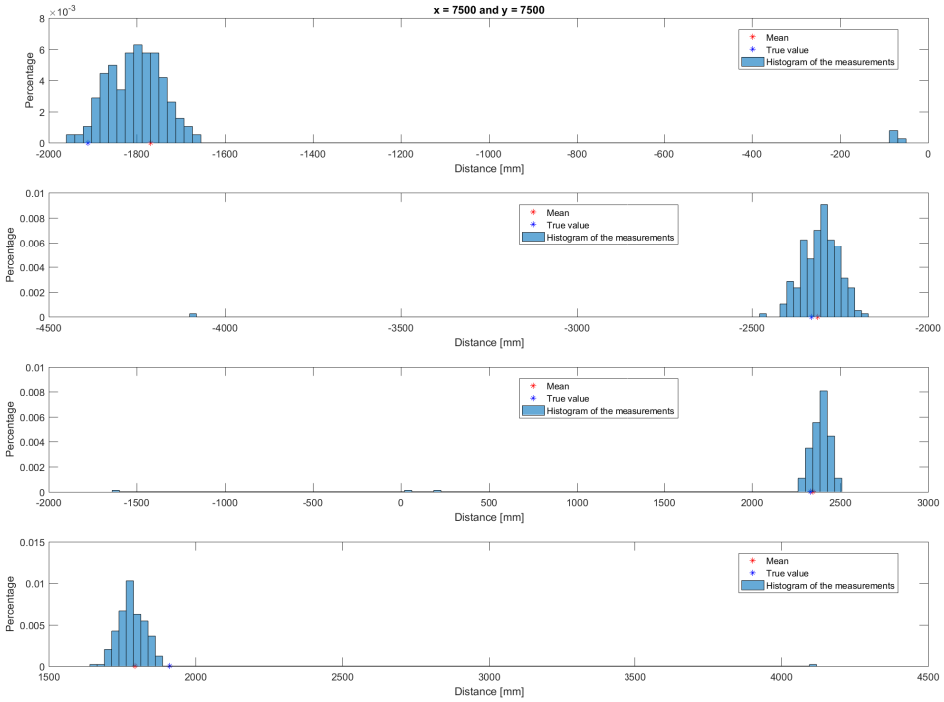

Figure B.8: Plot which shows the distribution, mean value and true value for the distance difference measurements in the point $(7500, 7500)$ with TDOA.

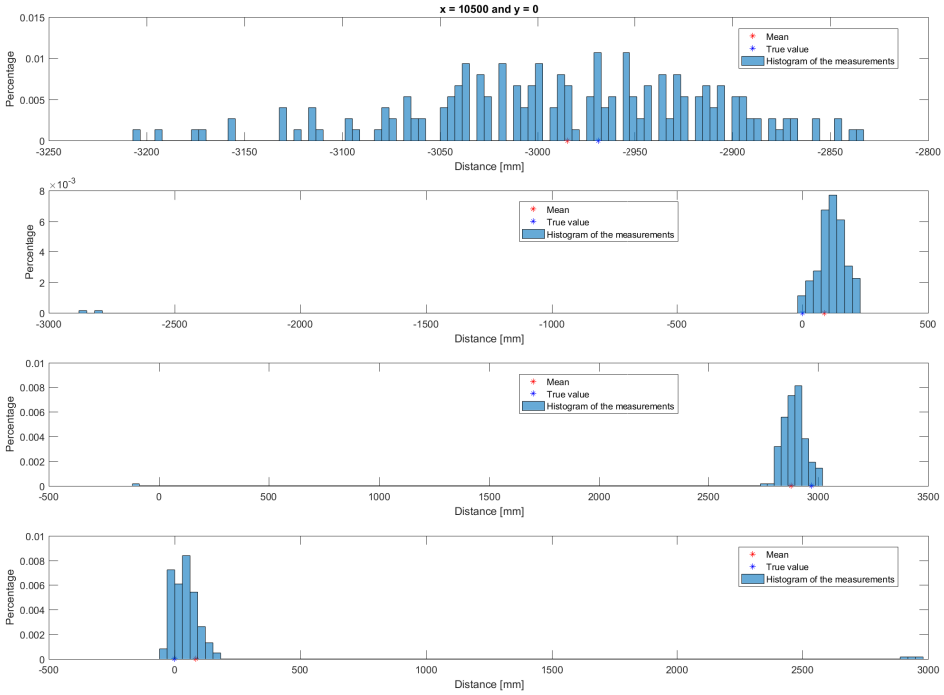

Figure B.9: Plot which shows the distribution, mean value and true value for the distance difference measurements in the point $(10500, 0)$ with TDOA.

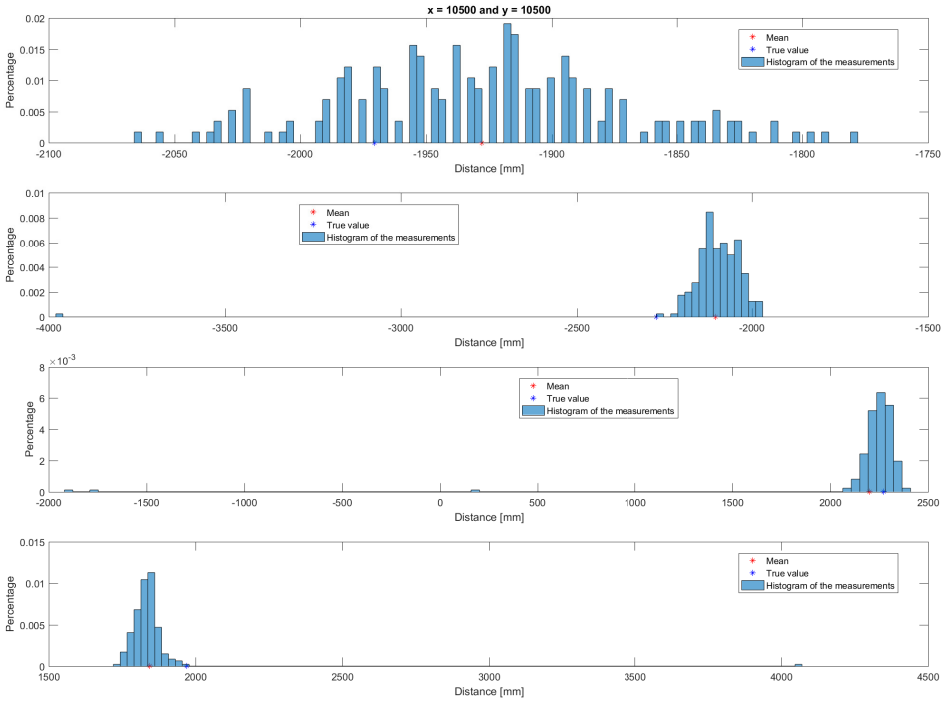

Figure B.10: Plot which shows the distribution, mean value and true value for the distance difference measurements in the point $(10500, 10500)$ with TDOA.

C

Appendix C

The plots in this appendix show how the result of the different methods, TWR and TDOA, is affected when moving away from the anchor setup as well as when noise is added to the measurements.

TWR

Figure C.1: Figure of obtained circles using TWR, when close, and far away from the anchors.

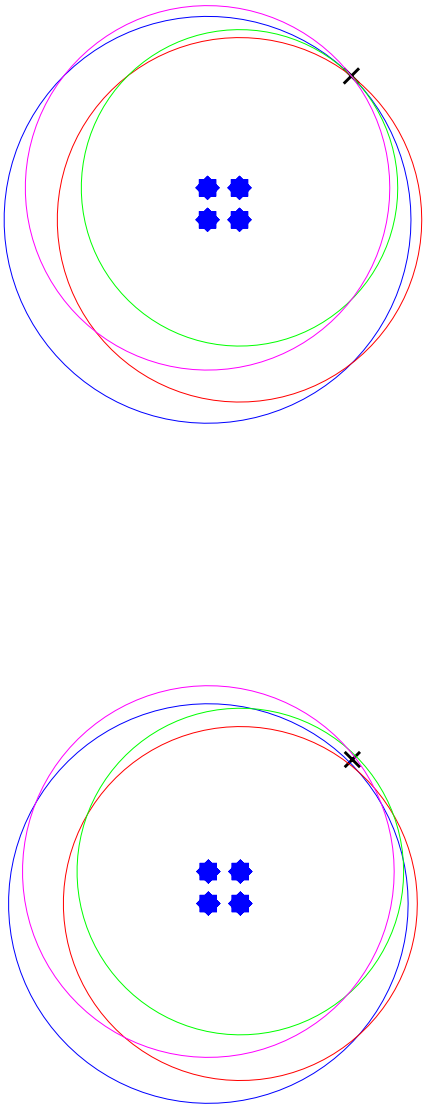

Figure C.2: Figure of obtained circles when using TWR. Top plot without noise, bottom plot with ±300 mm noise.

TDOA

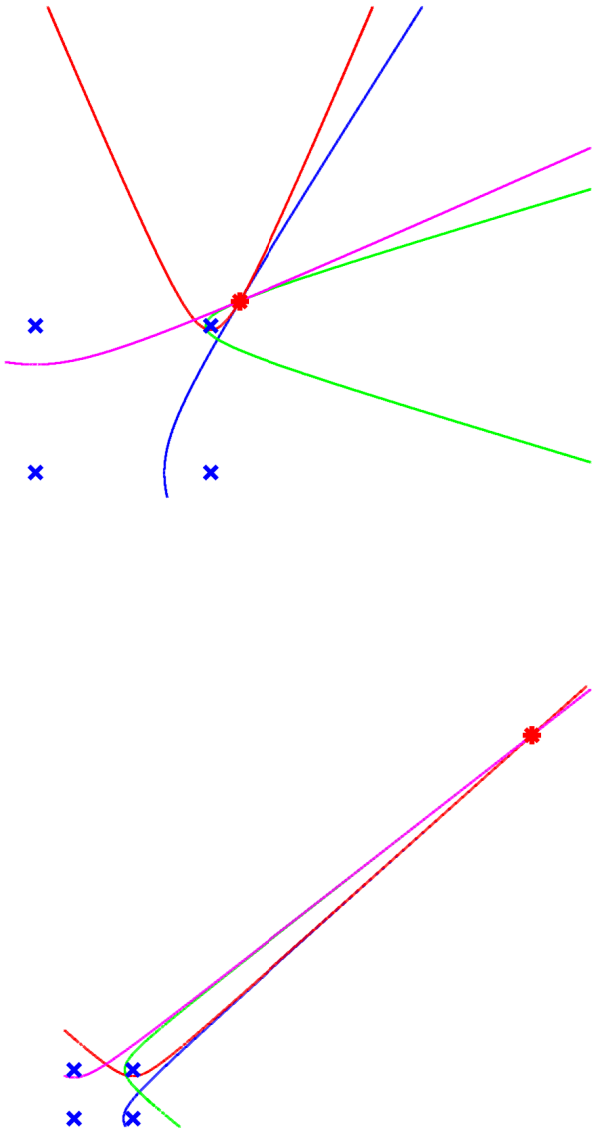

Figure C.3: Figure of obtained hyperbolas using TDOA, when close, and far away from the anchors.

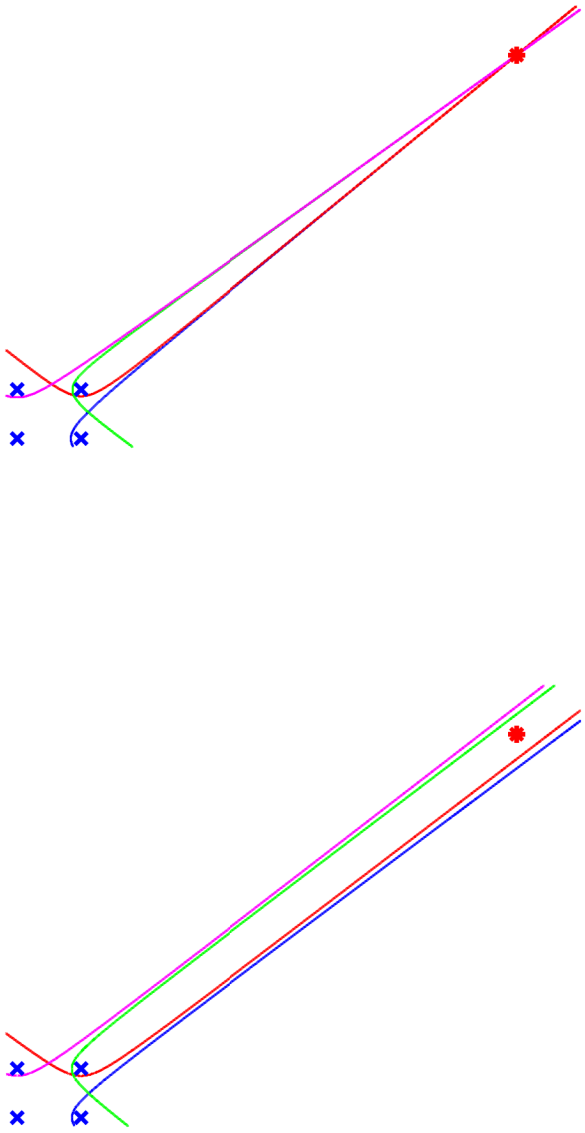

Figure C.4: Figure of created hyperbolas when using TDOA. Top plot without noise, bottom plot with ±100 mm noise.

D

Appendix D

Additional plots of the dynamic TDOA testing when moving around the machine in a circular trajectory.

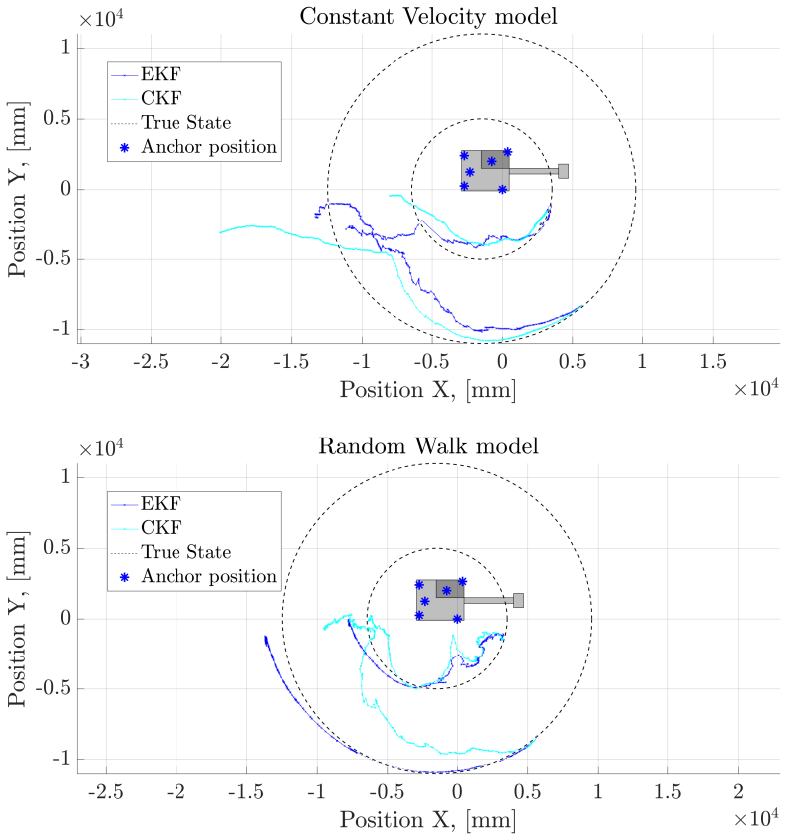

Figure D.1: Plot of dynamic tests on a real machine. The tag is moving in circular trajectory at 5 m and 11 m away from machine, behind it. Position estimation using EKF and CKF. The filters are using a constant velocity model and random walk model.

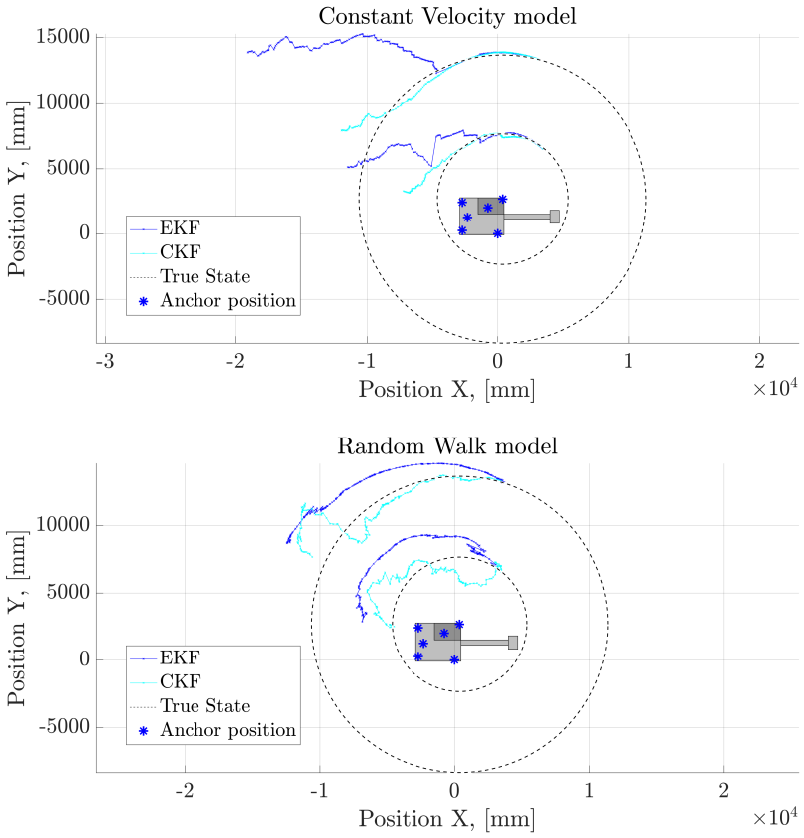

Figure D.2: Plot of dynamic tests on a real machine. The tag is moving in circular trajectory at 5 m and 11 m away from machine, behind it. Position estimation using EKF and CKF. The filters are using a constant velocity model and random walk model.